A WHOLLY ELECTROSTATIC FLAT CATHODE RAY TUBE FOR TELEVISION

A thesis submitted by HUGH ALFRED WILLIAM TOTHILL, B.Sc.(Eng.), A.C.G.I. for the degree of Doctor of Philosophy of the University of London.

April, 1965.

Electrical Engineering Department
Imperial College of Science and Technology,
London, S.W.7.

Supervisor: Professor D. Gabor, F.R.S.

ABSTRACT.

An account is given of the writer's contribution to the development of an electrostatic version of the Gabor-N.R.D.C. flat television tube. An earlier design had been found to have serious disadvantages, so a new design was proposed by D. Gabor in 1960. The writer was concerned with the electron optical aspects of this version of the tube.

The development undertaken by the writer included two important new components :-

1. A wide angle electrostatic deflection system giving a deflection angle of $\pm$ 60° in one plane for the line scan.
2. An electrostatic collimating lens to follow the deflection system, so that, on leaving this lens, the beam remains parallel to the axis of symmetry, but is displaced sideways by a distance which depends on the deflecting voltage. Initially, a theoretical design was available for this component, but many improvements had to be made.

In addition, a study was made of the action of the scanning array, which consists of a series of horizontal parallel conductors behind the viewing screen. The electron beam is deflected onto the screen by an electric wave which travels vertically up and down the scanning array to provide the frame scan. The position of this wave is changed by charging or discharging conductors of the scanning array. In the new design, this is effected by two beams from two additional electron guns, instead of by the writing beam. This arrangement has advantages which outweigh the complications of fitting two extra guns.

A digital computer was used to calculate electron trajectories in the deflection system and in the scanning array; it was found to be a powerful aid in the design.

CONTENTS.

		Page
Abstract		2.
Acknowledgments		5.
CHAPTER 1 - INTRODUCTION.		
1.1.	General	6.
1.2.	A description of the flat tube	6.
1.3.	Application of the flat tube to colour television	13.
1.4.	Advantages of the flat tube	16.
1.5.	Previous work on the flat tube	17.
1.6.	Other flat television tubes	20.
CHAPTER 2 - APPARATUS AND EXPERIMENTAL TECHNIQUES.		
2.1.	Introduction	22.
2.2.	The demountable vacuum tanks	22.
2.3.	Electrical supplies	25.
2.4.	Construction of the vacuum models	28.
2.5.	Measurement techniques	34.
2.6.	The electrolytic tank	37.
CHAPTER 3 - DEFLECTION SYSTEMS.		
3.1.	The development of the deflection system	38.
3.2.	Design procedure for a deflection system	41.
3.3.	Theoretical aspects of the deflection system	48.
3.4.	A program for a digital computer	62.
3.5.	Results of measurements and computations	72.

CHAPTER 4 - THE COLLIMATOR AND REVERSING LENS.

4.1. Requirements of a collimator 90.

4.2. Theory and design of the collimator 91.

4.3. Practical work on the collimator 95.

4.4. The reversing lens 105.

CHAPTER 5 - THE SCANNING ARRAY.

5.1. Introduction 113.

5.2. A digital computer program for the scanning array 115.

5.3. Results of computations for the scanning array 125.

5.4. The scanning action 133.

5.5. The screen region 148.

CHAPTER 6 - CONCLUSIONS. 160.

Appendix - Paraxial ray and c-error equations 164.

References 169.

ACKNOWLEDGMENTS.

The writer wishes to acknowledge with thanks the help he has received from a large number of sources, far too many to mention individually. Particular thanks are due to his supervisor, Professor D. Gabor, F.R.S., who invented the flat tube and has been an unfailing source of advice.

Thanks are due, as well, to the National Research Development Corporation, who hold the patent rights, and to Professor Sir Willis Jackson, F.R.S. for making available the facilities of the workshops in the Electrical Engineering Department. Among the many who have made apparatus for the project, Mr. P. Robinson, who has spent a considerable proportion of his time on the construction of experimental models, and Mr. M.J. Albert, who made the printed circuits, deserve special thanks.

The writer is deeply in debt to those who have worked on the flat tube before; their Theses have been consulted frequently. Acknowledgment must be made to Dr. P.R. Stuart and Mrs. G. Whittington, formerly Miss J.E. Smith, for permission to include their drawings in this thesis. Thanks are due to the other members of the Applied Electron Physics Section for many useful discussions, and especially to Mrs. John E. Talbot for typing this thesis.

CHAPTER 1. INTRODUCTION

1.1. General.

The Gabor-N.R.D.C. flat television tube was invented in 1952[1]; since then the development of the tube has been carried out in the Electrical Engineering Department of Imperial College by a number of workers[2,3,4,5,6]. Inevitably the resources available have been limited, although some assistance has been received from a number of industrial organisations. Thus it has been impossible to produce a complete sealed off tube of the standard required to display a television picture. However, the principles of operation of the tube were demonstrated in 1958 using a continuously pumped model.[7]

The writer has been concerned with the electron-optical problems of an entirely electrostatic form of the tube.[8] To solve these problems it has been necessary to make use of an electrolytic tank and a digital computer, but most of the work has been carried out using a demountable vacuum system and electrode structures which could be easily modified.

1.2. A Description of the Flat Tube

The latest proposed form of the Flat Tube is illustrated in Fig. 1.1. The envelope, which may be made from glass or less conventional materials, has the shape of a shallow box, about thirteen inches high, thirteen inches wide and $3\frac{1}{2}$ inches deep,

Third angle projection

HALF FULL SIZE

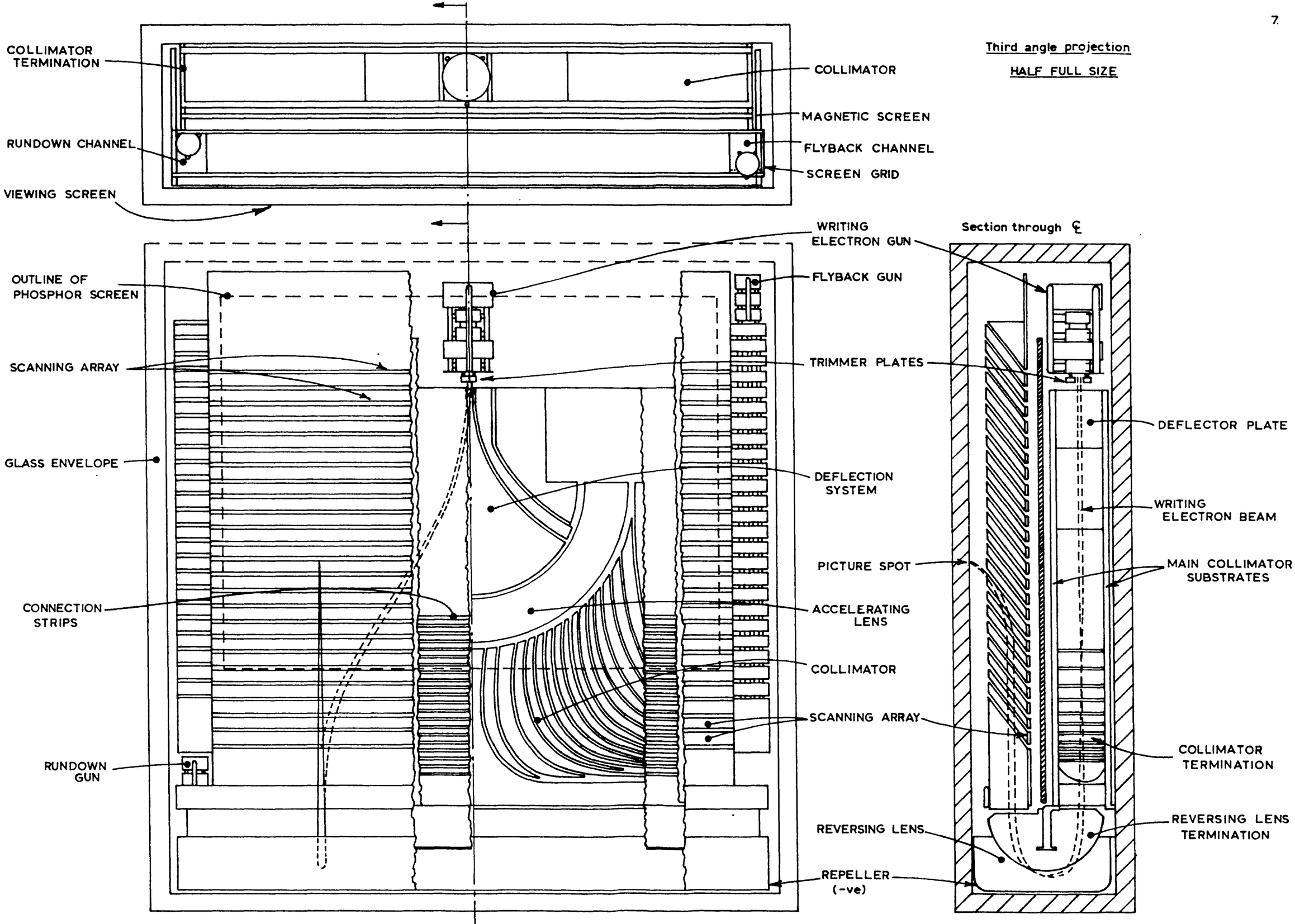


Fig. 1·1 THE FLAT TELEVISION TUBE (1965)

for a tube with a screen diagonal of 12 inches. For most of its height, the tube is divided in two by a magnetic screen, which runs parallel to the viewing screen.

The main electron gun emits a beam of electrons vertically downwards from the top of the rear half of the tube. The final anode of the gun is at one quarter of the viewing screen potential, or 'ultor potential', with respect to the cathode. Slightly modified versions of commercial electron guns are suitable for black and white displays.

After passing between a pair of electrostatic trimmer plates, which deflect it in the plane perpendicular to the screen, the beam enters the electrostatic deflection system which provides the line scan (Fig. 1.2). This deflects the beam through the unusually large angle of $\pm 60^{\circ}$, in the plane parallel to the screen. The upper half of this component is essentially a conventional parallel plate deflection system, but, in the lower half, the deflector plates are curved away from the axis and two central plates are fitted between them. The central plates lie on either side of the beam, in planes which are parallel to the screen, and they are maintained at the mean potential of the deflector plates. Thus the field is concentrated near the deflector plates in the lower part of the system. If the beam is strongly deflected in the upper part of the system, so that it passes close to the deflector plates, it

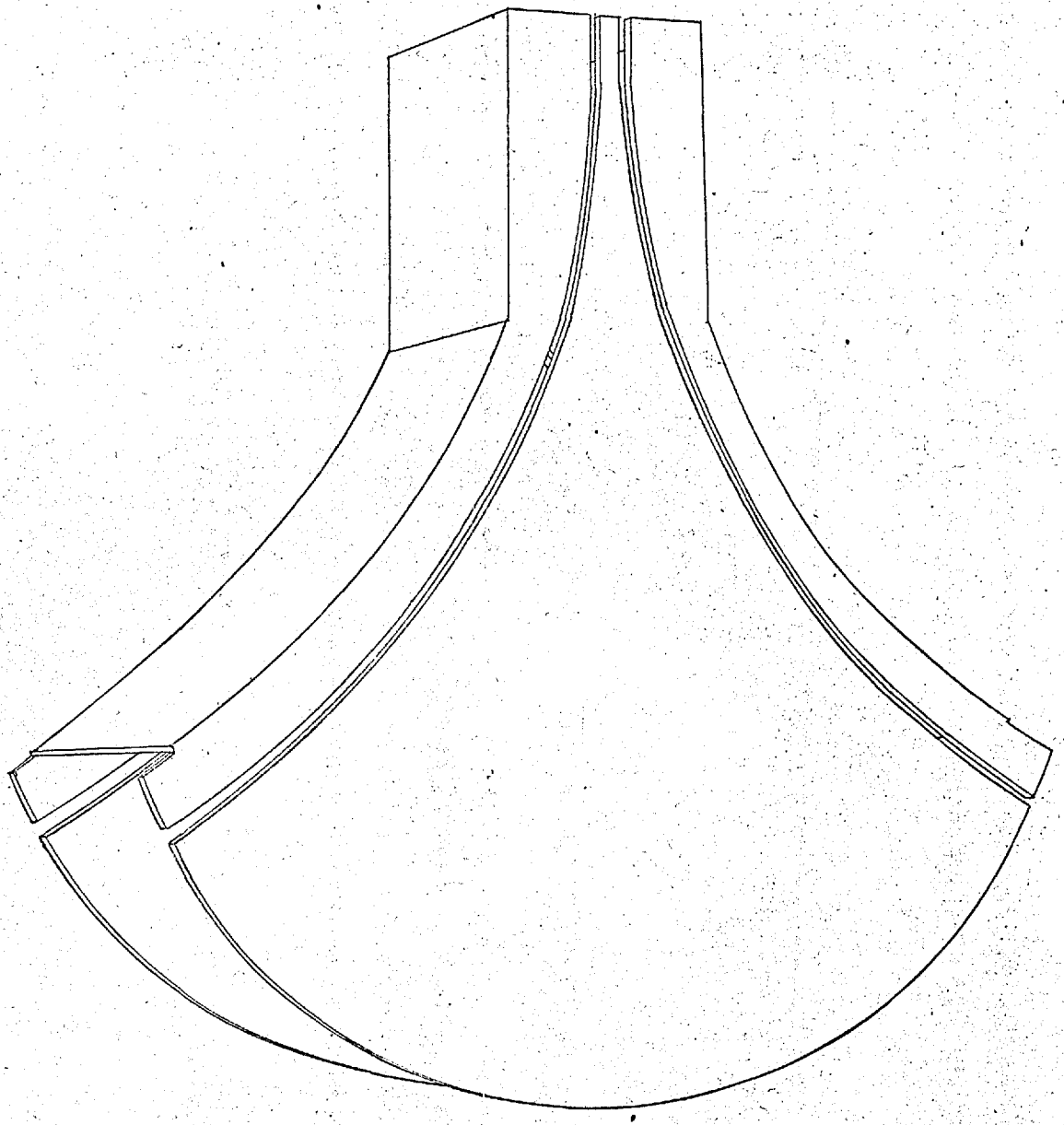


Fig. 1.2, Electrostatic Deflection System.

continues to be strongly deflected in the lower part. Furthermore, the deflection-focusing from the two parts is of opposite sign and tends to cancel.

When the electrons leave the deflection system, they are accelerated; the intermediate plates of the accelerating lens can be used as a further pair of trimmer plates, compensating for errors in alignment. After being accelerated, the electrons enter the collimator, which is a large, two-dimensional, plane electrostatic lens. The potential is most positive near the axis and in the lower part of the lens; it is nearest to cathode potential in the upper corners of the lens, away from the axis. The effect of the resulting field is to bend the beam downwards, so that it leaves the collimator parallel to the vertical axis, but displaced horizontally in the plane parallel to the screen. The field for the collimator and accelerating lens is produced by a number of electrodes at the bounding surfaces. These electrodes are made using evaporation or printed circuit techniques with insulating substrates; the central electrodes of the deflection system are also on these substrates.

The beam now enters the reversing lens and is deflected away from a trough-shaped electrode in the bottom of the tube, which is at cathode potential and is known as the repeller. The beam swings through 180° into the front half of the tube, so that it travels vertically upwards on leaving the lens.

In the front half of the tube, the beam passes between the viewing screen and an array of horizontal strips which run parallel to the screen and form the scanning array. As the upper strips are at, or near, cathode potential and the lower strips and the screen are at ultor potential, the beam is undeflected until it reaches the transition of potential, but at the level of this transition, the field bends the beam over towards the screen and also focusses it in the vertical plane. The potentials of the strips of the scanning array are controlled by two scanning guns which are mounted on either side of the screen. The ends of the strips are bent round to form two channels which surround the beams from the scanning guns; the loops which form the channels are staggered in such a way that the strips on which the scanning beams land are the ones where the potential transition occurs (Fig. 1.3). In one channel the secondary emission is suppressed and the electrons of the scanning beam charge each strip negatively in turn, but, in the other channel, the strips are coated with a good secondary emitter and a screen grid at ultor potential is provided, so the strips are charged positively when struck by the electrons of the scanning beam. Hence the transition can be moved down as the frame scan progresses and up during the flyback period.

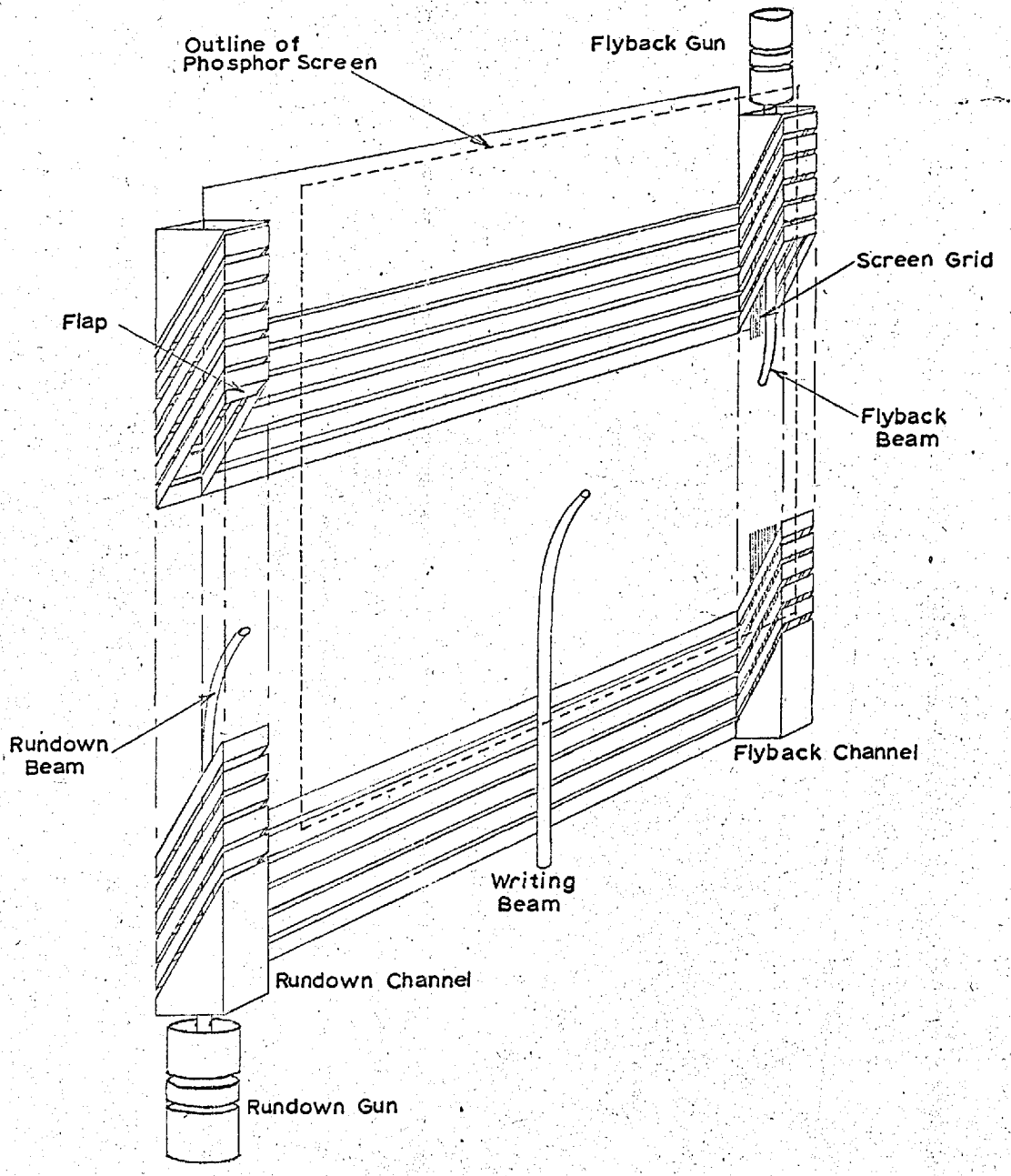


Fig. 1.3, Scanning Array.

1.3. Application of the Flat Tube to Colour Television

The focusing action of the field of the scanning array, makes the flat tube particularly suitable for colour television. It could either be used as a three-beam shadowmask tube or as a single gun sequential scanning tube.

If the tube were to be used with a shadowmask, the electron gun would have three separate cathodes, mounted in a line perpendicular to the screen; all the other electrodes would be common to the three beams. Such a gun was developed by Stuart[2] for the earlier version of the tube. The three beams would pass through the deflection system, accelerating lens and collimator together and would leave the reversing lens side by side. On being bent over onto the screen, the beams would land together, but at different angles of incidence (Fig. 1.4). A shadow mask, consisting of a large number of horizontal strips, would be used to select the correct electron beam for each colour of phosphor; this would be laid in horizontal strips. The difference between the angles of incidence of the three beams would be greater than for a conventional shadowmask tube, so the problems of alignment of the shadowmask in manufacture would be reduced. This method of colour selection is described in detail in the paper by Gabor, Stuart and Kalman[7].

In a single-gun "indexing" tube, where one beam lands on phosphors of different colours in turn, the spot must be very small, so sophisticated electron guns and deflection systems are

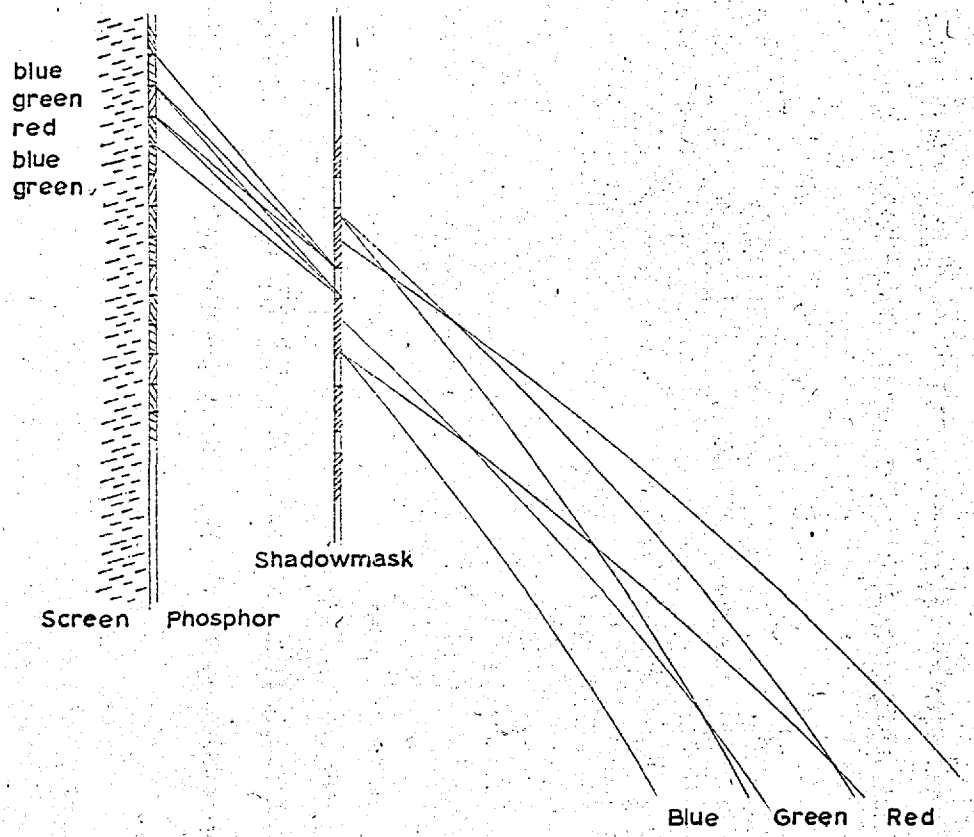


Fig. 1.4, Shadowmask Method of Colour Selection.

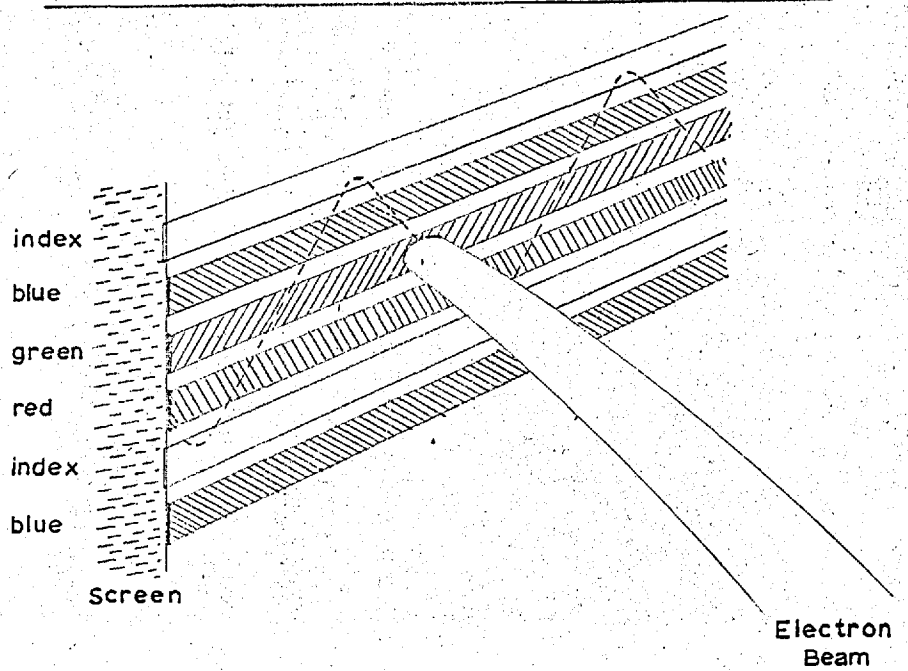


Fig. 1.5, Colour Selection for Single Gun Indexing Tube.

normally required. However, it may well be possible to obtain a spot which is small enough in the vertical direction, using the focusing field of the scanning array in the flat tube with an ordinary electron gun. The spot would be of normal size in the horizontal direction, but this would not be significant as the phosphors would again be laid in horizontal strips. The spot must be made to oscillate vertically, in order to strike the strips of different colours; immediately after striking one of the three colour strips, an index signal would be initiated (Fig. 1.5). The index signal is required, because it would be impossible to scan sufficiently accurately to ensure that the beam would land on phosphor of the right colour, without some form of feedback. A number of methods of producing the index signal have been proposed for conventional single gun tubes, but a particularly suitable one is an adaptation of a photo-electric technique[9]. Although, in the flat tube, the coloured phosphors would be laid in the normal way and would not be in optical contact with the glass, the index strips would consist of phosphor evaporated on to the glass. The index phosphor would be in optical contact with the glass, and every time electrons struck an index strip the resulting pulse of light would be detected by a photo-multiplier at one edge of the glass plate forming the front of the tube. Hardly any light from the picture phosphors would be detected by the photo-multiplier, because they would not be in optical

contact with the glass. Indexing light losses would not be very great owing to the high efficiency of total internal reflection, which would contain the light pulses.

1.4. Advantages of the Flat Tube.

In recent years, domestic television sets have been made with shorter and shorter tubes, while cabinet designers have adopted many tricks to make the sets look slimmer. Furthermore, due to improvements in circuitry and the use of transistors, the proportion of the volume of a set which is occupied by the tube is increasing. Until now the trend has been to use larger deflection angles in tubes of conventional shape, although this introduces distortion and increases the power which is needed for scanning. In portable sets, it has been necessary to use low voltage tubes and to restrict the deflection angle in order to reduce the scanning power, even though this involves an increase in the volume of the set. In fact the demand for a true flat television tube becomes greater every year.

In addition to the obvious advantages in the design of cabinets, the small physical size of the flat tube will reduce the problems of transportation and storage and permit more compact processing plant than is necessary for a conventional tube. The use of an electrostatic line deflection system greatly reduces the scanning power and will probably reduce the size, weight and cost of the associated circuitry. This makes the tube particularly

suitable for portable sets. However, on account of the complexity of the flat tube, it is unlikely that it will ever be as cheap as a conventional monochrome tube, although a colour version of the tube might well be competitive with other colour tubes.

1.5. Previous Work on the Flat Tube.

In 1953, work started on the electron optical problems of the flat tube[2]; the technological problems, including the glass envelope, were considered from 1953[3]. In 1958, although it was not possible to show a picture, the tube was described in a lecture to the Institution of Electrical Engineers[7]. At this time, a great effort was made to try to develop the tube to a stage where it would have commercial prospects, so all the components were tested, though a sealed off model of the tube could not be built.

Although the basic layout of the tube was similar to the present version, there were considerable differences in the components (Fig. 1.6). The envelope was to be made of two prestressed glass shells; a prestressing process was developed especially for this purpose. The electron gun, with its final anode at ultor potential, was mounted in the same position as in the present version, so was the line deflection system, but two pairs of trimmer plates were fitted between the deflection system and the reversing lens. The line deflection system gave a maximum deflection angle of $\pm$ 16° and was shaped to minimise deflection

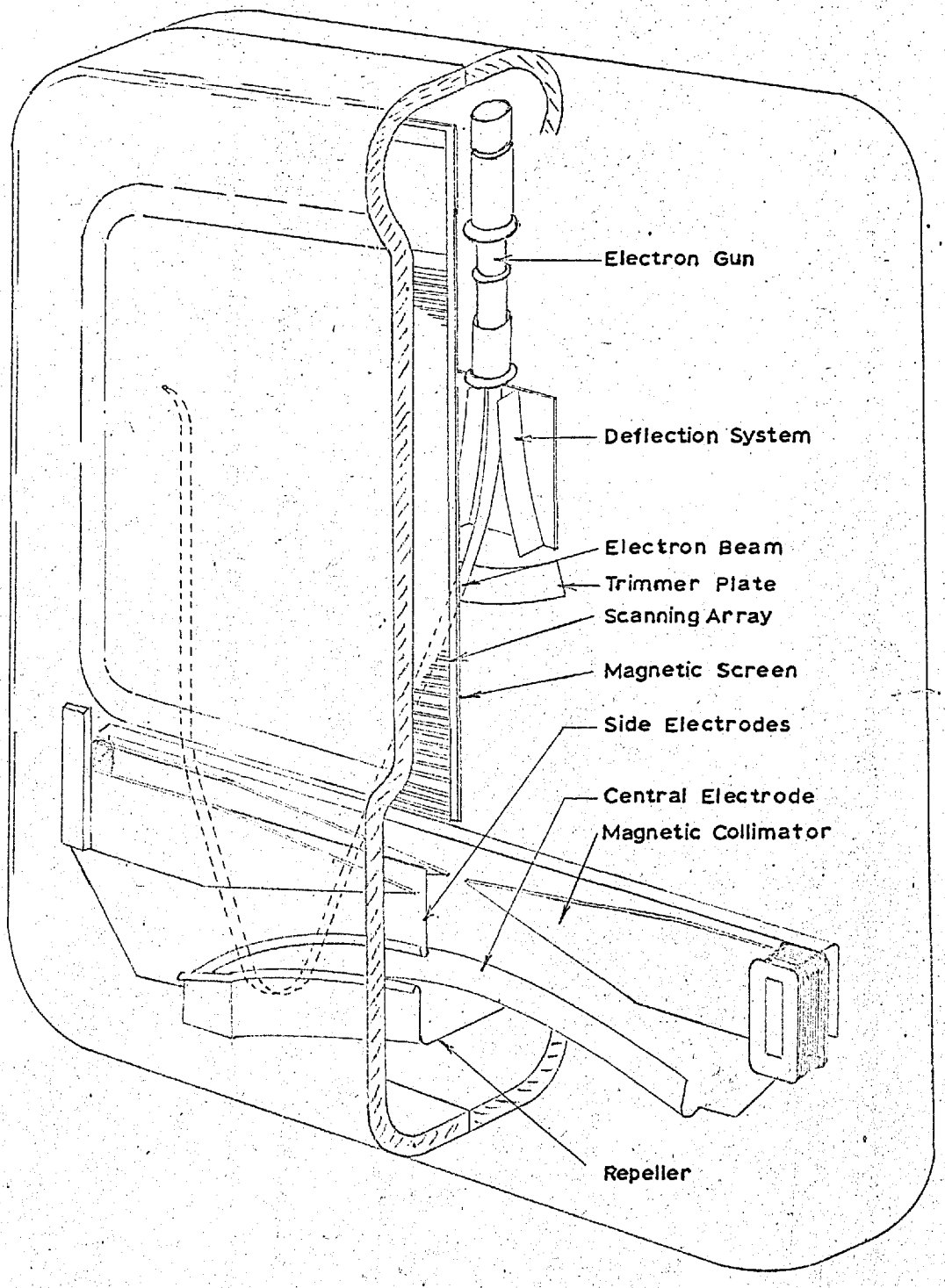


Fig. 1.6, The Flat Tube in 1958.

defocussing. The beam then went to the reversing lens, which was curved, and, in addition to bending the beam into the front half of the tube, increased the deflection angle to $\pm$ 60°; it also compensated for the aberrations from the other components. The beam passed through a magnetic collimator immediately below the screen region and was bent upwards. The screen region was essentially similar to the present arrangement, but at extreme horizontal deflection angles, the main beam passed along the channels of the scanning array and performed the function of the beams from the scanning guns.

After the lecture to the Institution of Electrical Engineers, it became clear that the flat tube was too complicated to be a commercial proposition; in particular, the magnetic collimator required a stabilised magnetizing d.c. supply of several hundred milliamps, which had to be at the screen potential, and the E.H.T. had to be stabilised as well. Furthermore, there were certain inherent aberrations in the magnetic collimator, so it was decided that it should be replaced by an electrostatic one. Development was hindered by a requirement that the electrostatic collimator should be as short as the magnetic one, though it soon became clear that this was impossible and that a large number of electrodes would be required. Work was then concentrated on a combined reversing lens and collimator, using printed circuit techniques to provide suitable electrodes, as described by Zollman[4] and Upadhyay[5].

Although a fully satisfactory reversor-collimator was never built, the theory which had been developed for its design and the practical insight into the problems were of great value later.

In 1960, the flat tube was redesigned in its present form. The main problems were the design of a suitable wide angle deflection system and a collimator. The theory, which had originally been developed for the reversing lens and was extended for the earlier electrostatic collimator, was modified and used by Smith[6] to calculate the shape of the electrodes. The deflection system could not be designed using the same approach, so no attempt was made to design it theoretically. At this stage, in October 1961, the writer started work, using an electrolytic tank to confirm the calculations on the collimator and to develop a wide angle deflection system.

1.6. Other Flat Television Tubes

A flat television tube is a most attractive proposition and a number of other designs have been put forward. Notable among these is the "Thin Cathode-Ray Tube" proposed by Aiken[10,11]. In this tube, the electron gun is in one corner and emits a horizontal beam parallel to the screen. The beam is deflected into a vertical path and then onto the screen by two travelling deflecting fields. The vertical scanning array has only seven conductors, but each is connected to a special valve which must be rated for at least 10 kilovolts. The horizontal scanning array

has ten elements, but the potential variation is only about 1 kilovolt. This is the type of flat tube which has recently been considered for very large displays, covering more than ten square feet.

Another proposal for a relatively thin tube is the "Reflected Beam Kinescope"[12]. In this tube, the electron gun is in the conventional position and a conventional deflection system is used, but the face plate, which is transparent, is at cathode potential and the screen is on a fine mesh several inches from the faceplate. The beam passes through the mesh, but is repelled by the faceplate and returns to the phosphor which is deposited on the mesh. A considerable increase in deflection is achieved, at the cost of picture brightness, because some electrons are stopped by the mesh.

Photo-luminescent devices[13] give the possibility of a completely solid state television set, but much development will be required before these can be used to produce a television picture. One difficulty which has yet to be overcome is that of scanning hundreds of lines without an excessively complicated switching network.

CHAPTER 2. APPARATUS AND EXPERIMENTAL TECHNIQUES.

2.1. Introduction

When the writer started working on the flat tube, no practical work had been done on the project for more than a year. Unfortunately, much of the apparatus which had previously been used for research on the flat tube had been damaged or lost; furthermore, it was impossible to discuss details of experiments with those who had been working on the project before. Thus a completely fresh start was made, both in experimental techniques and in the construction of the models which were tested under vacuum (printed circuit had, however, been used previously in vacuum models). Some of the electrical equipment, such as resistance chains, could be used after reconditioning and modification, although most of it was later replaced.

There has, in fact, been a considerable difference between the apparatus which the writer used and that which has been described before, notably by Stuart[2]. For this reason, the experimental techniques and apparatus which the writer has employed are described in this chapter. Obviously, many improvements and modifications have been made in the course of the project, so only the latest designs and methods are described.

2.2. The Demountable Vacuum Tanks.

The demountable vacuum tanks which were used for most of the experiments had been used before for work on the flat tube.

The internal dimensions are 18" by 18" and they are about 7" deep. The lower parts are made of mild steel, but the lids are of armour plate glass 3/8" thick. The glass plates are protected from scratches by sheets of perspex and are supported near the centre by rubber pads which rest on metal frames. These frames also prevent the neoprene cords, which form the vacuum seals between the glass and the flanges of the tanks, from being sucked in.

For early experiments, a tank was used which was fitted with a four inch oil diffusion pump. However, in July 1962, the Electrical Engineering Department moved to a new building, so the opportunity was taken to fit a six inch oil diffusion pump to another tank. This tank has been used for all subsequent experiments. The backing pump is a single stage rotary pump which has a speed of 150 l/min; it is fitted with a magnetic isolation and air admittance valve. The effective pumping speed for air of the diffusion pump is about 180 l/sec., but the pumping speed for vapours is much higher because a stainless steel cold trap is fitted immediately above the diffusion pump. An 11" baffle valve is fitted between the trap and the bottom of the tank, so the tank can be let up to atmospheric pressure for adjustments without emptying the liquid nitrogen from the trap or switching off the diffusion pump. A hot filament ionisation gauge is used to measure the pressure inside the tank and a Pirani gauge is used to monitor the backing pressure. The best vacuum which has so far been achieved in this tank is 10^{-6} torr.

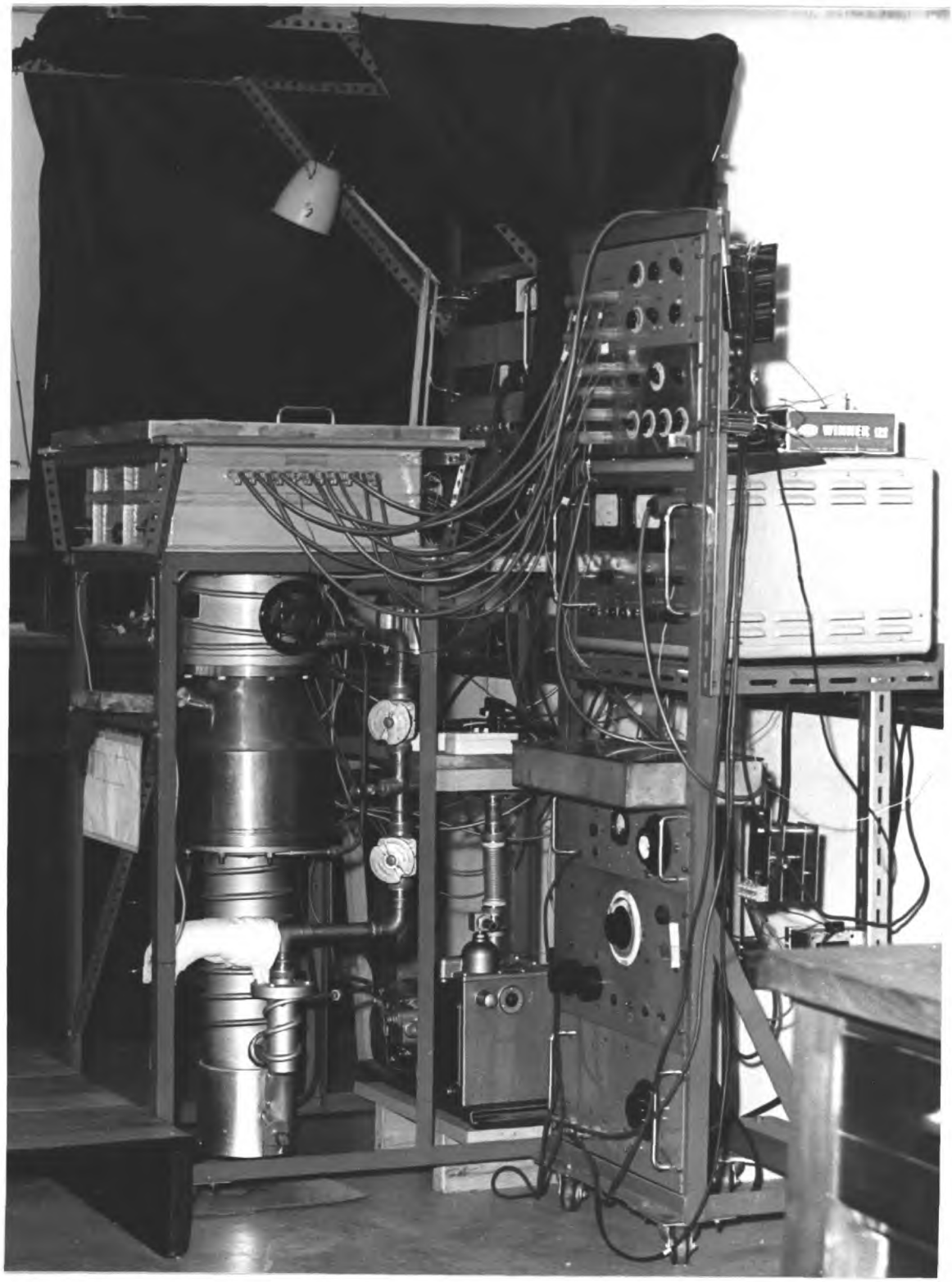


Fig. 2.1 : The Demountable Vacuum System.

Up to six steel rods can be used to transmit mechanical motion to the assembly inside the tank, although it has been found to be preferable to open the tank for adjustments rather than to build a complicated linkage. Vacuum seals for the rods are provided by neoprene O-rings. Electrical connections pass through ceramic bushes which are mounted in the sides of the tank; in addition, extra leads enter through glass pinches fitted to the bottom of the tank.

A number of materials such as perspex and phenolic laminates have been used in the vacuum, although they are definitely not vacuum materials and outgass for a long time. In order to cut down the time which was wasted while these were outgassing, a protection circuit was designed and built, so that the vacuum system could be left running overnight. Protection circuits of this design have since been fitted to most of the vacuum stands in the laboratory.

2.3. Electrical supplies.

The electrical requirements of the different vacuum models have varied considerably, so it has been necessary to make the supplies very flexible. The source of E.H.T. is a unit capable of giving 2 milliamps at 15 kilovolts, and this feeds the double potential-dividing chain shown in Fig. 2.2; each half of the main chain has a resistance of 10 megohms and the two halves are connected together at both ends and four intermediate points. Potentiometers which are incorporated in one half supply the

writing electron gun and the deflector plates; the other half, which consists of 200, 50 kilohm resistors, provides tapping-off points at intervals of 0.5% of the total E.H.T. voltage. Where finer division is required, for example supplies for the trimmer plates, a 1 megohm potentiometer is connected across one of the 50 kilohm resistors. As the collimator requires some 20 different potentials and there is a limit to the number of leads which can pass into the tank, 200 megohm chains have been incorporated in each collimator to supply these potentials and connections have been taken out from these chains to the main chain at five points; rotary switches permit adjustment of the tapping points on the main chain. In general, the screen has been near earth potential and the cathode has been at E.H.T. negative, but, when the scanning array has been used, the screen has been at E.H.T. positive and the cathode has been near earth potential.

The deflector plates are supplied from a double potentiometer, but a fairly complicated switching system which includes a change-over switch is required because this potentiometer will only cover one quarter of the necessary voltage range. A source of 50 c/s a.c., which can be applied to the deflector plates to simulate a line scan, is available, and, in addition, a circuit has been built which gives a sawtooth waveform of 800 volts amplitude. The anodes of the scanning guns are supplied from the main chain, but the grids are supplied from a battery via

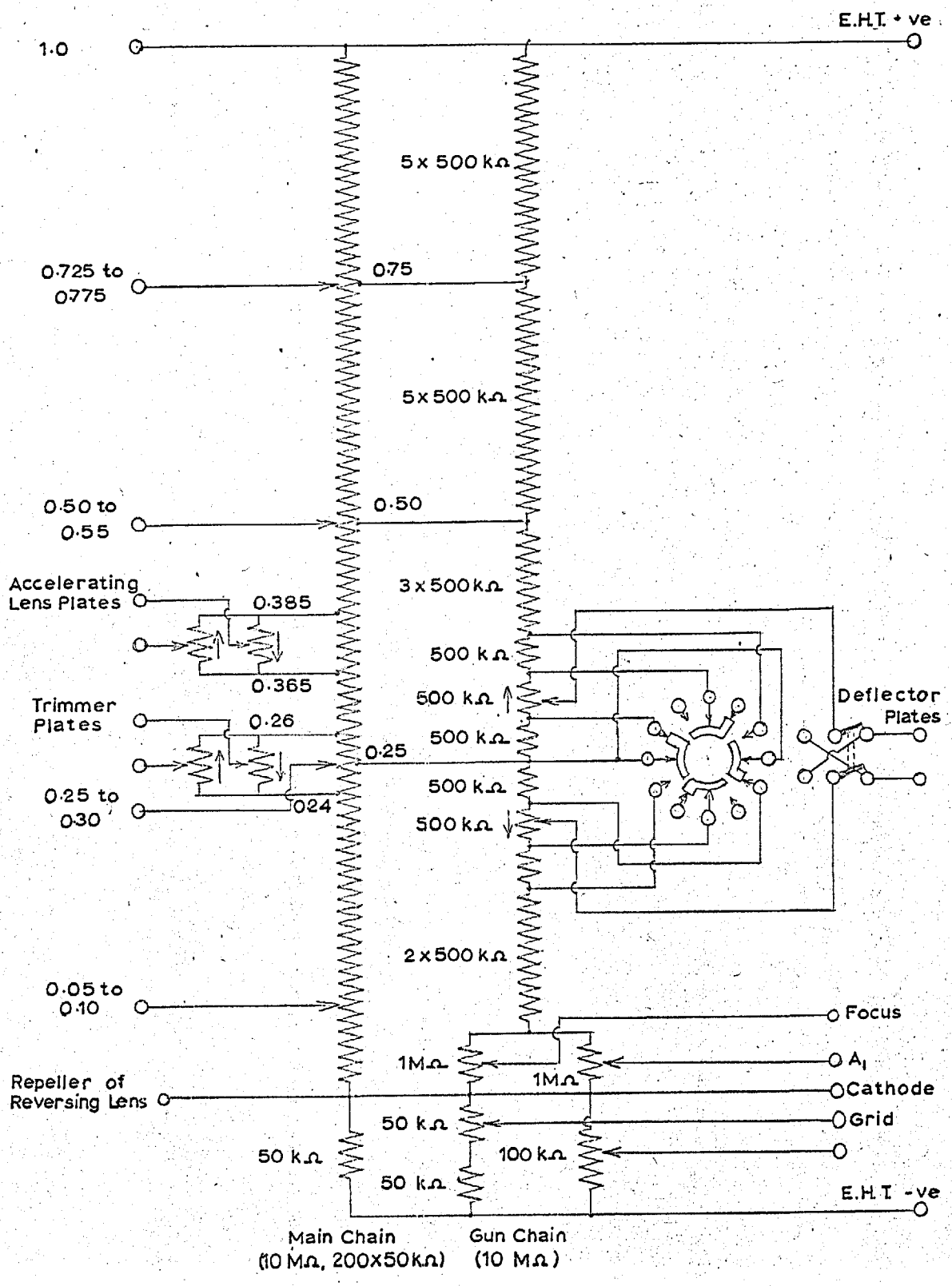


Fig. 2.2, E.H.T. Supplies.

a change-over switch; one gun is cut-off when the other is giving a beam. Alternatively, the grids can be fed from two pulse generators so that dynamic measurements can be made.

The heating current for the tungsten hairpin which forms the cathode of the writing electron gun is rectified d.c. and is isolated for 10 kilovolts; the voltage is controlled by a 'Variac' variable ratio auto-transformer. The supply for the cathodes of the scanning guns which is not rectified, is also controlled by a 'Variac', but it is only isolated for 1.5 kilovolts.

2.4. Construction of the Vacuum Models.

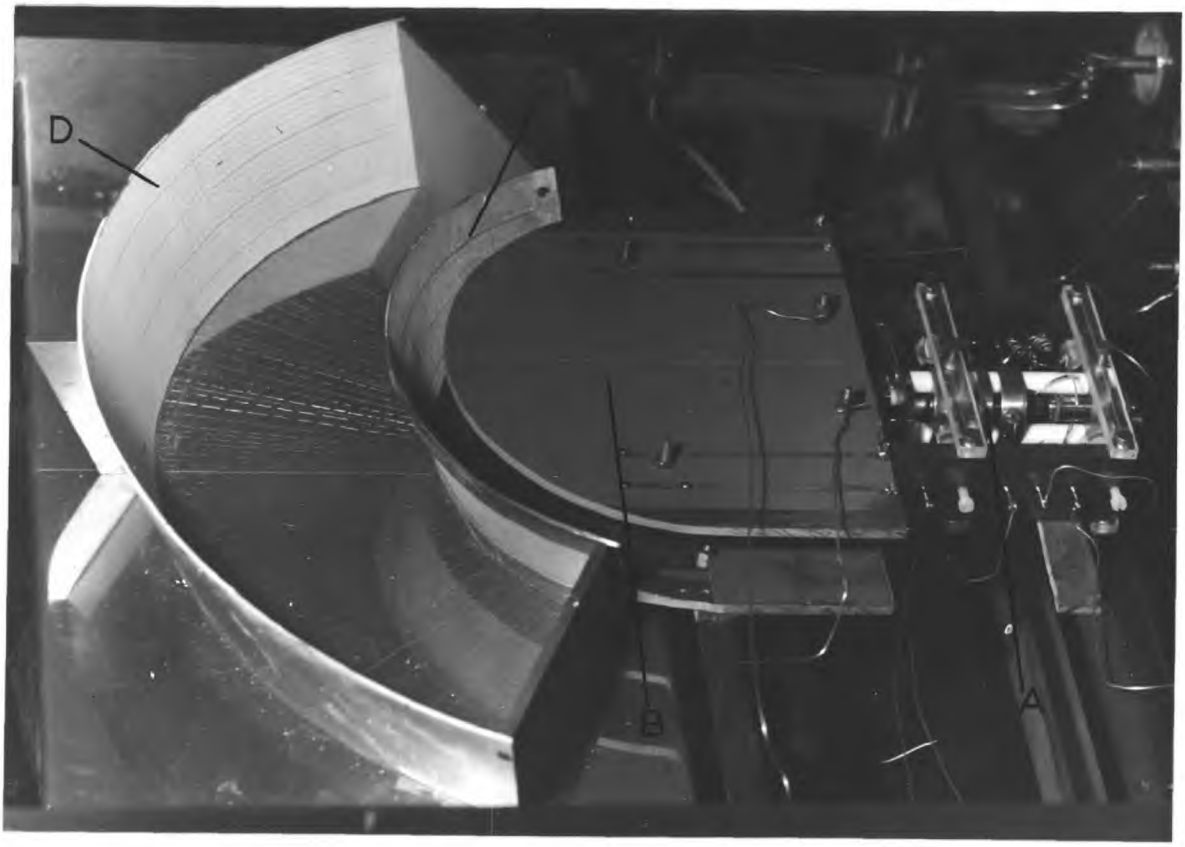
As the vacuum tank is only 7" deep, the vacuum models are placed so that the viewing screen, if it were fitted, would be immediately below the lid. A brass frame, with two threaded lead screws, rests on the bottom of the tank and the models are mounted on this.

One of the limitations of a demountable vacuum system is the poisoning of oxide cathodes which occurs when the system is let up to atmospheric pressure. For this reason, tungsten hairpins have been used as the cathodes of the electron guns. Commercial guns, suitably modified, have been fitted, but they tend to become distorted in the course of time; this is unimportant in the scanning guns, where the size of the beam is not critical, but a more robust version of the commercial guns had to be made for the writing gun. This gun is constructed so that modifications to the electrode spacing can easily be made and the position of the

hairpin can be adjusted. Adjustments are provided for the horizontal and vertical position of the writing gun, but only for the vertical positions of the scanning guns. The writing gun has been aligned with the aid of a jig, but the scanning guns have been aligned by trial and error; however, the height has normally been checked with a cathetometer before the array was put into the tank.

The deflector plates were machined from brass, so that they cannot be distorted; the mounting for the writing gun is screwed to them. The other electrodes of the deflection system are incorporated in the printed circuits which make up the collimator. When the deflection system was being tested by itself, smaller printed circuits were used, which have only the electrodes of the deflection system and accelerating lens (Fig. 2.3).

The collimator is formed entirely from printed circuits; the two main boards are parallel to the viewing screen, but there are terminating strips between them on three sides; these prevent distortion due to the accumulation of electrostatic charge on the insulating surfaces which would otherwise be exposed. The printed circuits are reinforced by Perspex sheets, which serve the additional function of protecting the connection strips on the back of the main boards. Connections were made between the electrodes and these connection strips with copper rivets; the resistors which form the 200 megohm collimator chain are fitted at the ends of the strips (Fig. 2.4). When the design of the collimator had been finalised, a 'Mumetal' magnetic screen was



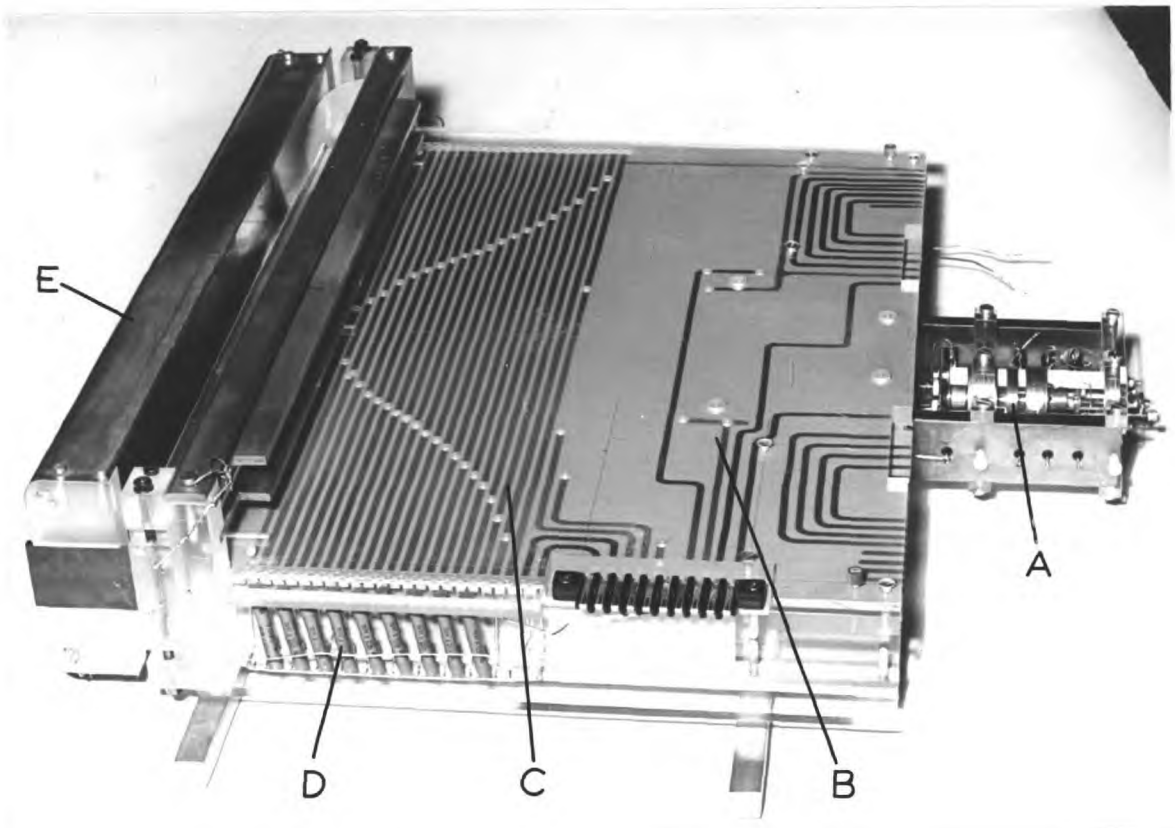
A. Electron gun

B. Deflection system

C. Phosphor coated gauze

D. Phosphor coated screen

Fig. 2.3 : Deflection System No.11 in the Vacuum Tank.



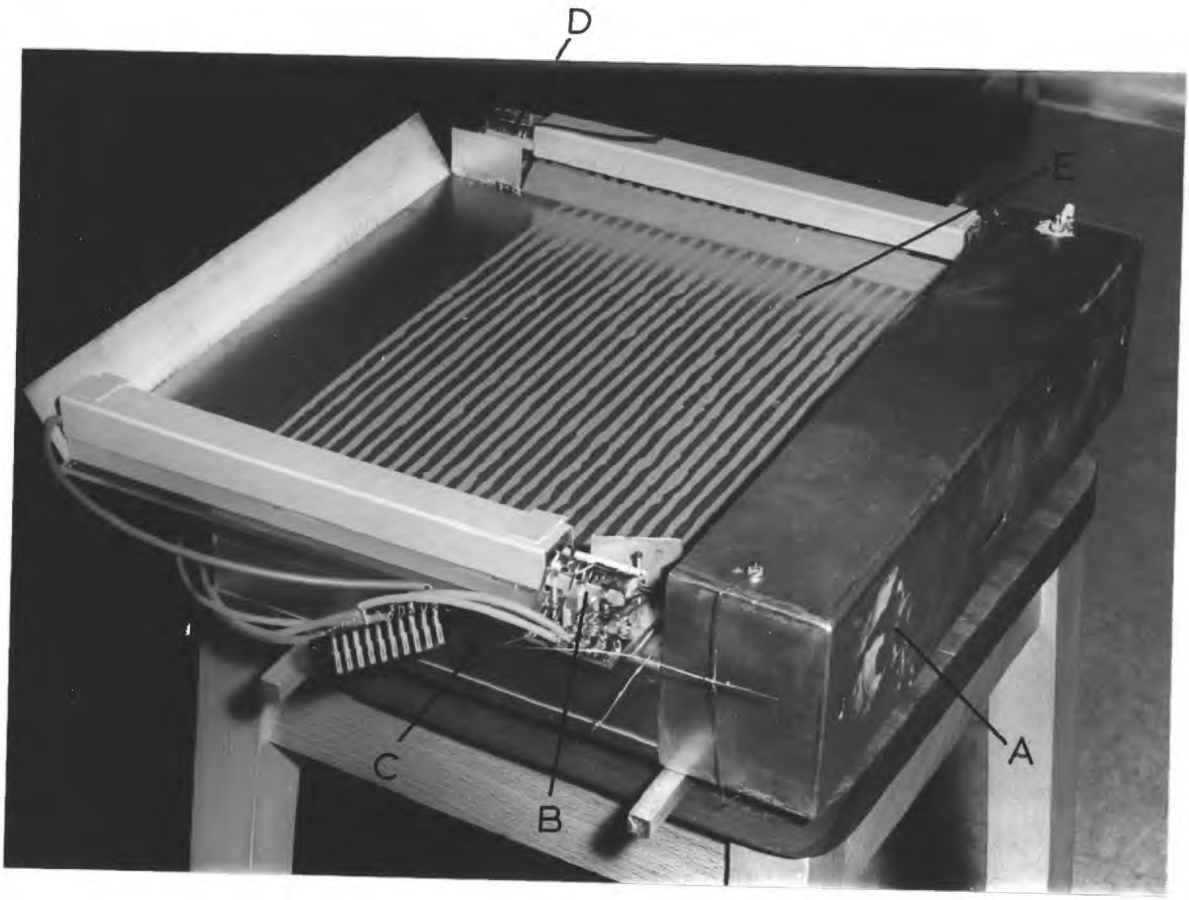
A. Electron gun
B. Printed circuit board
C. Connection strips
D. Resistors forming collimator chain
E. Repeller

Fig. 2.4 : Vacuum Model of Deflection System and Collimator with Reversing Lens.

obtained which fitted around the outside of the collimator; this was found to be necessary, even though a coil had been wound round the outside of the vacuum tank in order to neutralise the vertical component of the earth's magnetic field. The electron trajectories are particularly susceptible to stray magnetic fields, because it is normally impossible to raise the E.H.T. voltage above 5 kilovolts without flashover; to make matters worse, the magnetic field inside the carbon-steel vacuum tank is very irregular.

The reversing lens is mounted on the collimator, but it is possible to adjust the position of the repeller relative to the rest of the lens. In an earlier model, this could be done from outside the tank by means of the lead screws, but, when a magnetic screen was fitted, this became impossible. Like the electrodes in the collimator, the electrodes in the reversing lens have been gold-plated to eliminate the formation of insulating layers; these could cause distortion by attracting electrostatic charges.

The scanning array was made from a printed circuit with a sheet of Perspex as a base. Grooves were milled in the back of the printed circuit board, then it was bent to form the scanning channels. The insulating surfaces between the strips were painted with Green Chromic Oxide, which forms a slightly conducting layer preventing charging up and reducing the tendency to flashover. Inside the rundown channel, an angled copper strip was soldered to each strip of the array where the electrons land. The projecting parts of these strips prevent secondary



A. Magnetic screen for Reversing lens
B. Rundown electron gun
C. Magnetic screen for collimator
D. Flyback electron gun
E. Scanning Array

Fig. 2.5 : Complete Vacuum Model with Viewing Screen Removed.

electrons from cascading down the array. In the flyback channel the electrons land on plates of Beryllium Nickel which have been oxidised and soldered onto the strips of the array; this surface is a good secondary emitter of electrons. The secondary electrons are attracted to a grid several millimeters away from the Beryllium Nickel which is maintained at ultor potential. Fluorescent screens have been fitted at the opposite ends of the scanning channels to the electron guns; one has also been fitted at the opposite end of the scanning array to the reversing lens. These screens have been used for alignment of the beams. The scanning guns are mounted at opposite corners of the array and the strips of the array are staggered near the edges in order to save space. A transparent fluorescent screen which occupies the place of the viewing screen has been used to observe the position of the main beam when the array was in operation.

Recently another scanning array has been constructed in which the use of a printed circuit was avoided by making each strip separately, a laborious process.

2.5. Measurement Techniques.

In order to measure the convergence of the main beam, an aperture in the form of a cross was fitted in the final anode of the electron gun. The convergence of the beam as it left the gun was found by connecting all the electrodes, other than those in the gun, to the final anode and observing the diameter on a fluorescent screen. Two fluorescent screens, one of which was

actually a gauze coated with phosphor, were used to measure the position and convergence of the beam, after it had passed through a component. Both screen and gauze were marked every 2 mm in the vertical plane and every 5 mm. in the horizontal plane. By observing the position and diameter of the beam on both the screen and the gauze it was possible to deduce the diameter in a reference plane, the convergence angle and the angle of the beam with the axis. It was necessary to measure the diameter of the beam, both in the horizontal and in the vertical direction, because of the astigmatism of the components. When taking measurements on the collimator, it was possible to see the shadow of the gauze on the screen; knowing the mesh size of the gauze, when the number of shadows in a given distance on the screen had been counted, the convergence angle of the beam could be calculated more accurately. It was not possible to use this technique for the reversing lens because aberrations prevented the gauze from casting a clear shadow; nor was it possible to use it for the deflection system because the gauze was curved so the apparent mesh size was uneven. It was essential to use curved screens for measurements on the deflection system because of the large deflection angle.

It was not easy to find a good method of measuring the performance of the scanning array. Initially measurements were made by timeing the rundown and flyback times with a stop-watch for low scanning beam currents. When larger beam currents were used, pulse generators were connected to the grids of the scanning

guns and the distance travelled by the writing spot was measured. The linearity of the scan was checked by applying a horizontal deflection voltage in synchronism with the pulses to the grids. The potential on individual strips when the rundown was completed was found by connecting a strip to one of a pair of deflector plates; the other plate was connected to the main chain. The deflector plates, which were fitted immediately after the reversing lens, deflected the main beam in the plane of the screen. To measure the potential on the strip, the tapping point on the main chain was adjusted until the main beam was undeflected; the potentials on the two plates were then equal. This method of measurement caused the minimum amount of disturbance to the array, but none of these methods was entirely satisfactory.

Recently an oscilloscope with a very sensitive differential amplifier has become available, and this has been used to examine the scanning action by observing the potential variation of one or more strips. In order to reduce the disturbance to the array, a capacitor voltage divider was used, in which the value of the high voltage capacitor was about 1 picofarad; the low voltage capacitor had a value of 0.05 microfarads. A x10 attenuating probe, with an input resistance of 10 megohms, was used to measure the voltage across this capacitor. The potential divider was calibrated by applying a 100 volt square wave to the strip; the overall attenuation ratio of the voltage divider and

the probe was 500,000 : 1. The main difficulty of this method was poor low frequency response, which could only be improved by increasing the attenuation ratio; hence the requirement for an oscilloscope with high sensitivity. Measurements were made by triggering the oscilloscope from the grid of one of the scanning guns and taking photographs of the trace.

The size of the writing spot with a sharp voltage transition was investigated using two plates to simulate the scanning array.

2.6. The Electrolytic Tank.

An electrolytic tank was used to plot the equipotentials in the earliest deflection systems and collimator. The tank which was used has been described by Stuart[2] and was virtually unchanged. The models of the deflection system were made of copper and copper-laminate and they were three times full size. They were, in fact, half models, as the water plane was in the plane of symmetry parallel to the viewing screen. The collimator, which was also a half model, was twice full size and was made of a printed circuit with suitable terminating strips. The current for all the electrodes was supplied from a potentiometer wire, but great care was required when setting up the potentials because the electrodes drew a considerable current. The potential of each electrode was found by placing the probe very close to it; the tapping point on the potentiometer was then adjusted until the probe was at the correct potential. Electron trajectories were plotted using the circle method and the trajectory tracing trolley, as described by Stuart.

CHAPTER 3. DEFLECTION SYSTEMS.

3.1. The Development of the Deflection System

One of the writer's first tasks, when he started working on the new version of the flat tube, was to establish whether it would be possible to make a suitable wide angle deflection system. In the earlier version of the tube, the deflection system had a maximum deflection angle of $\pm 16^{\circ}$, but even with this angle deflection defocusing was a problem. The difficulty had been overcome by using the deflection system shown in Fig. 3.1 where the central plates were maintained at the mean potential of the deflection system. This system reduced the defocusing in the direction of deflection, but only by introducing defocusing in the normal direction; fortunately it was possible to compensate defocusing in this direction with the reversing lens.

In the new version of the flat tube, the requirements for a deflection system are:-

(i) A maximum deflection angle of at least $\pm 55^{\circ}$;

(ii) High deflection sensitivity;

(iii) The electrode configuration should not be complicated;

(iv) The electrodes should only be at the potentials of the deflector plates or at the mean potential;

(v) Minimum deflection defocusing.

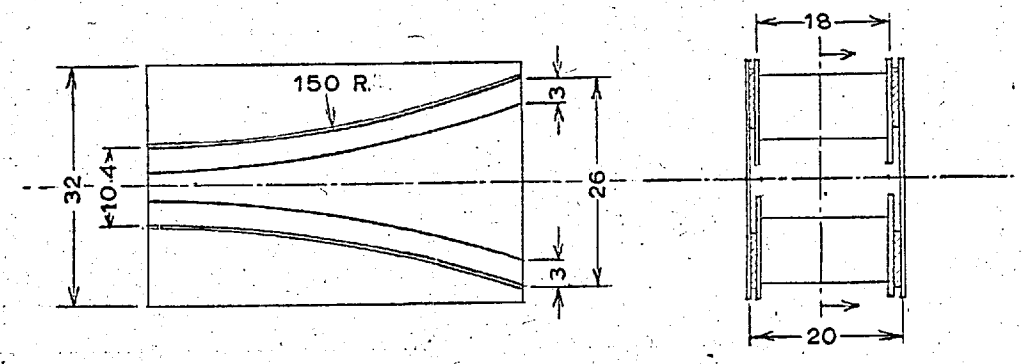


Fig. 3.1, Deflection System for Tube of 1958 (dimensions in millimeters).

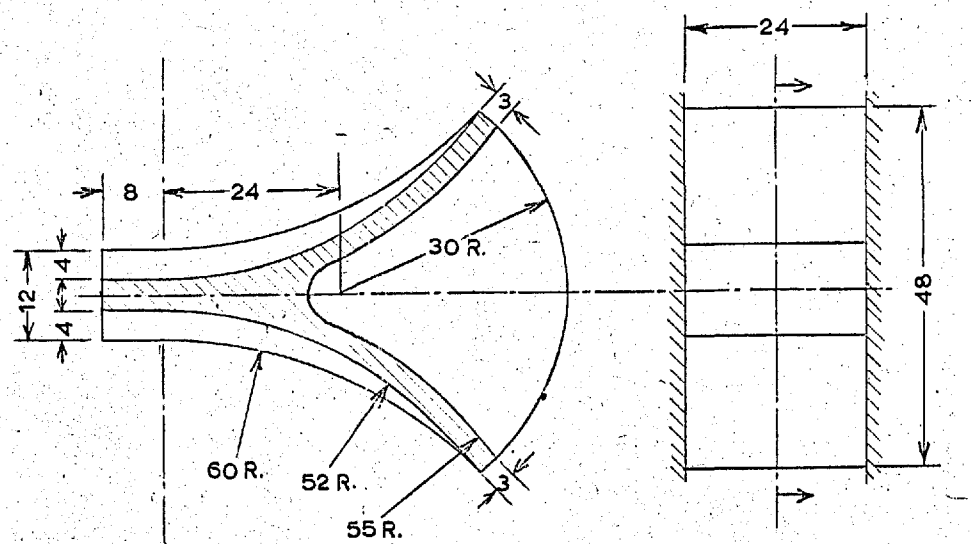


Fig. 3.2, Deflection System No. 1.

The presence of the collimator permits the deflection defocusing to be much worse than would otherwise be possible; but even so these requirements are very hard to fulfil.

In the new design of 1960, D. Gabor proposed a deflection system which was a wide angle form of the design which had been used before (Fig. 3.2). This system was tested in the electrolytic tank, although at this stage defocusing was not considered. It was found that the maximum deflection angle was only $\pm 48^{\circ}$; the next design, in which the deflector plates were curved with a smaller radius, was not much better.

The next deflection system was designed using the technique which is described in section 3.2. The deflector plates were parallel for as great a distance as possible; just before the position where the beam would strike them at maximum deflections they were bent back and were curved for the rest of their length in such a way that the beam would always be close to them, but would not quite touch them. With this design, at extreme deflections, the beam travelled in a strong deflecting field for the entire length of the system, but the electrode configuration was quite simple. The design was very promising and has been the basis of all later designs.

Many of the modifications, which were made to the design of the deflection system in order to reduce the defocusing, were unsuccessful because some other requirement was not satisfied. Eventually a design was chosen which seemed to be a good compromise. This was deflection system No. 11.

3.2. Design Procedure for a Deflection System.

This procedure relates only to the principal electron trajectories; deflection defocusing is not considered. The procedure predicts a configuration of the deflector plates, in the plane of deflection, with which good sensitivity may be achieved. The system is considered in two parts; the first region is where the deflector plates are straight and parallel, the second region is where the deflector plates are curved.

Parallel Plate Region.

This part of the system may be considered, as an approximation, to be a simple parallel plate condenser with no fringing fields (see Fig. 3.3). The plates are assumed to lie in the planes $x = d$, $x = -d$ and to be at potentials (V_o+V_d), (V_o-V_d) respectively; they extend from $z = 0$ to $z = L$ and from $y = +\infty$ to $y = -\infty$. An electron beam is assumed to enter the system along the z-axis and to be deflected through an angle θ; $\theta = \theta_1$ at the end of the region.

The equations of motion for an electron of mass m and charge e are

$$m \frac{d^2x}{dt^2} = - e \frac{V_d}{d} \qquad (3.1)$$

$$\frac{1}{2}m \left(\frac{dz}{dt}\right)^2 = - e V_o \quad . \qquad (3.2)$$

Integration of these equations and elimination of t gives the well known formula

$$x = \frac{1}{4} \frac{V_d}{V_o} \frac{z^2}{d} \quad . \tag{3.3}$$

This equation may also be expressed parametrically in terms of θ as

$$x = d \frac{V_o}{V_d} \tan^2\theta \tag{3.4}$$

$$z = 2d \frac{V_o}{V_d} \tan\theta \quad . \tag{3.5}$$

At the maximum value of V_d, the beam will graze the end of the positive plate, so here,

$$x = d - \frac{b}{\cos(\theta_1)_{max}} \tag{3.6}$$

where the diameter of the beam is $2b$.

Combining (3.4) and (3.6)

$$\left(\frac{V_d}{V_o}\right)_{max} = \frac{\sin(\theta_1)_{max} \tan(\theta_1)_{max}}{\cos(\theta_1)_{max} - \frac{b}{d}} \tag{3.7}$$

From (3.5)

$$L = 2d \frac{\cos(\theta_1)_{max} - \frac{b}{d}}{\sin(\theta_1)_{max}} \quad . \tag{3.8}$$

Thus, for given b and d, the maximum value of θ_1 determines L and the maximum value of V_d/V_o .

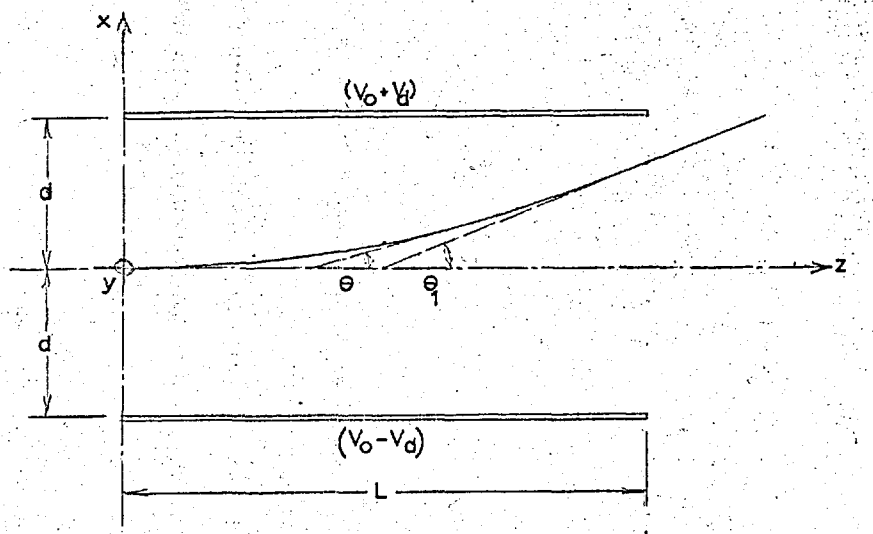


Fig. 3.3, Parallel Plate Condenser.

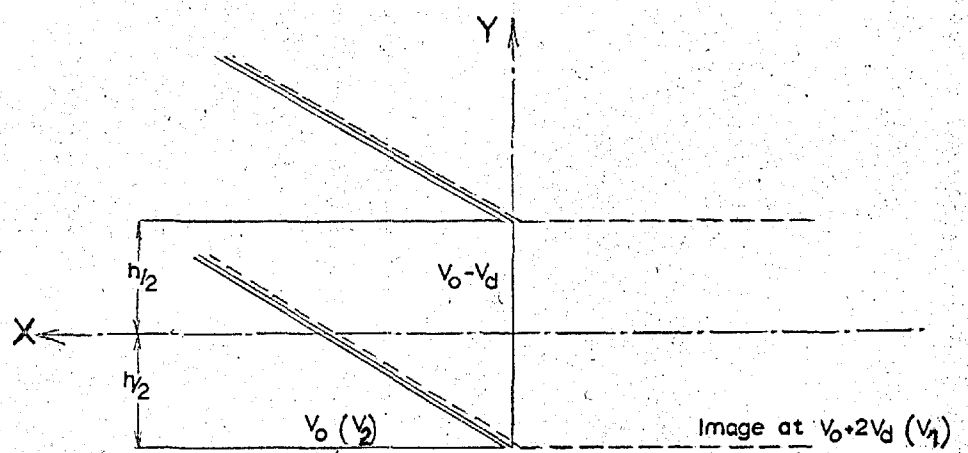


Fig. 3.4, Assumed Configuration in Curved Region.

Curved Region.

In this part of the system, close to one of the deflector plates, the field is given approximately by assuming that the deflector plate is straight and neglecting the presence of the other deflector plate (Fig. 3.4). Let X be the distance of a general point from the deflector plate under consideration; let Y be written for y. When these assumptions are made, the potential is given[14] by the equation

$$V = V_2 - (V_1-V_2)\frac{1}{\pi}\tan^{-1}\left(\frac{\cos\frac{\pi Y}{h}}{\sinh\frac{\pi X}{h}}\right) \qquad (3.9)$$

where $V_2 = V_o$ (potential of the central plates),

$V_1 = V_o + 2V_d$ (potential of the images of the central plates in the plane of the deflector plates)

and h = separation between the central plates.

This equation can be rewritten as

$$V = \frac{V_1+V_2}{2} - (V_1-V_2)\frac{1}{\pi}\tan^{-1}\left(\frac{\sinh\frac{\pi X}{h}}{\cos\frac{\pi Y}{h}}\right) \qquad (3.10)$$

When $Y = 0$, this equation becomes

$$V = \frac{V_1+V_2}{2} - (V_1-V_2)\frac{1}{\pi}\tan^{-1}\left(\sinh\frac{\pi X}{h}\right) \qquad (3.11)$$

and

$$\frac{\partial V}{\partial X} = -(V_1-V_2)\frac{1}{h}\frac{1}{\cosh\frac{\pi X}{h}} \qquad (3.12)$$

Now,

$$\sinh a = a + \frac{a^3}{3!} + \cdots\cdots$$

$$\tan a = a + \frac{a^3}{3} + \cdots\cdots$$

$$\cosh a = 1 + \frac{a^2}{2!} + \cdots\cdots$$

Hence for small X,

$$V = \frac{V_1+V_2}{2} - (V_1-V_2)\frac{X}{h} \qquad (3.13)$$

and

$$\frac{\partial V}{\partial X} = -\frac{V_1-V_2}{h\left\{1+\frac{1}{2}\left(\frac{\pi X}{h}\right)^2\right\}} \qquad (3.14)$$

Using the well known formula for the radius of curvature (R) of an electron trajectory

$$\frac{1}{R} = \frac{E_n}{2V}$$

(where E_n is the component of field normal to the trajectory)

the radius of curvature of an electron trajectory at distance X from a deflector plate is

$$\left[\frac{-(V_1+V_2)h + 2(V_1-V_2)X}{V_1-V_2}\right] \cdot \left[1+\frac{1}{2}\left(\frac{\pi X}{h}\right)^2\right]$$

$$\simeq -\left\{\frac{V_o+V_d}{V_d}\left[1+\frac{1}{2}\left(\frac{\pi X}{h}\right)^2\right]h - 2X\right\} \qquad (3.15);$$

the $-$ sign occurs because the direction of deflection is opposite to the direction of X.

Ideally, the deflector plates should have a radius of curvature such that, at maximum deflection, the deflector plate is always half the nominal beam diameter away from the centre of the beam. Therefore, substituting b for X in (3.15), the radius of curvature of the deflector plate, R', is given by

$$R' = \left[\frac{1}{\left(\frac{V_d}{V_o}\right)_{max}} + 1 \right] \left[h + \frac{(\pi b)^2}{2h} \right] - 3b \qquad (3.16)$$

Although it is possible to substitute for $\left(\frac{V_o}{V_d}\right)_{max}$ in this equation, the expression then becomes unduly complicated, so it is more useful for design purposes in its present form.

It will be shown that defocusing is minimised by making a deflection system as large as possible, but the accelerating lens limits the size of the system especially as the deflector plates should meet the lens at right angles (Fig. 3.5). By simple trigonometry, the distance of the centre of curvature of the deflector plates from the z-axis, X', is

$$d + R'\cos(\theta_1)_{max} .$$

Hence the maximum deflection angle of the system, $(\theta_2)_{max}$, is given by

$$(\theta_2)_{max} = \tan^{-1}\left(\frac{R_a}{R'}\right) + \cos^{-1}\left(\frac{d+R'\cos(\theta_1)_{max}}{\sqrt{R_a^2 + R'^2}}\right) \qquad (3.17)$$

where R_a is the radius of curvature of the accelerating lens.

From these calculations, it is apparent that, in a system which is designed for maximum sensitivity, there are only two dimensions of a deflection system which can be varied independently. It might be desirable, however, not to design the system for maximum sensitivity, if, by doing so, it were possible to reduce the deflection defocusing.

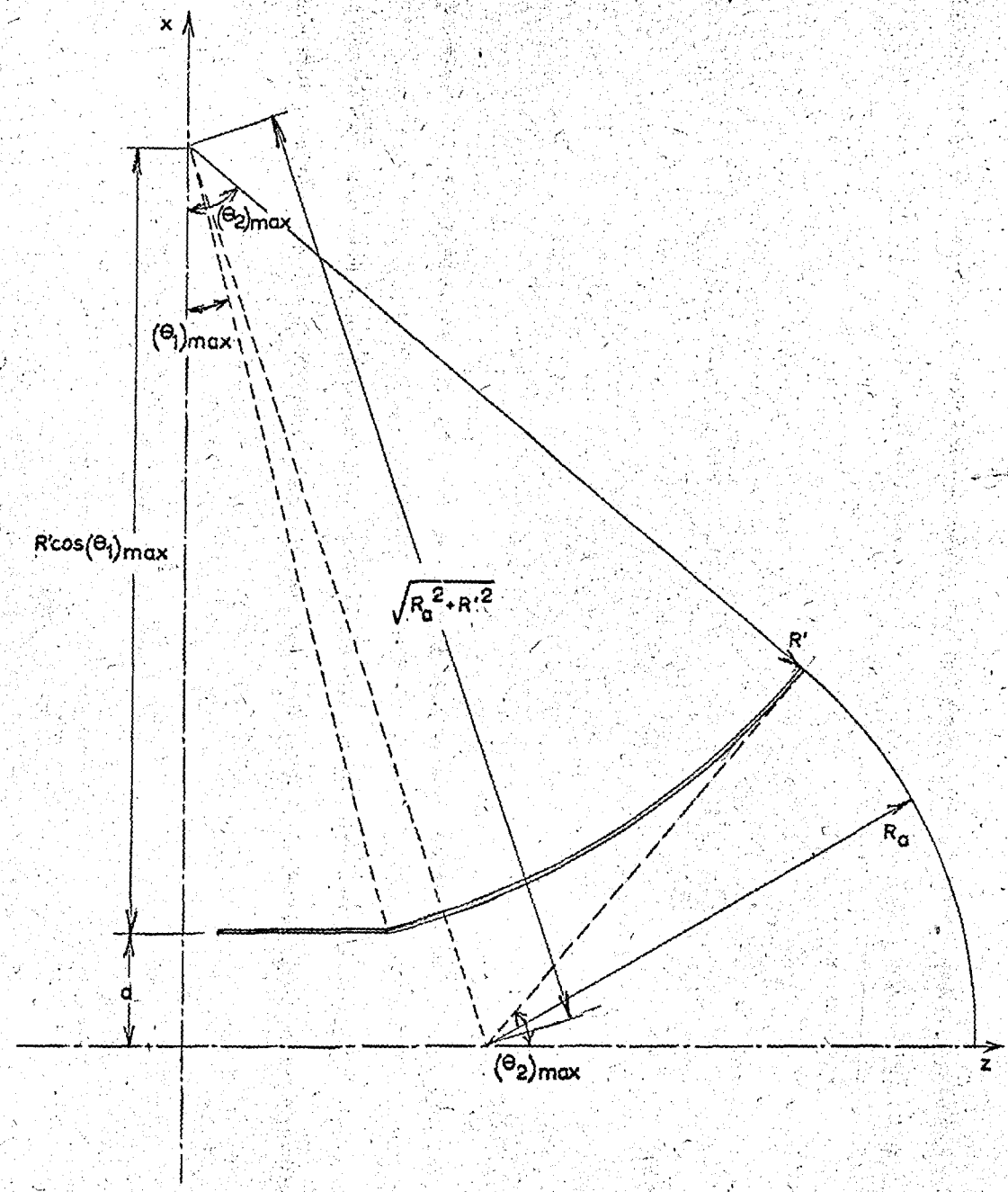
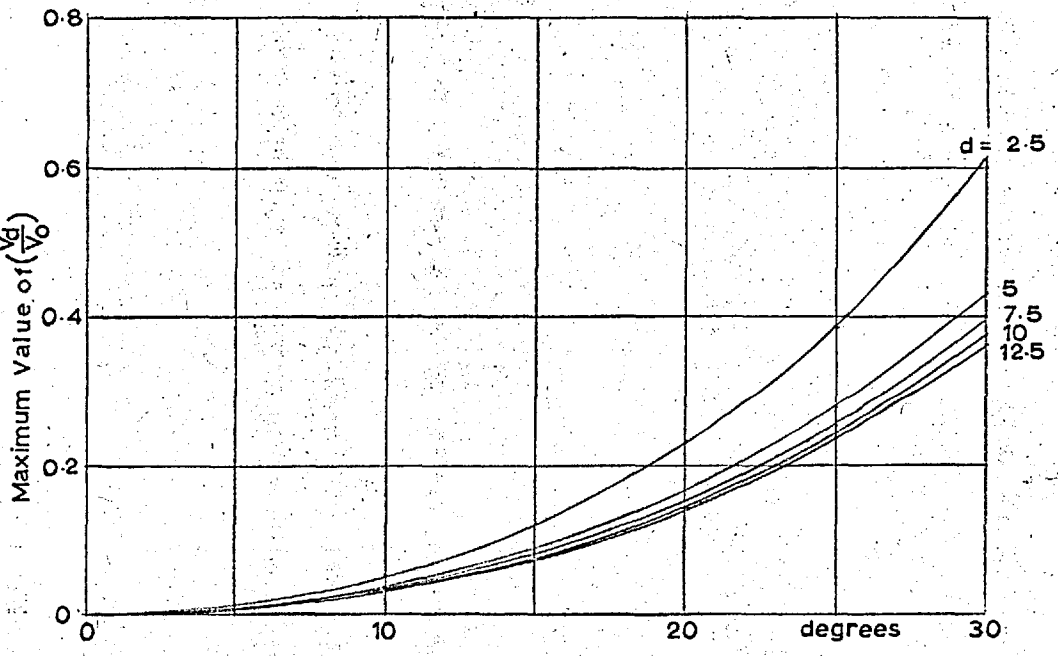


Fig. 3.5, Deflector Plates and Accelerating Lens.

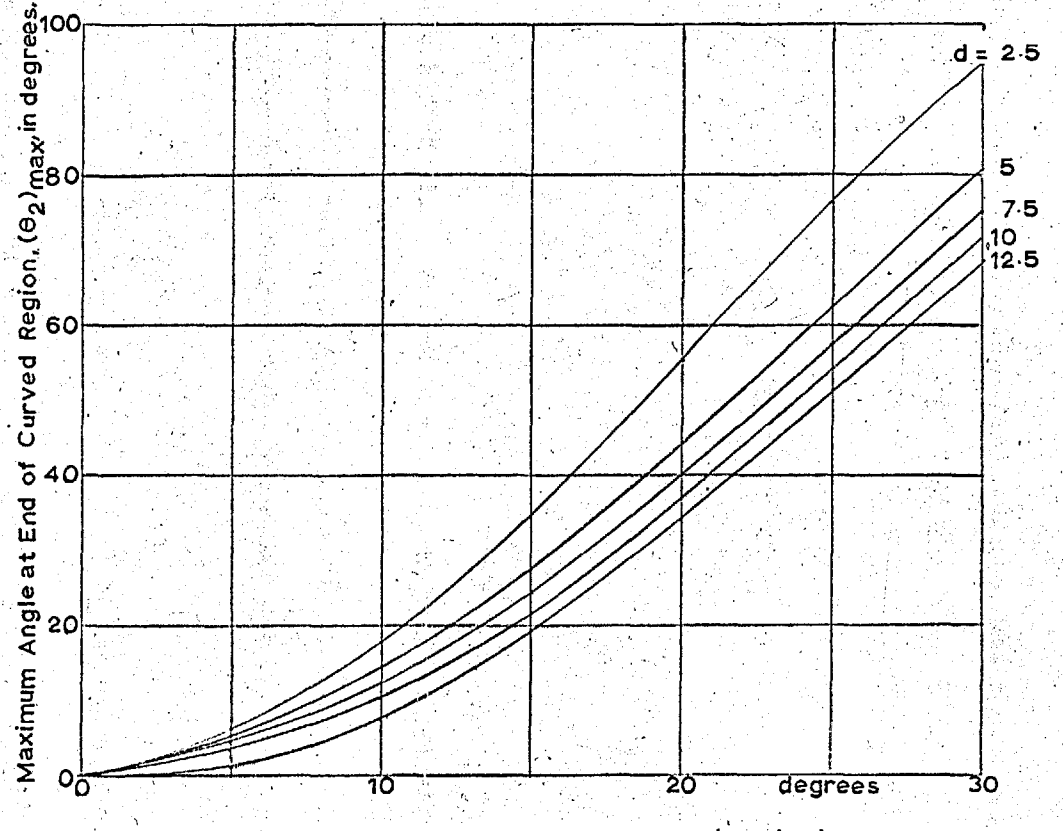
The formulae which are derived above have been used in the calculations for the curves of Fig. 3.6. These illustrate the variation of $(\theta_2)_{max}$ and $\left(\frac{V_d}{V_o}\right)_{max}$ with $(\theta_1)_{max}$ for several values of d. Typical values of b and R_a have been assumed. From these curves it is possible to calculate $\left(\frac{V_d}{V_o}\right)_{max}$ for a given value of $(\theta_2)_{max}$. Within the range considered, $\left(\frac{V_d}{V_o}\right)_{max}$ is almost independent of d for any given value of $(\theta_2)_{max}$, so d may be chosen to give minimum deflection defocusing.

3.3. Theoretical Aspects of the Deflection System.

The most important difference between conventional electrostatic deflection systems and the deflection system which is used in the flat tube is that, in the former, the potential distribution is essentially two dimensional, whereas it is three dimensional in the latter. As a result, accurate analysis on the deflection system of the flat tube is impossibly complicated and many simplifying approximations must be made, also it is essential that the beam always lies in the plane $y = 0$, so the electron gun must be very accurately aligned. However, these disadvantages are outweighed by the large deflection angle and relatively high sensitivity of this system. Furthermore, at large deflection angles the curved region becomes more effective which improves the sensitivity; this improvement in sensitivity helps to compensate for nonlinearities in the amplification of the deflection voltage.



a)



b)

Fig. 3.6, Design Curves for Deflection Systems.

It is not possible to design a deflection system theoretically by starting from the required electron trajectories and deriving the potential distribution because, even if the trajectories were such that a realisable potential distribution existed, a large number of electrodes would be required. As the voltage on each electrode would not be constant, but would be varied at a high frequency, the complications of supplying a considerable number of electrodes are unacceptable. Thus the only method of designing a deflection system of this type is to start with a certain configuration of electrodes, and then try to improve it by trial and error. This is not easy, as any change in the dimensions usually has more than one effect and the side effects are sometimes far from obvious, so some theoretical background can be very useful.

When the defocusing of the electron beam is under consideration, it is convenient to use the paraxial ray equations for curvilinear coordinates. These equations deal with rays (or trajectories) close to a principal trajectory; they are derived in the Appendix, although they are quite well known. The equations are:-

$$\frac{d^2n}{ds^2} + \frac{1}{2V}\frac{\partial V}{\partial s}\frac{dn}{ds} = \left(-\frac{3}{R^2} + \frac{1}{2V}\frac{\partial^2 V}{\partial n^2}\right) n \qquad (3.18)$$

$$\frac{d^2y}{ds^2} + \frac{1}{2V}\frac{\partial V}{\partial s}\frac{dy}{ds} = \left(\frac{1}{2V}\frac{\partial^2 V}{\partial y^2}\right) y \qquad (3.19);$$

where s is in the direction of the principal trajectory and n is normal to it in the plane of deflection.

In the parallel plate region, the field is assumed to be uniform so the second differential of V in any direction is zero;

also $$V = V_o + V_d \frac{x}{d} \qquad (3.20)$$

$$= V_o \sec^2\theta \qquad \text{Using (3.4),} \qquad (3.21)$$

and $$\frac{\partial V}{\partial x} = \frac{V_d}{d} \qquad \text{while} \quad \frac{\partial V}{\partial z} = 0,$$

so $$\frac{\partial V}{\partial s} = \frac{V_d}{d} \sin\theta \qquad \text{and} \qquad \frac{\partial V}{\partial n} = \frac{V_d}{d} \cos\theta \ ;$$

but $$\frac{1}{R} = \frac{\frac{\partial V}{\partial n}}{2V}$$

$$= \frac{1}{2d} \frac{V_d}{V_o} \cos^3\theta \qquad (3.22).$$

Now $$dz = ds \cos\theta$$

and from (3.5)

$$dz = 2d \frac{V_o}{V_d} \sec^2\theta \, d\theta \ ,$$

hence $$\frac{d\theta}{ds} = \frac{1}{2d} \frac{V_d}{V_o} \cos^3\theta$$

so $$\frac{d}{ds} = \frac{1}{2d} \frac{V_d}{V_o} \cos^3\theta \frac{d}{d\theta}$$

and $$\frac{d^2}{ds^2} = \frac{1}{4d^2} \left(\frac{V_d}{V_o}\right)^2 \cos^6\theta \left(\frac{d^2}{d\theta^2} - 3 \tan\theta \frac{d}{d\theta}\right)$$

Thus the paraxial ray equations in terms of θ are:-

$$\frac{d^2n}{d\theta^2} - 2 \tan\theta \frac{dn}{d\theta} + 3n = 0 \qquad (3.23)$$

$$\frac{d^2y}{d\theta^2} - 2 \tan\theta \frac{dy}{d\theta} = 0 \qquad (3.24)$$

If these equations are solved and written in terms of $\frac{d}{ds}$ instead of $\frac{d}{d\theta}$,

$$n = n_o \cos 2\theta \sec\theta + z \left(\frac{dn}{ds}\right)_o \cos\theta \qquad (3.25)$$

$$\frac{dn}{ds} = -\frac{n_o}{z}(1 + 2\cos^2\theta)\sin^2\theta + \left(\frac{dn}{ds}\right)_o \cos^4\theta \qquad (3.26)$$

$$y = y_o + z \left(\frac{dy}{ds}\right)_o \qquad (3.27)$$

$$\frac{dy}{ds} = \left(\frac{dy}{ds}\right)_o \cos\theta \qquad (3.28)$$

where the suffix 'o' indicates the value at $z = 0$.

These results could also have been obtained by considering trajectories starting from the points $(n_o,0,0)$ and $(0,y_o,0)$ at initial angles with the z-axis of $\left(\frac{dn}{ds}\right)_o$ and $\left(\frac{dy}{ds}\right)_o$ respectively.

If $\left(\frac{dn}{ds}\right)_o$ is taken to be zero (the beam is initially parallel) equations (3.25) and (3.26) can be written approximately as

$$n = n_o\left(1 - \frac{3\theta^2}{2}\right) \qquad (3.29)$$

$$\frac{dn}{ds} = -\frac{3n_o}{z}\theta^2(1 - \theta^2) \qquad (3.30).$$

Since (3.3) is the equation of a parabola, the tangents at $z = L$ to the principal rays cut the z-axis at $(0,0,\frac{L}{2})$ and this point is known as the deflection centre of this region. A length which is of interest is the distance between the point where $n = 0$ and the deflection centre: it is approximately $L\left(\frac{1-\theta_1^2}{3\theta_1^2}\right)$ for an initially parallel beam. This length can be considered as the focal length of the parallel plate part of the deflection system, though only in the plane of deflection. Ideally, if there were no deflection defocusing, this length would be infinite for all θ, but in a practical system it should be as great as possible. Since the length is proportional to L, this result may be generalised to indicate that, in order to decrease deflection defocusing, a deflection system should be as large as possible.

In the curved region it is essential to make drastic approximations, otherwise the paraxial ray equations may become very difficult to solve. It is again necessary to assume that one deflector plate is straight and to neglect the other. In order that the paraxial ray equations may have constant coefficients, we must assume that R, V, $\frac{\partial^2 V}{\partial n^2}$ and $\frac{\partial^2 V}{\partial y^2}$ are constant over the whole length of a trajectory in this region; it is convenient to assume that this length is the same for all trajectories. These assumptions imply that $\frac{\partial V}{\partial s} = 0$, so the paraxial ray equations simplify to

$$\frac{d^2n}{ds^2} = \left(-\frac{3}{R^2} + \frac{1}{2V}\frac{\partial^2 V}{\partial n^2} \right) n \qquad (3.31)$$

and

$$\frac{d^2y}{ds^2} = \left(\frac{1}{2V}\frac{\partial^2 V}{\partial y^2} \right) y \qquad (3.32)$$

These have the general form

$$\frac{d^2\eta}{d\xi^2} = \kappa^2 \eta \qquad (3.33)$$

or

$$\frac{d^2\eta}{d\xi^2} = -\lambda^2 \eta \qquad (3.34)$$

where κ and λ are constants.

The general solution of (3.33) is

$$\eta = \alpha \cosh \kappa\xi + \beta \sinh \kappa\xi \qquad (3.35)$$

with

$$\frac{d\eta}{d\xi} = \alpha \kappa \sinh \kappa\xi + \beta \kappa \cosh \kappa\xi \qquad (3.36)$$

and the general solution of (3.34) is

$$\eta = \alpha \cos \lambda\xi + \beta \sin \lambda\xi \qquad (3.37)$$

with

$$\frac{d\eta}{d\xi} = -\alpha \lambda \sin \lambda\xi + \beta \lambda \cos \lambda\xi \qquad (3.38)$$

where α and β are the values of η and $\frac{1}{\kappa}\frac{d\eta}{d\xi}$ or $\frac{1}{\lambda}\frac{d\eta}{d\xi}$ respectively at $\xi = 0$.

Differentiating (3.12) and substituting for $(V_1 - V_2)$

$$\frac{\partial^2 V}{\partial n^2} = \frac{2\pi V_d}{h^2} \frac{\sinh \frac{\pi X}{h}}{\cosh^2 \frac{\pi X}{h}}.$$

Now we are in effect assuming a two dimensional system, so, using Laplace's equation,

$$\frac{\partial^2 V}{\partial y^2} = - \frac{2\pi V_d}{h^2} \frac{\sinh \frac{\pi X}{h}}{\cosh^2 \frac{\pi X}{h}} \qquad (3.39)$$

Using (3.12) and remembering that the direction of n is opposite to the direction of X,

$$\frac{1}{R} = \frac{V_d}{V h \cosh \frac{\pi X}{h}} \qquad (3.40)$$

Hence, if V is assumed to be V_o,

$$- \frac{3}{R^2} + \frac{1}{2V} \frac{\partial^2 V}{\partial n^2} = \frac{V_d}{V_o} \left(\frac{- 3 \left(V_d / V_o \right) + \pi \sinh \frac{\pi X}{h}}{V_o h^2 \cosh^2 \frac{\pi X}{h}} \right) = N^2 \qquad (3.41)$$

and

$$\frac{1}{2V} \frac{\partial^2 V}{\partial y^2} = - \pi \frac{V_d}{V_o} \left(\frac{\sinh \frac{\pi X}{h}}{\cosh^2 \frac{\pi X}{h}} \right) = Y^2 \qquad (3.42)$$

In order to reduce these to functions of X it is necessary to express $\left(\frac{V_d}{V_o} \right)$ as a function of X; this is not easy, but a reasonable approximation, which is based on deflection system No. 11, is

$$\frac{V_d}{V_o} = \left(\frac{V_d}{V_o} \right)_{max} \exp \left(- \frac{\pi X}{2h} \right).$$

For the purpose of this calculation, we will assume that $\left(\frac{V_d}{V_o} \right)_{max} = 0.4$ and that the total length of a trajectory in this region is 2.5 h: these values are also based on deflection system No. 11.

Substituting for $\left(\frac{V_d}{V_o}\right)_{max}$ in (3.41) and (3.42)

$$N = \frac{\sqrt{0.4 \exp\left(-\frac{\pi X}{2h}\right)\left\{\pi \sinh \frac{\pi X}{h} - 1.2 \exp\left(-\frac{\pi X}{2h}\right)\right\}}}{h \cosh \frac{\pi X}{2h}} \qquad (3.43)$$

$$Y = \frac{\sqrt{0.4\,\pi \exp\left(-\frac{\pi X}{2h}\right) \sinh \frac{\pi X}{h}}}{h \cosh \frac{\pi X}{h}} \qquad (3.44)$$

The values of N and Y have been plotted against $\frac{X}{h}$ in Fig. 3.7.

The solutions of the paraxial ray equations for an initially parallel beam of unit diameter are given by substituting for κ, λ, ξ and η in (3.35), (3.36), (3.37) and (3.38) with $\alpha = 1$ and $\beta = 0$. The values of n and y at the end of the region have been plotted against $\frac{X}{h}$ in Fig. 3.8; the values of $\frac{dn}{ds}$ and $\frac{dy}{ds}$ have been plotted in Fig. 3.9. The values of n and $\frac{dn}{ds}$ at the end of the parallel plate region are also shown in Fig. 3.8 and Fig. 3.9. These have been plotted on the basis of (3.29) and (3.30) with $\theta = -0.175X + 0.49$ and $z = 30$ for an initially parallel beam. The expression for θ and the value of z are based on deflection system No. 11. Unfortunately the curves have little application to a practical deflection system because of the approximations which have been made in order to obtain them. However, the abrupt variations in the curved region particularly where $\frac{X}{h}$ is small are important because they indicate that it is impossible to compensate the deflection defocusing from the two regions for all angles.

Since N and Y are proportional to $\frac{1}{h}$, and $\frac{dn}{ds}$ and $\frac{dy}{ds}$ depend on N and Y, it is desirable to make h large. However, h is determined by the separation of the main collimator plates and cannot be changed. A possibility is to scale down all the other dimensions of the deflection system, but we have already seen that there are disadvantages in doing this. Actually, the two effects counteract each other and there is no advantage to be gained from scaling down all the dimensions except h. Another possibility is to simulate a larger value of h by employing gradual changes of potential between the deflector plates and the central plates. Although the problems of electrical supplies rule out the possibility of electrodes at intermediate potentials in a deflection system, it is possible to achieve the same effect by using channel shaped deflector plates. Instead of completely covering the surface between the deflector plates, the central plates stop some distance short of the deflector plates, and the remaining area is at the same potential as the deflector plates. In effect this splits the discontinuity in potential near a deflector plate into two; one transition is the mirror image of the other in the deflector plate. With this arrangement, the variations in deflection defocusing are less abrupt, but they occur further away from the deflector plates.

A disadvantage of any deflection system, in which the field is three-dimensional, is that rays which do not lie in the plane

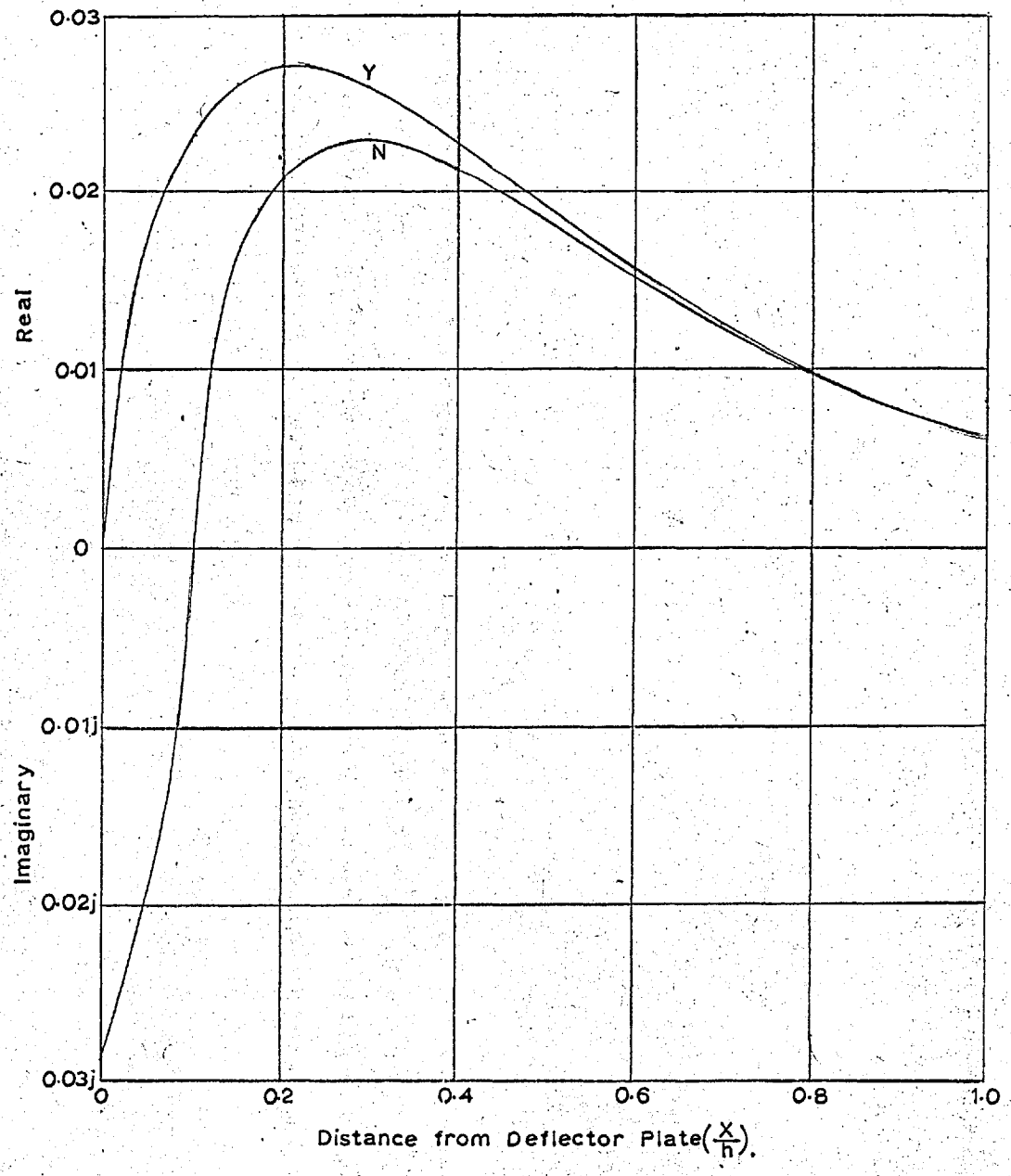


Fig. 3.7, Curved Region: N and Y Against $\frac{X}{h}$.

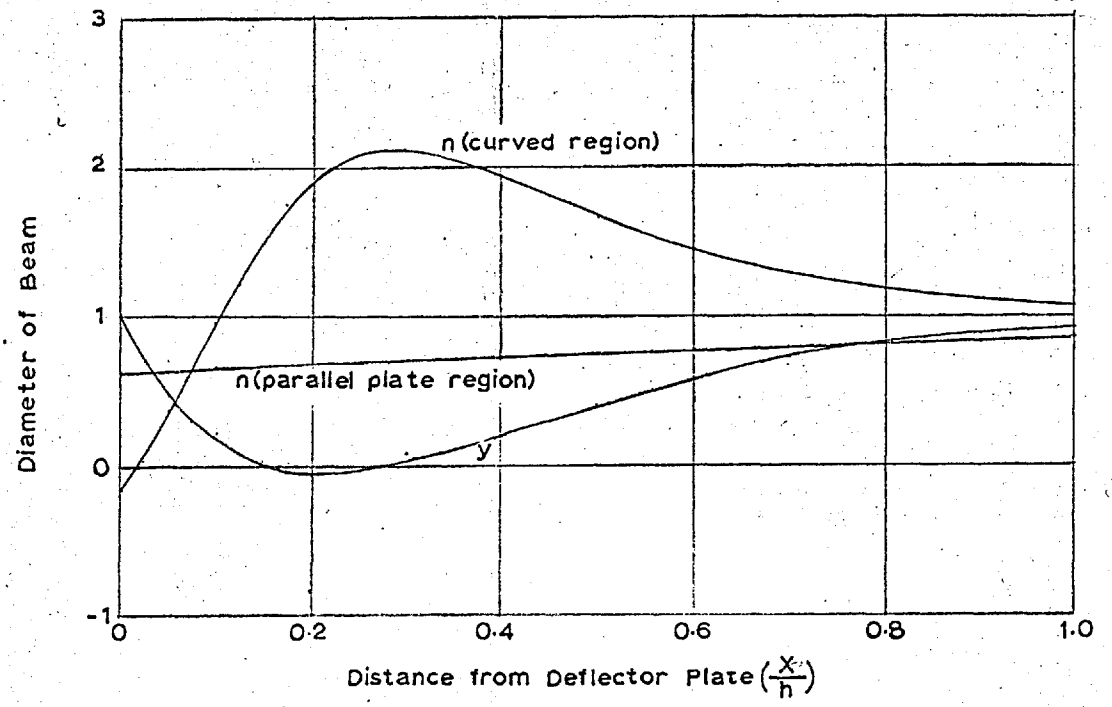


Fig. 3.8, Diameter of Beam (n and y) Against $\frac{X}{h}$.

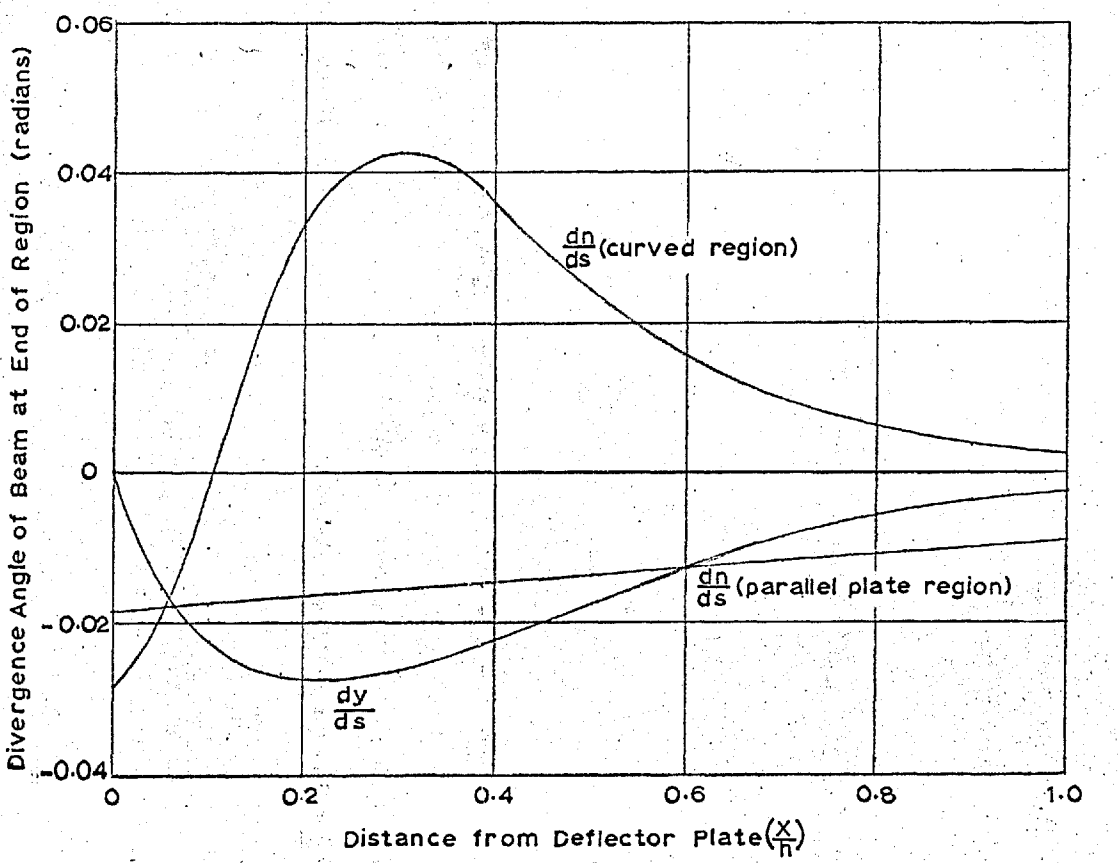


Fig. 3.9, Divergence Angle of Beam ($\frac{dn}{ds}$ and $\frac{dy}{ds}$) Against $\frac{X}{h}$.

of deflection will be deflected through a different angle to those which do. A beam, which is initially a straight line in the plane $x = 0$, will appear, after deflection, to be shaped like a C, so this aberration is described as the "c-error". It is possible to derive an equation for the c-error which is similar to the paraxial ray equations for curvilinear coordinates. This is done in the Appendix; the equation is

$$\frac{d^2c}{ds^2} + \frac{1}{2V}\frac{\partial V}{\partial s}\frac{dc}{ds} = \left(-\frac{3}{R^2} + \frac{1}{2V}\frac{\partial^2 V}{\partial n^2}\right)c + \frac{y^2}{2V}\left(\frac{1}{2}\frac{\partial^3 V}{\partial n \partial y^2} - \frac{1}{R}\frac{\partial^2 V}{\partial y^2}\right) \tag{3.45}$$

In the parallel plate region we assumed a two-dimensional field so there will be no c-error from this region. The coefficients of (3.45) are the same as those of (3.18), but there is an extra term which is independent of c; this term will be assumed to be constant for each trajectory in the curved region. In this region, if the same approximations are made as for (3.31), (3.45) has the form

$$\frac{d^2\eta}{d\zeta^2} = K^2\eta + \mu \tag{3.46}$$

or

$$\frac{d^2\eta}{d\zeta^2} = -\lambda^2\eta + \mu \tag{3.47}$$

where μ is constant.

The particular integrals for these equations are

$$\eta = -\frac{\mu}{K^2}$$

and

$$\eta = +\frac{\mu}{\lambda^2}$$

We obtain the general solutions by adding the particular integrals to the complimentary functions, but the complimentary functions are (3.35) and (3.37). The coefficients α and β are easily found because $\eta = \frac{d\eta}{ds} = 0$ at $\xi = 0$. Hence the general solution of (3.46) is

$$\eta = \frac{\mu}{K^2} \cosh K\xi - \frac{\mu}{K^2} \tag{3.48}$$

and the general solution of (3.47) is

$$\eta = -\frac{\mu}{\lambda^2} \cos \lambda\xi + \frac{\mu}{\lambda^2} \tag{3.49}.$$

Differentiating (3.39) with respect to n and remembering that n is in the opposite direction to X,

$$\frac{\partial^3 V}{\partial n \partial y^2} = \frac{2\pi^2 V_d}{h^3} \left(\frac{1 - \sinh^2 \frac{\pi X}{h}}{\cosh^3 \frac{\pi X}{h}} \right)$$

so, using (3.39) and (3.40) and assuming that $y = \frac{1}{2}$ and $V = V_o$

$$\frac{y^2}{2V} \left(\frac{1}{2} \frac{\partial^3 y}{\partial n \partial y^2} - \frac{1}{R} \frac{\partial^2 V}{\partial y^2} \right) = \frac{\pi}{8h^3} \left(\frac{V_d}{V_o} \right) \left\{ \pi \left(1 - \sinh^2 \frac{\pi X}{h} \right) - 2 \left(\frac{V_d}{V_o} \right) \sinh \frac{\pi X}{h} \right\} \frac{1}{\cosh^3 \frac{\pi X}{h}}$$

$$= M \tag{3.50}$$

The values of M have been plotted against $\frac{X}{h}$ in Fig. 3.10 with the same assumptions as were made in the calculation of N and Y.

Now the solution of (3.45) may be written in terms of M, N and n as

$$c = \frac{M}{N^2}(n - 1) \qquad (3.51)$$

so c is easily calculated and it has been plotted against $\frac{X}{h}$ in Fig. 3.11. This curve is of interest because it indicates that the c-error will only be a problem at large deflection angles and that, when channel shaped deflector plates are used, the maximum magnitude of the c-error will be reduced although it will be significant at rather smaller deflection angles.

These calculations on the aberrations of deflection systems give a qualitative idea of where the aberrations arise. Unfortunately, they are too inaccurate to be used for the design or optimisation of a deflection system, but they do suggest a method of calculating the electron trajectories and aberrations of a realistic deflection system using a digital computer.

3.4. A program for a digital computer.

We have seen in the previous sections that it is possible to design a deflection system for maximum sensitivity, but no similar procedure exists for minimising deflection defocusing; indeed, the direct theoretical treatment is of little use as far as aberrations in this deflection system are concerned. For this reason, the optimisation of the deflection system for the flat tube was carried out largely on a trial and error basis.

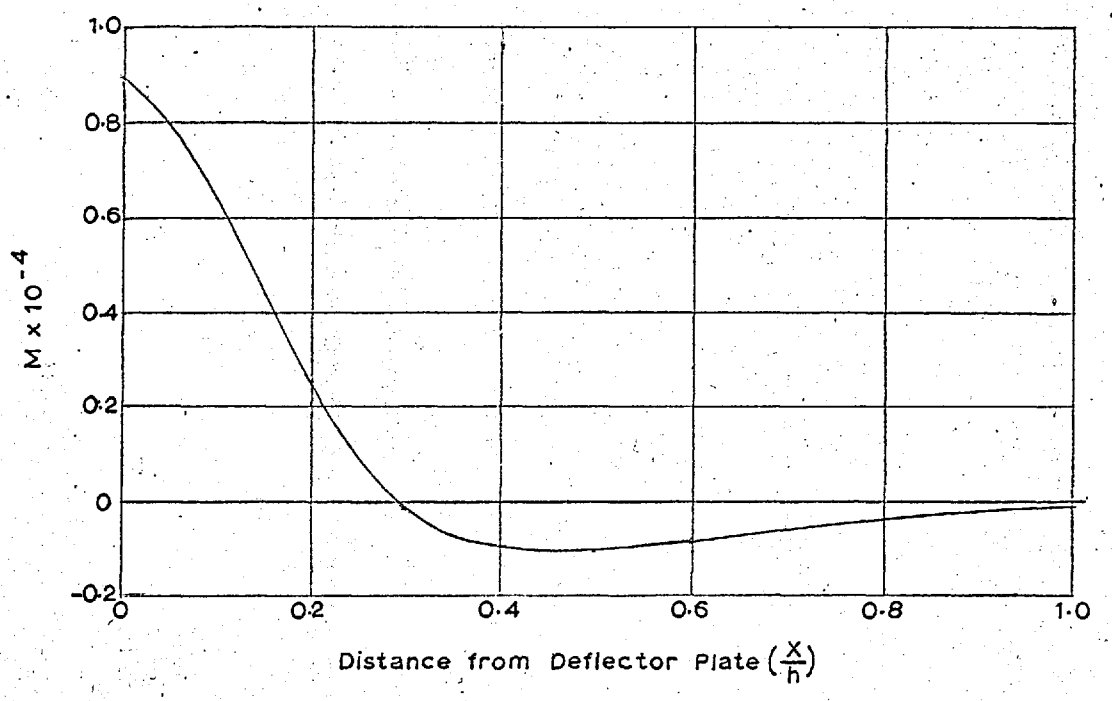


Fig. 3.10, c-error: M Against $\frac{X}{h}$.

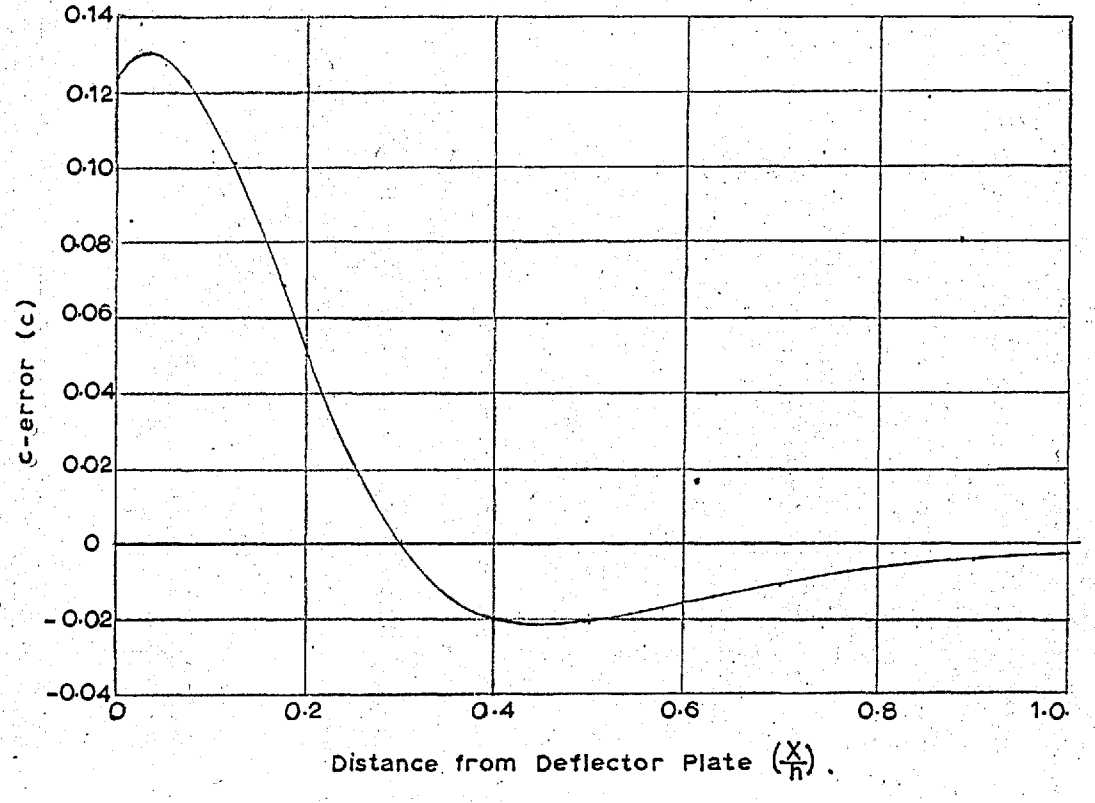


Fig. 3.11, c-error for Beam of Unit Diameter (c) Against $\frac{X}{h}$.

However building and testing a large number of deflection systems was distinctly laborious, and the accuracy of measurements on the aberrations was low, so there were incentives to find an easier way of comparing deflection systems. A program for a digital computer which simulates a deflection system, is particularly attractive for this purpose.

A program to compute the trajectories and aberrations in an electron optical system of this type must carry out the following operations:

i) Solve Laplace's equation for the given electrode configuration;

ii) Calculate the principal trajectories;

iii) Solve the paraxial ray equations and the c-error equation.

Digital computers are not very suitable for the direct solution of Laplace's equation, but, if an analytical solution can be found, the machine can be used to do the substitutions, even if the expression is very long and complicated. Although an exact analytical expression for the field in the deflection system does not exist, it is possible to find an approximate one which is based on the expression in (3.9). The method of images can of course be used with great effect because, with a computer, it is possible to consider a large number of them. If even an approximate analytical solution is available, not only can the

gradients of the field be obtained very easily, but it is only necessary to solve Laplace's equation at the points where a solution is required.

Once Laplace's equation has been solved, the solution of the trajectory equations and the paraxial ray equations present no difficulty and can best be carried out using a step by step method. A technique which is especially suitable for calculating the trajectories is a direct adaptation of the "circle method" mentioned in section 2.6; it is particularly convenient to use this method if comparisons are to be made between trajectories based on electrolytic tank plots and computer results. The paraxial ray equations and the c-error equation are straightforward second order differential equations with variable coefficients, which present no difficulty when the solution is by step method.

We have seen in section 3.2 that the potential distribution between two pairs of semi-infinite plates, which are at V_1 if $X < 0$ but V_2 if $X > 0$, is given by

$$V = V_2 + (V_1-V_2)\frac{1}{\pi}\tan^{-1}\left(\frac{\cos\frac{\pi Y}{h}}{\sinh\frac{\pi X}{h}}\right) \qquad (3.9)$$

If the boundary between V_1 and V_2 is not straight, but curves with radius a, the system has cylindrical symmetry. A first approximation for V in this case is, writing $(r-a)$ for X in (3.9),

$$V = V_2 + (V_1-V_2)\frac{1}{\pi}\tan^{-1}\left(\frac{\cos\frac{\pi Y}{h}}{\sinh\frac{\pi(r-a)}{h}}\right) \qquad (3.51)$$

However, as $a \gg h$, a better approximation is

$$V = V_2 + (V_1-V_2)\left\{\frac{1}{\pi}\tan^{-1}\left(\frac{\cos\frac{\pi Y}{h}}{\sinh\frac{\pi(r-a)}{h}}\right) - \frac{1}{a\pi^2}\left(\frac{\cosh\frac{\pi(r-a)}{h}\cos^2\frac{\pi Y}{h}}{\sinh^2\frac{\pi(r-a)}{h} + \cos^2\frac{\pi Y}{h}}\right)\right\} \quad (3.52)$$

This may be verified by differentiating partially twice with respect to r and Y and substituting in Laplace's equation for cylindrical coordinates. The expression can be greatly simplified because we are only interested in the case where $Y = 0$.

In order to obtain an approximate solution for the potential in a deflection system, it is necessary to divide the system into a number of regions and consider each separately. Each region is assumed to have a fixed basic shape, although the proportions can be varied, so the range of deflection systems which can be simulated is somewhat limited. However, as the program is intended for a deflection system of the general form of No. 11, it has been possible to use it to test a wide range of variations of this system. The four regions into which a deflection system must be divided are:-

i) Where the deflector plates are straight and the edges of the central plate are also straight;

ii) Where the deflector plates are straight but the edges of the central plates are curved;

iii) Where the deflector plates are curved;

iv) Near the first part of the accelerating lens.

In the first region, using the principle of superposition, there are an infinite number of images of the gaps between the central plates and the electrodes connected to the deflector plates; these images are reflections of the gaps and reflections of reflections in the planes of the deflector plates. Hence the potential in the first region is given exactly by the sum of an infinite number of expressions of the form of (3.9). If the deflector plates and the gaps are at distances d and b from the center-line respectively, where $b < \frac{d}{3}$, the distances of a point $(x,0,z)$ from the images of the gaps are:

$$x-b+2d; \quad x+b+2d; \quad x-b+4d; \quad x+b+4d; \quad \ldots\ldots$$

and $$x-b-2d; \quad x+b-2d; \quad x-b-4d; \quad x+b-4d; \quad \ldots\ldots$$

Now if $X > \frac{h}{2}$

$$\frac{1}{\pi} \tan^{-1}\left(\frac{1}{\sinh \frac{\pi X}{h}}\right) = \frac{2}{\pi} \exp\left(-\frac{\pi X}{h}\right) \quad \text{within 2\%} \qquad (3.53)$$

and if $X < -\frac{h}{2}$

$$\frac{1}{\pi} \tan^{-1}\left(\frac{1}{\sinh \frac{\pi X}{h}}\right) = 1 - \frac{2}{\pi} \exp\left(\frac{\pi X}{h}\right) \quad \text{within 2\%} \qquad (3.54)$$

Substituting for X in (3.53) and (3.54), the potential due to the images can be written as

$$\frac{V_d}{\pi} \sinh \frac{\pi X}{h} \cosh \frac{\pi b}{h} \frac{\exp\left(-\frac{\pi d}{h}\right)}{\sinh \frac{\pi d}{h}}$$

The potential within the region is given by adding the potential due to the images to that due to the two gaps; the field and the gradient of the field can be found by differentiating the expression for the potential.

It is not possible to find such a convenient expression for the potential due to the images in the second region because they are curved, so only the first eight are considered in the program; the effect of the others is almost negligible anyway. In this case, values of r are calculated for each image and the two gaps; these values are then substituted in (3.52).

In the third region, the reflecting surfaces are curved instead of straight so the shape of the images is very complicated. However, in the program, only two are considered and these are assumed to be cylindrical. These images are constructed in such a way as to compensate to some extent for the missing ones. (3.51) is used in this region instead of (3.52) because it gives a more accurate representation of the potential near the deflector plates.

In experimental models, the disturbing influence of the fluorescent screens on the potential distribution inside the

deflection system was minimised if the first part of the accelerating lens was included. It has been included in the program in order to help the comparison of experimental results with those from the computer. The potential due to the accelerating lens, which is computed using (3.52), is simply added to that due to the remainder of the system, although this introduces considerable errors near the deflector plates.

The program was written in Mercury Autocode and it first ran on the London University Mercury computer. Shortly after the program had been debugged, the London University Atlas came into commission; since then, the program has been run on this machine, but it has not been necessary to make any changes to it. A flow diagram of the program is given in Fig. 3.12, and a flow diagram of the chapter in which the solution of Laplaces Equation is computed is given in Fig. 3.13. At each point the following are printed out:

- the coordinates of the point,
- the angle of the beam with the z-axis,
- the diameter of the beam in the x and y directions,
- the c-error,
- and the potential.

At the end of each trajectory, the divergence angle of the beam in both the x and the y directions and the divergence angle of the c-error are also printed out. This is more data than is

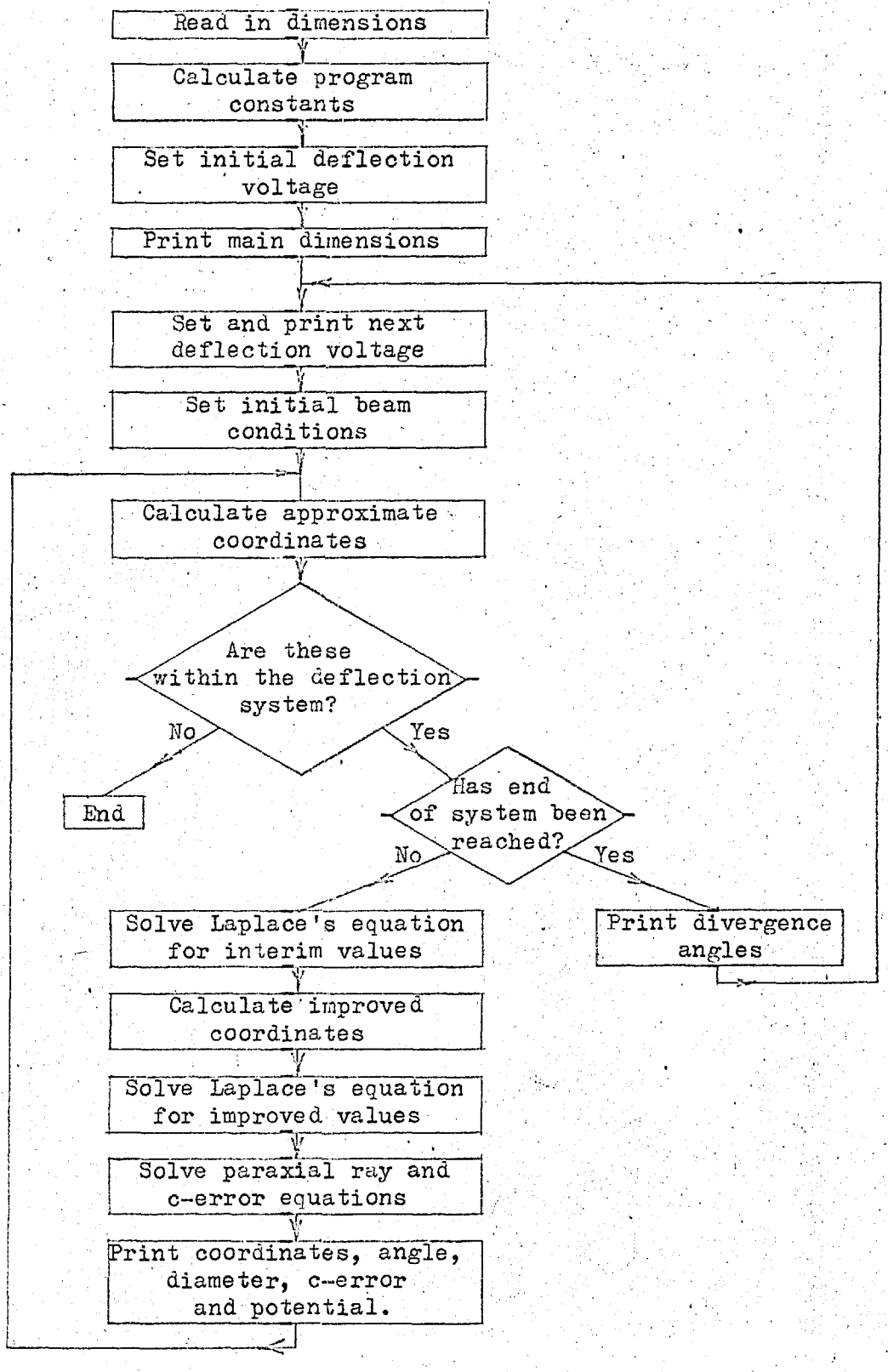
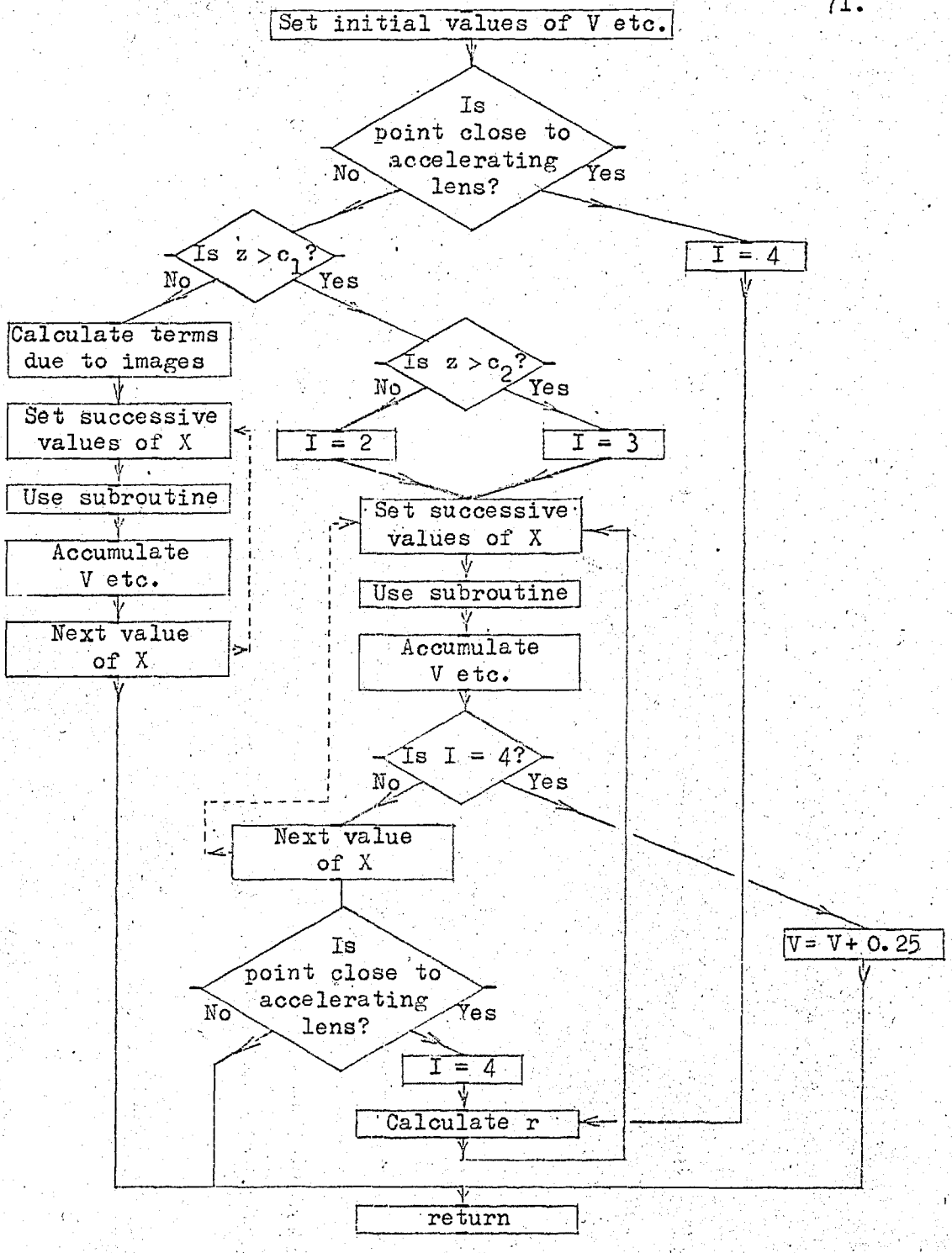


Fig. 3.12, Flow Diagram For Deflection System Program.



c_1 and c_2 are the values of z at the transitions between the regions. The subroutine substitutes for X or $(r-a)$, depending on the value of I, in (3.11) or (3.52) and the corresponding equations for the field and the gradient of the field.

Fig. 3.13, Flow Diagram for Computation of Laplace's Equation.

required for a simple comparison of deflection systems, but it is useful when trying to discover in which part of the system the aberrations arise.

A comparison of the experimental results for deflection system No. 11 with the results from the computer for the same deflection system and initial conditions for the beam is given in section 3.5. The discrepancies between these results at extreme deflections are almost certainly due to the approximations which were made for the field in the curved region, particularly in the area close to both the accelerating lens and the deflector plates. Otherwise, the results are in good agreement and indicate that the computer program simulates the deflection system with a reasonable degree of accuracy.

3.5. Results of measurements and computations.

A large number of deflection systems have been built and tested, so lack of space prevents details of the results for them all from being included. In addition to results for the final choice, deflection system No. 11, some of the results obtained for deflection system No. 8 are given too, because the aberrations in this system were less than any other, although the number of electrodes made it unacceptable. The results of analysis of deflection system No. 11 using the computer program are also given.

Deflection systen No. 8 (Fig. 3.14) was designed as a flexible system which could be used to test a number of different configurations of electrodes. The deflector plates were split into two parts, so that measurements could be made on the parallel plate region by itself, and variation of the separation of the parallel plates could be simulated by supplying them with a fraction of the total deflection voltages. The surfaces between the central plates and the curved parts of the deflector plates were divided into a number of strips; separate connections were made to each strip so that it was possible to supply them with different fractions of the deflection voltage. Thus the system could be used to simulate a system in which the separation between the central plates (h) was much larger, as suggested in section 3.4; in fact the results for this system (Fig. 3.15 and Fig. 3.16) were obtained with the system connected in this manner.

Deflection system No. 11 (Fig. 3.17) was developed from the experiments on deflection system No. 8; it has no electrodes at intermediate potentials, but the areas between the deflector plates and the central electrodes are at the potential of the deflector plates. In addition to the experimental results for this deflection system, the computed results are also given in Fig. 3.18 and Fig. 3.19.

When the results for the deflection systems are compared, it is important to remember that the accuracy of the measurements on

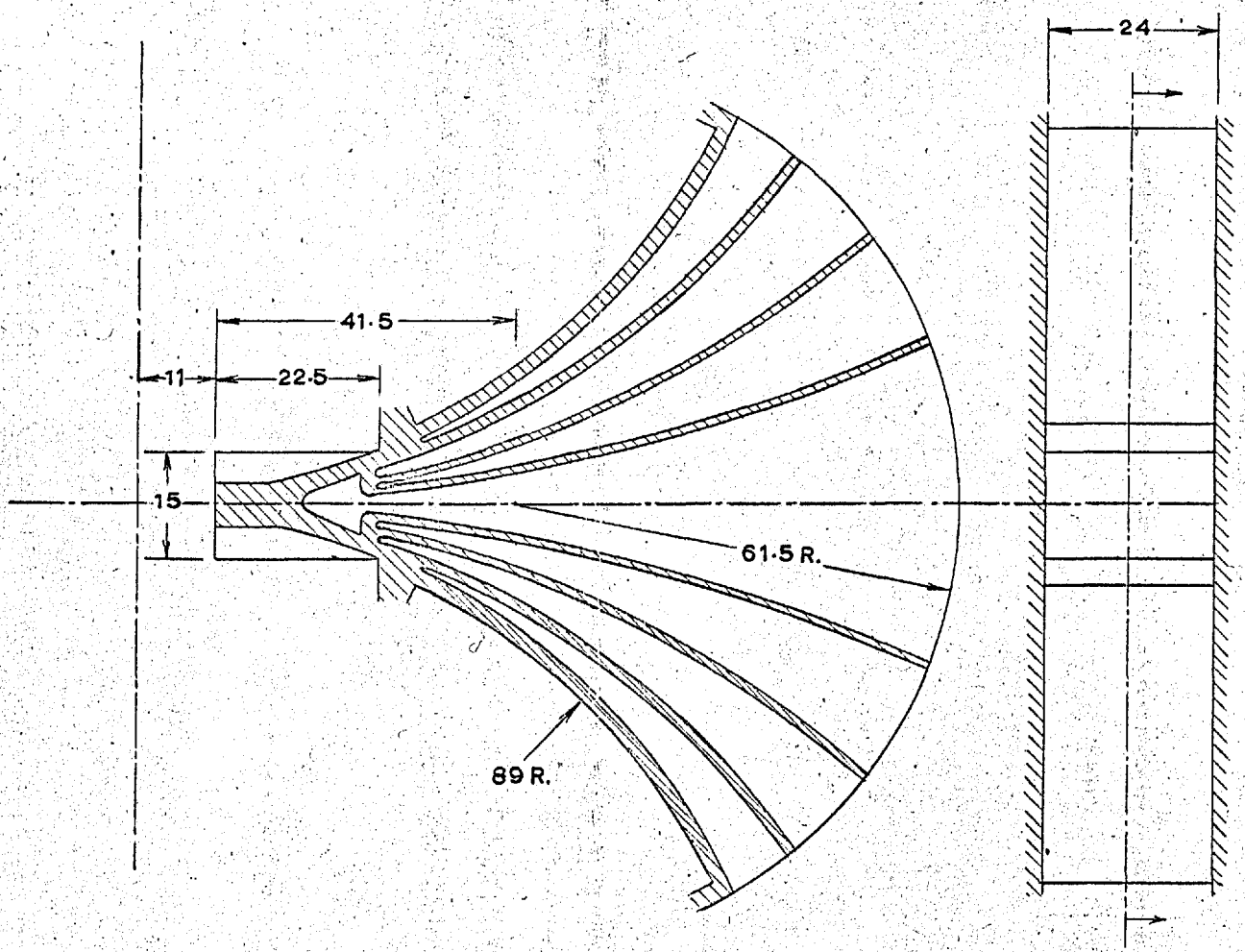


Fig. 3.14, Deflection System No. 8.

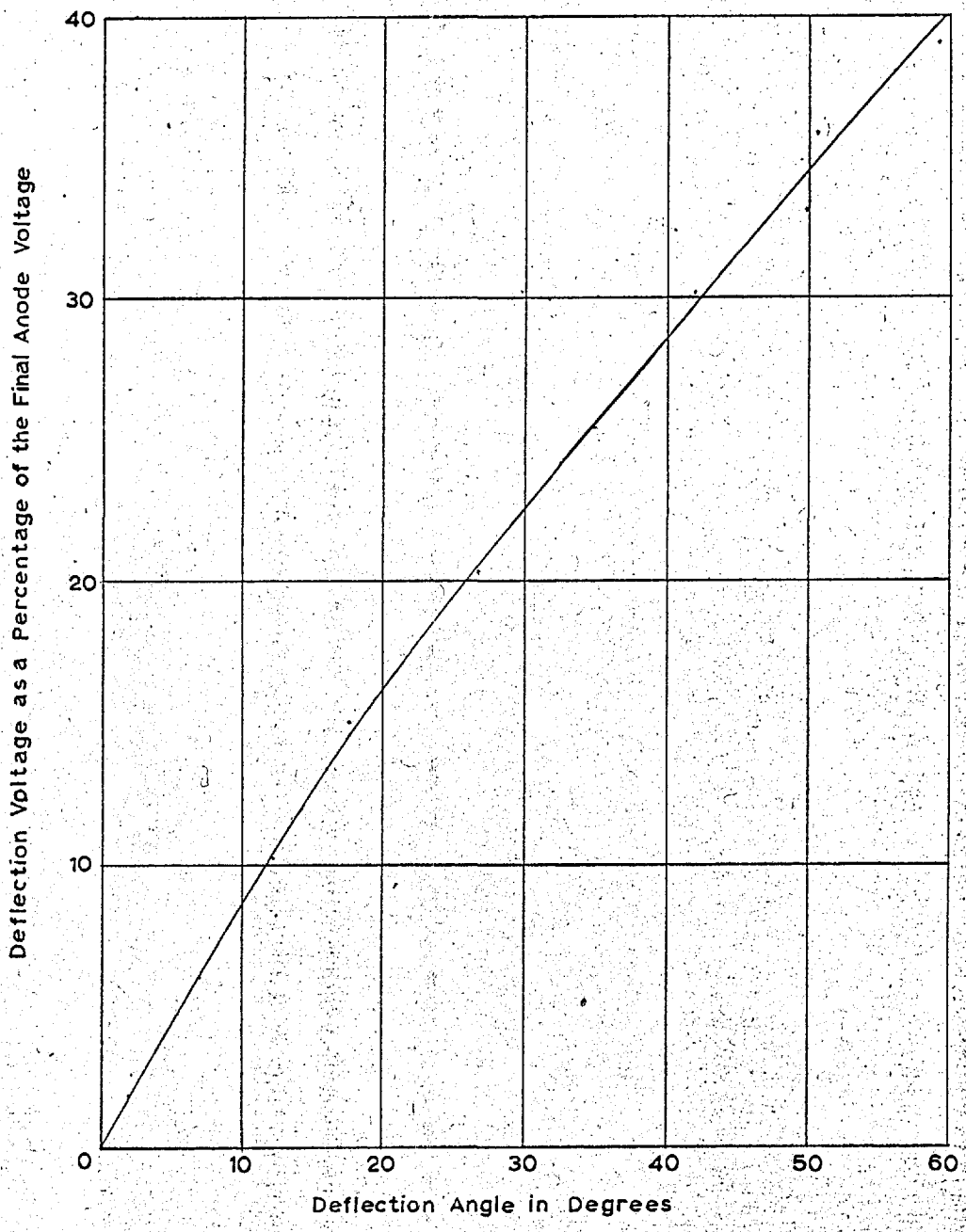
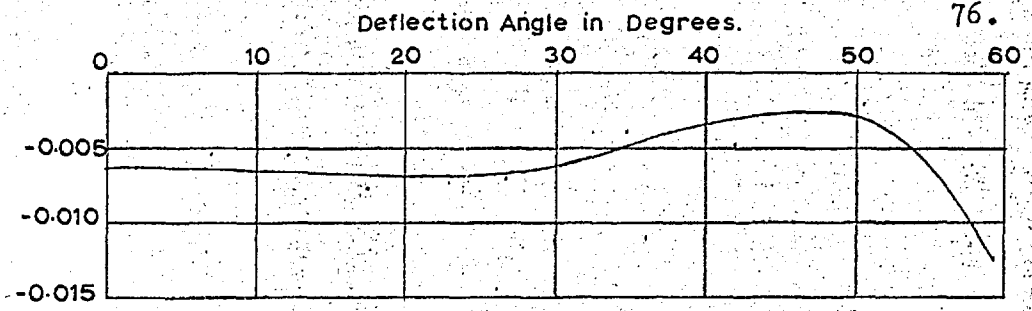
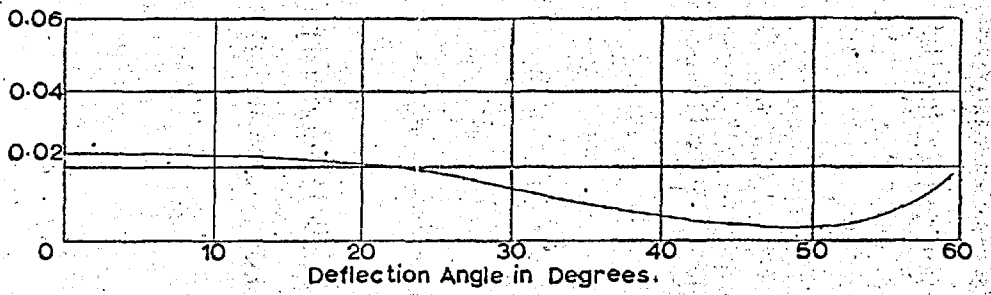


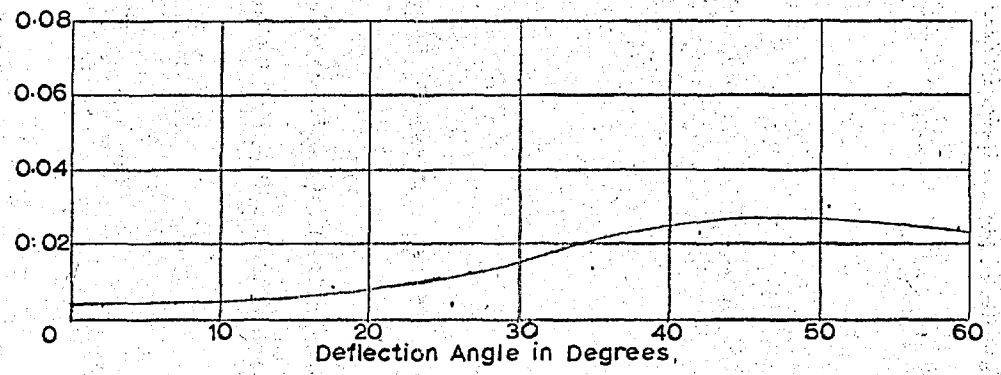
Fig. 3.15, Deflection Curve for Deflection System No. 8.



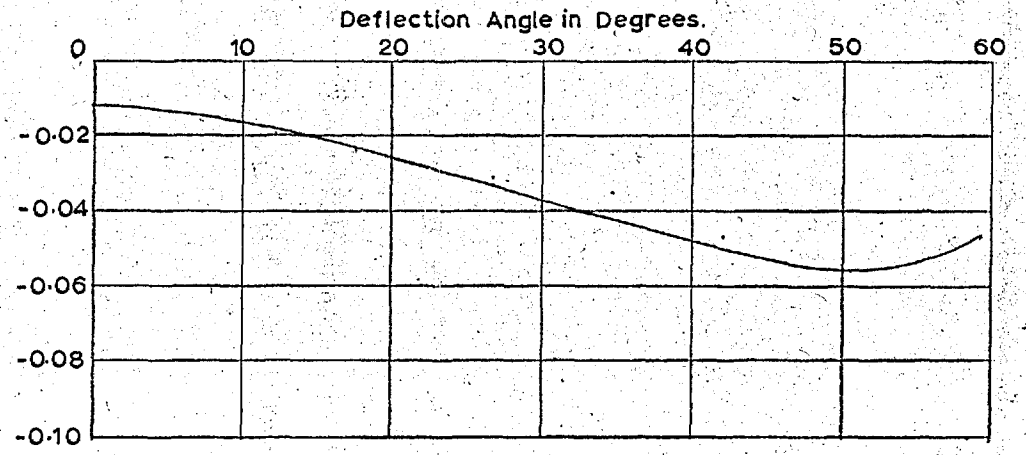
a). Reciprocal of Distance of Horizontal Crossover in Front of Accelerating Lens.



b) Horizontal Divergence Angle in Radians.



c). Reciprocal of Distance of Vertical Crossover in Front of Accelerating Lens.



d). Vertical Divergence Angle in Radians.

Fig. 3.16, Divergence of Beam leaving Deflection System No.8.

the aberrations is low, so there is considerable scatter of points, and that a deflection system is intended to be combined with a collimator which has aberrations too. Thus any measurements on a deflection system alone are of limited value in assessing the merit of the system; the best deflection system for the flat tube is not necessarily the one with minimum aberrations.

For each deflection system, the deflection voltage has been plotted against the deflection angle, although the angle is usually plotted against the voltage, because the divergence angle of the beam and the distance of the crossover from the middle of the accelerating lens have also been plotted against the deflection angle for both horizontal (x) and vertical (y) directions. The sign of the horizontal divergence angle has been assumed to be unaffected when the horizontal crossover moves inside the deflection system from in front of it. Unfortunately the length of the component means that any calculations of the focal length using the thin lens approximation is of little significance, while errors of measurement make the accuracy of calculations of the properties of the equivalent thick lens unacceptably low.

A comparison of deflection system No. 8 with deflection system No. 11 indicates that the latter had better deflection sensitivity but the former had less aberrations. Indeed, a horizontal crossover occurred within deflection system No. 11. This bears out the prediction, made in Section 3.3, that it is

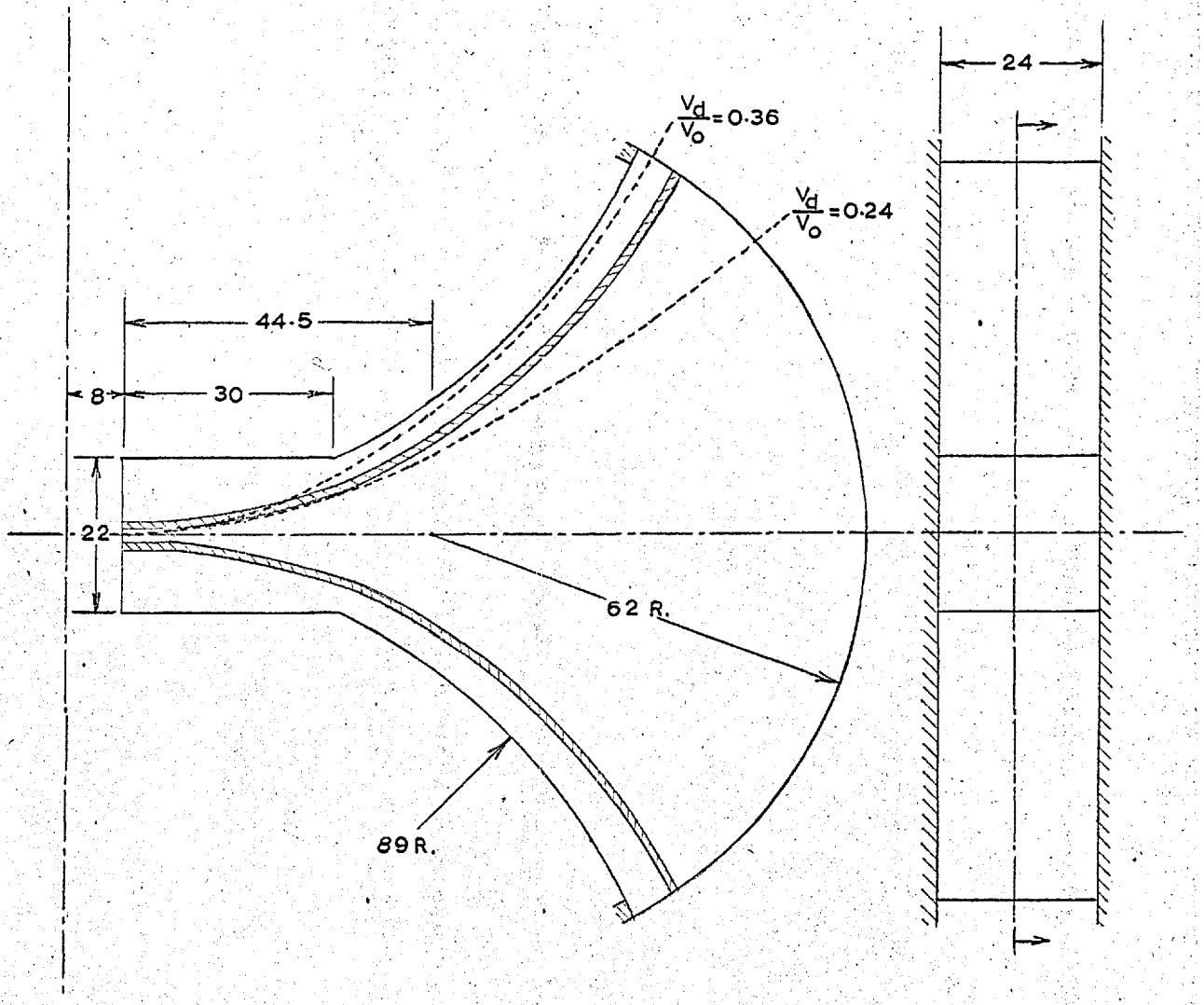


Fig. 3.17, Deflection System No. 11.

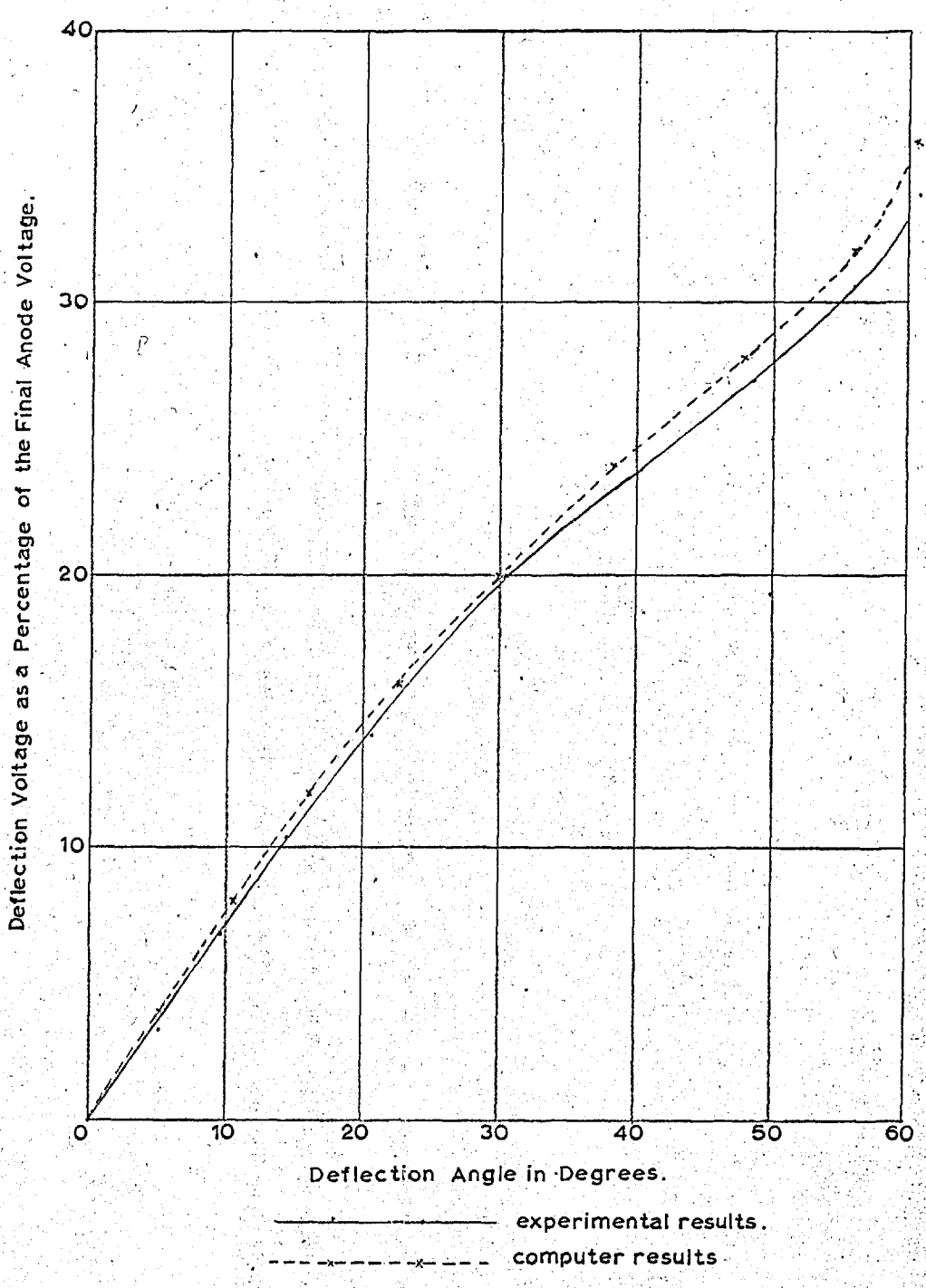
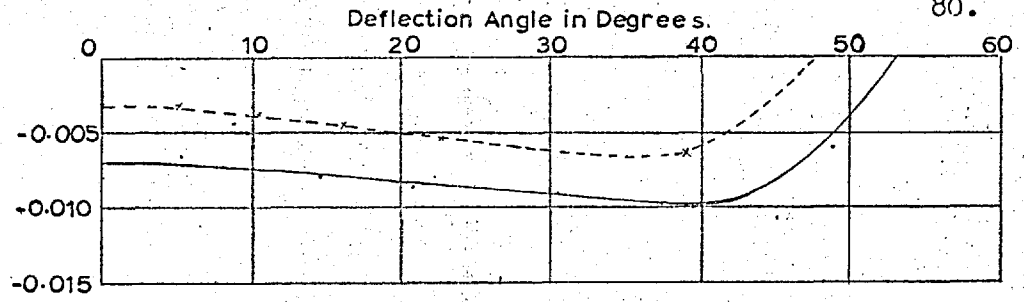
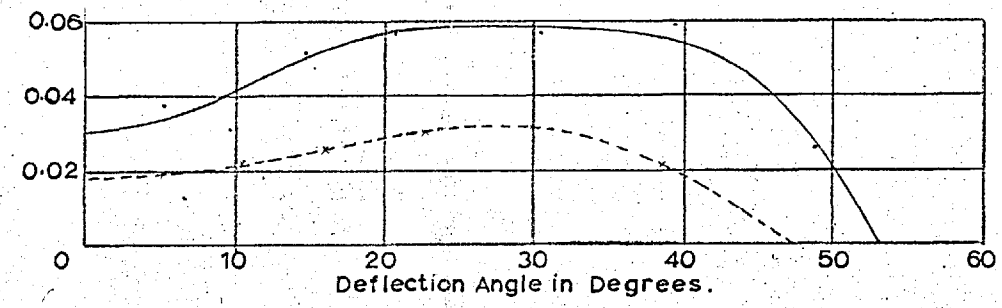


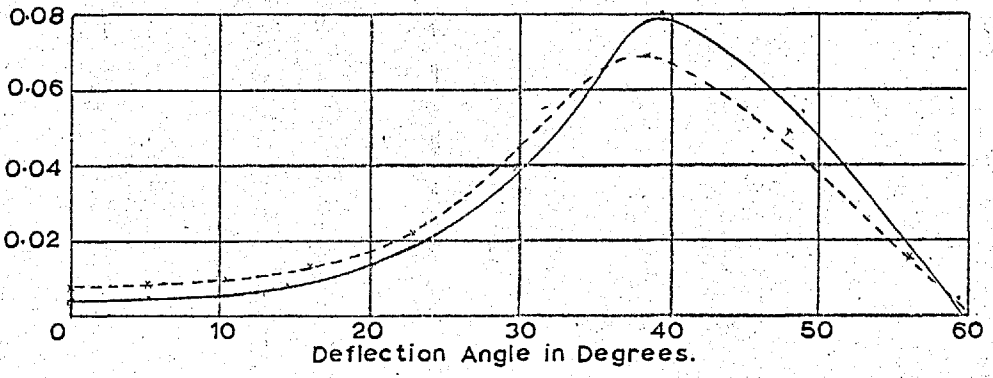
Fig. 3.18, Deflection Curve for Deflection System No. 11.



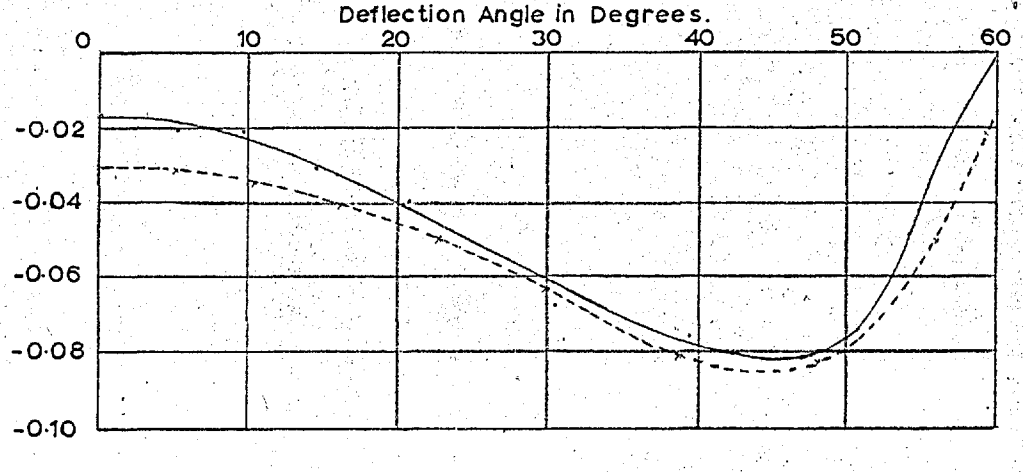
a). Reciprocal of Distance of Horizontal Crossover in Front of Accelerating Lens.



b). Horizontal Divergence Angle in Radians.



c). Reciprocal of Distance of Vertical Crossover in Front of Accelerating Lens.



d). Vertical Divergence Angle in Radians.

Fig. 3.19, Divergence of Beam Leaving Deflection System No. 11.

possible to reduce the aberrations in a system of this type by using electrodes at intermediate potentials. The results from the computer are in reasonable agreement with the experimental results for deflection system No. 11, although it seems as if the initial conditions of the beams were not quite the same in the x direction. This may have been due to a systematic error in the measurements on the deflection system, caused by the markings on the phosphor coated gauze, or it may have been due to an error in measuring the initial conditions of the beam. The discrepancy between the two curves in Fig. 3.18 at extreme deflection angles is almost certainly due to an inaccurate approximation for the field close to both the accelerating lens and the deflector plates. In the program, the potential due to the accelerating lens is added to the potential due to the remainder of the system, but, close to the deflector plates, the potential is, in a real system, hardly affected by the presence of the accelerating lens; thus, in the program, the potential in this area may be considerably higher than in a real system. The effect should be to decrease the angle through which the beam is deflected, which is exactly what has happened.

In both Fig. 3.15 and Fig. 3.18, the gradient of the deflection voltage against the deflection angle decreases with the deflection angle, but it increases again, in the case of deflection system No. 11 at extreme deflection angles. Now differentiating

(3.5) with respect to θ shows that this gradient is proportional to $\sec^2\theta_1$ in the parallel plate region; as $\sec\theta$ increases with θ, this seems to contradict the results of the measurements. However, the deflecting field in the curved region was very weak near the centre line of a system, but became stronger towards the deflector plates, so, in this region, the gradient under consideration decreases with the deflection angle. Thus the two regions have opposite effects on the gradient of the combined curve, but the curved region is the more important of the two. Close to the deflector plates of deflection system No. 11, the deflecting field became weaker, in the curved region, because of the presence of the electrodes which were maintained at the potential of the deflector plates, and lay between the central plates and the deflector plates. Hence the gradients of the curves in Fig. 3.18 start to increase at extreme deflection angles.

A comparison between the two deflection systems with regard to deflection defocusing is of particular interest because, in deflection system No. 8 (Fig. 3.16), the defocusing has been reduced by simulating a system with a larger value of h, whereas, in deflection system No.11 (Fig. 3.19), channel shaped deflector plates have been used. However, if a comparison is to be made, it must be reemphasized that the accuracy of the measurements was low and the initial conditions of the beams were not exactly the same. For both systems a beam was used which was initially

slightly diverging, because it was not possible to obtain a parallel beam of adequate diameter from the electron guns.

In deflection system No. 8, the effective value of h was quite large, so the magnitude of the variations of n and $\frac{dn}{ds}$, in the curved region, were much reduced compared to the variations indicated in Fig. 3.8 and Fig. 3.9, but the variations in the parallel plate region were not altered. Furthermore, in the curved region, the positions of the simulated deflector plates were the same as, or even outside, their actual positions, so the variations in n and $\frac{dn}{ds}$ were only significant at large deflections. Thus the horizontal divergence angle decreased, under the influence of the parallel plate region, until the deflection angle reached 45°, but beyond this angle the curved region became important, so the divergence angle started to increase again. The decrease in the divergence angle was accompanied by a decrease in the diameter, again due to the parallel plate region; this tended to keep the distance of the horizontal crossover from the accelerating lens constant, until the deflection angle reached 55°.

In deflection system No. 11, the curved region was far more important, because the effective value of h was much smaller than in the earlier system; the effects of the parallel plate region were small in comparison. Quite abrupt changes in the defocusing were produced by the transitions in potential, which occurred at the gaps between the central plates and the electrodes

at the potentials of the deflector plates, as if the deflector plates were inside their actual positions. Thus from Fig. 3.9, neglecting the effects of the parallel plate region, the horizontal divergence angle should increase for small deflection angles, but then decrease through zero, so that the beam should become converging at large angles of deflection. From Fig. 3.8, the diameter, after increasing for small deflection angles should decrease through zero to a negative value, indicating the presence of a horizontal crossover within the deflection system. Hence the horizontal crossover was initially at a fairly constant distance from the accelerating lens, well behind the deflection system; as the divergence angle went towards zero, the distance of the crossover from the accelerating lens tended to infinity, and the reciprocal of the distance went to zero. When the beam became converging, the crossover occurred in front of the system, but it shifted inside as the diameter became negative.

In the horizontal plane, the effect of the accelerating lens on the beam is negligible, because the radius of curvature of the equipotentials, although large, compensates almost exactly for the convergence which occurs when the electrons are accelerated. However, in the vertical plane the equipotentials have the shape and effect of a convex lens, so an initially divergent beam leaves the system, converging to a vertical crossover, which is in front of the accelerating lens. The strength of this converging lens depends on the voltage through which the electrons are accelerated,

so the lens is strongest at zero deflection and weakest for large deflection angles.

Apart from the accelerating lens, it is simpler to predict the defocusing in the vertical plane, because it only occurs in the curved region. We have seen that, in deflection system No. 8, the large effective value of h reduced the magnitude of the variations of n and $\frac{dn}{ds}$; it also reduced the magnitude of the variations of y and $\frac{dy}{ds}$. Thus the divergence angle slowly became more negative as the deflection angle increased, though, at extreme deflections, it started to become less negative. The distance of the vertical crossover in front of the accelerating lens decreased as the divergence angle became more negative, and the diameter decreased slightly; this tendency was reversed at extreme deflection angles. Deflection system No. 11 had a relatively small effective value of h, so, as in the horizontal plane, the variations in y and $\frac{dy}{ds}$ were much more marked and relatively abrupt changes occurred at smaller deflection angles. Thus the plots of vertical defocusing have the same general shape as those of deflection system No. 8, but the fluctuations in both the divergence angle and the position of the vertical crossover were much greater; also the transitions from increasing magnitude to decreasing magnitude occurred at smaller angles of deflection.

Although the theory in section 3.3 was extended to cover the c-error, the experimental measurements of this aberration were of little use, except as a check on the computer program, because the

errors were so large. However, as the computer program does calculate the c-error, it can be taken into account when deflection systems are compared using computer results only.

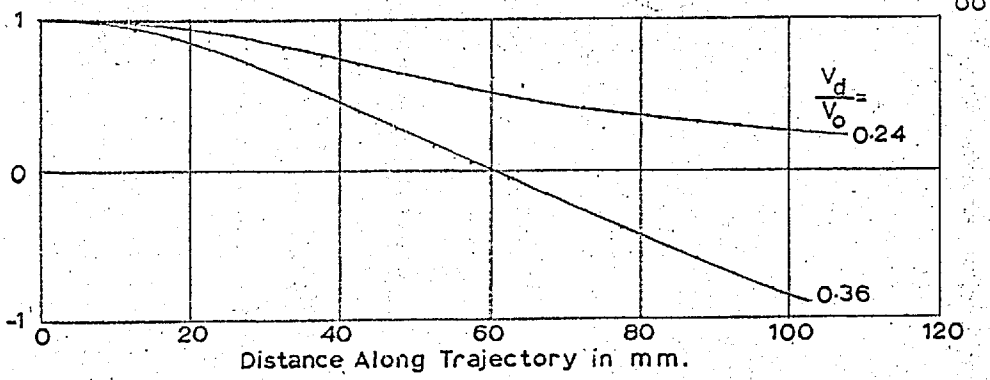
In addition to being used for comparing deflection systems without having to build and test physical models, the computer program may be used to find out in which part of a deflection system the aberrations arise. At each point of a trajectory the program prints out, among other information, the diameters of the beam in the x and y directions; thus a profile of the beam diameter can be plotted throughout the length of a trajectory. Although such a profile is of considerable interest, a better indication of the areas where the aberrations occur is given by plotting the change in divergence angle per unit length, over the length of a trajectory. As the points, at which the diameter is known, occur at regular intervals along a trajectory, the change in divergence angle per unit length may be obtained by taking the second difference of the diameters and dividing by the square of the interval between adjacent points.

In Fig. 3.20, the profiles of the beam in both the x and y directions have been plotted for deflection system No. 11, with three different values of deflection voltage; the beam was assumed to have been parallel and to have had a diameter of 1 millimetre, before it entered the deflection system. The changes in divergence angle per unit length were calculated, and these

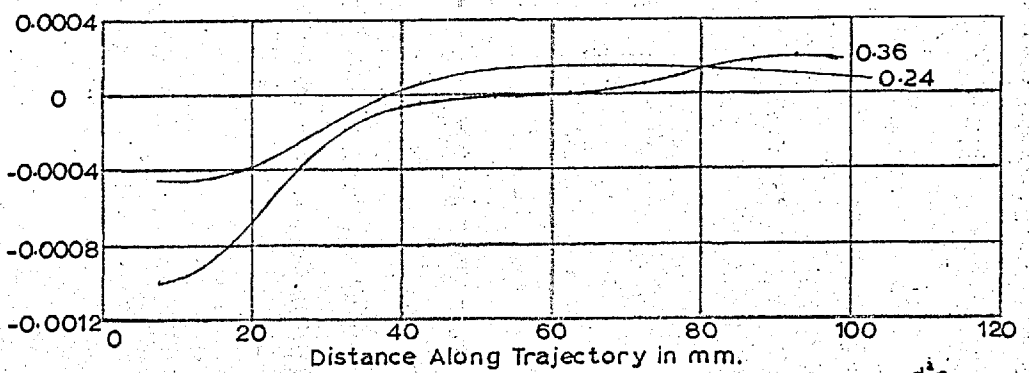
have been plotted in Fig. 3.20 too. The principal trajectories for these values of deflection voltage have been added to the drawing of deflection system No. 11, Fig. 3.17.

In the horizontal plane, the diameter of the beam remained unchanged when the deflection voltage was zero, but the beam tended to converge as the deflection voltage increased. The change in horizontal divergence angle per unit length, which is, in fact, $\frac{d^2n}{ds^2}$, was initially negative, particularly for the larger deflection voltages, but it rapidly decreased and was even slightly positive for the remaining two-thirds of the trajectories. Now the potential distribution which causes the defocusing is related to $\frac{d^2n}{ds^2}$ by (3.18), so the field which produced the convergent tendency occurred right at the back of the system, in the parallel plate region; the field tended to make the beam diverge slightly in the curved region, but this could not overcome the convergence from the parallel plate region.

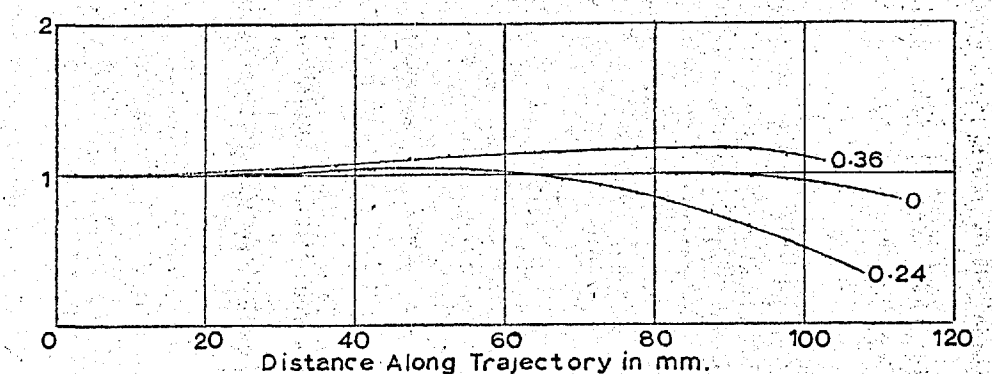
In the vertical plane, the accelerating lens made the beam converge near the end of all the trajectories, but the trajectory where $\frac{V_d}{V_o}$ was 0.24 converged more than either of the others. The reason is apparent in Fig. (3.20 d.). Although $\frac{d^2y}{ds^2}$ was slightly positive in the parallel plate region, it tended to become negative in the curved region, particularly for the trajectory where $\frac{V_d}{V_o}$ was 0.24. This trajectory lay just inside the edge of the central plate and (3.42) and Fig. 3.7 indicate



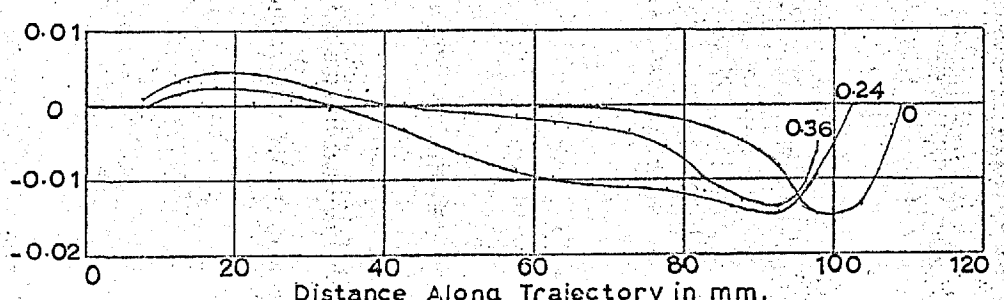
a). Horizontal Diameter, n.



b). Change in Horizontal Divergence Angle per Unit Length, $\frac{d^2n}{ds^2}$.



c). Vertical Diameter, y.



d). Change in Vertical Divergance Angle per Unit Length, $\frac{d^2y}{ds^2}$

Fig. 3.20, Beam Profiles for Initially Parallel Beam.

that the value of $\frac{d^2y}{ds^2}$ is likely to have a minimum here. The effect of the accelerating lens can clearly be seen in Fig. 3.20(d); it occurs at slightly different distances from the beginning of a trajectory, depending on the deflection angle.

CHAPTER 4. THE COLLIMATOR AND REVERSING LENS.

4.1. Requirements of a collimator.

We have seen that the collimator is an electrostatic lens which is used to straighten the electron beam after it has been deflected. It is essential that the electron beam should be vertical in the screen region, because the effect of a horizontal component of velocity is to produce severe distortion. In the earlier version of the tube a magnetic collimator was used which was sufficiently short to be placed between the reversing lens and the screen region. However, an electrostatic collimator must be much longer, so there is not enough room for it in that position. The only place for it is between the deflection system and the reversing lens, although the deflection system must then swing the beam through large angles in order to produce sufficient width of scan. This means that the deflection voltage will be excessive unless post deflection acceleration is used, so an accelerating lens must be incorporated in the collimator. In addition, it is desirable that the collimator should compensate some of the aberrations of the deflection system, although this is difficult to achieve in practice. Since the field inside the collimator does not vary with time, it is possible to use a large number of electrodes fed from a high resistance chain.

The problem of design can be divided into two stages:

1) design an ideal collimator,

2) modify it to compensate for aberrations in other components.

It was possible to use a theoretical method to design the ideal collimator, which was fortunate, because it would have been extremely difficult to do this experimentally, in view of the large number of electrodes. The accelerating lens was designed separately, also by a theoretical approach in which (3.9) was used, and then added to the collimator. The whole of the accelerating lens was originally considered with the collimator, but later part of it was considered with the deflection system for experimental convenience. First priority in the design of the collimator was given to the requirement that the principal trajectories should be deflected through the correct angle; the aberrations in the x-direction due to the collimator cannot be great if this is so. Once the collimator had been built and tested, experimental methods were used to find suitable modifications for compensation of aberrations in other components.

4.2. Theory and design of the collimator.

This section is a brief summary of the thesis by Miss J. Smith entitled: "An Electrostatic Collimator for the Flat Television Tube"[6] which was submitted for the Diploma of Imperial College in April 1962. This summary is included in order to permit comparison

between the methods used for the design of the deflection system and those used for the collimator.

The object was to design an electrostatic lens such that:

i) rays issuing from a deflection centre, C, (Fig. 4.1) in a plane fan should be deflected so as to form parallel rays at a line, c, in the plane;

ii) the potential near the deflection centre should be one quarter of the potential along c, which should be unity;

iii) there should only be one focus in the y-plane.

The method which was used was based on that developed by D. Gabor for designing the reversing lens of the earlier version of the tube. It involved finding the electrostatic potential distribution within the lens which gave the required trajectories.

An orthogonal curvilinear system of coordinates (u,v,w) was used, in which the principal ray surface lay in the plane $w = 0$ and the principal rays were the v = constant lines. For a system of this nature,

$$ds^2 = dx^2 + dy^2 + dz^2 = h_1 du^2 + h_2 dv^2 + h_3 dw^2$$

where h_3 may be taken as unity.

Two other important equations which were derived are:

$$h_{1\,u,o}\,\phi_{u,o} = h_{1\,u,v}\,\phi_{u,v} \qquad (4.1)$$

and

$$\phi\, w'' + \phi' w' = \frac{h_o \phi_o}{2\phi} \frac{\partial^2 \phi}{\partial w^2}\, w \qquad (4.2),$$

where ϕ is the potential and primes indicate differentiation with respect to u.

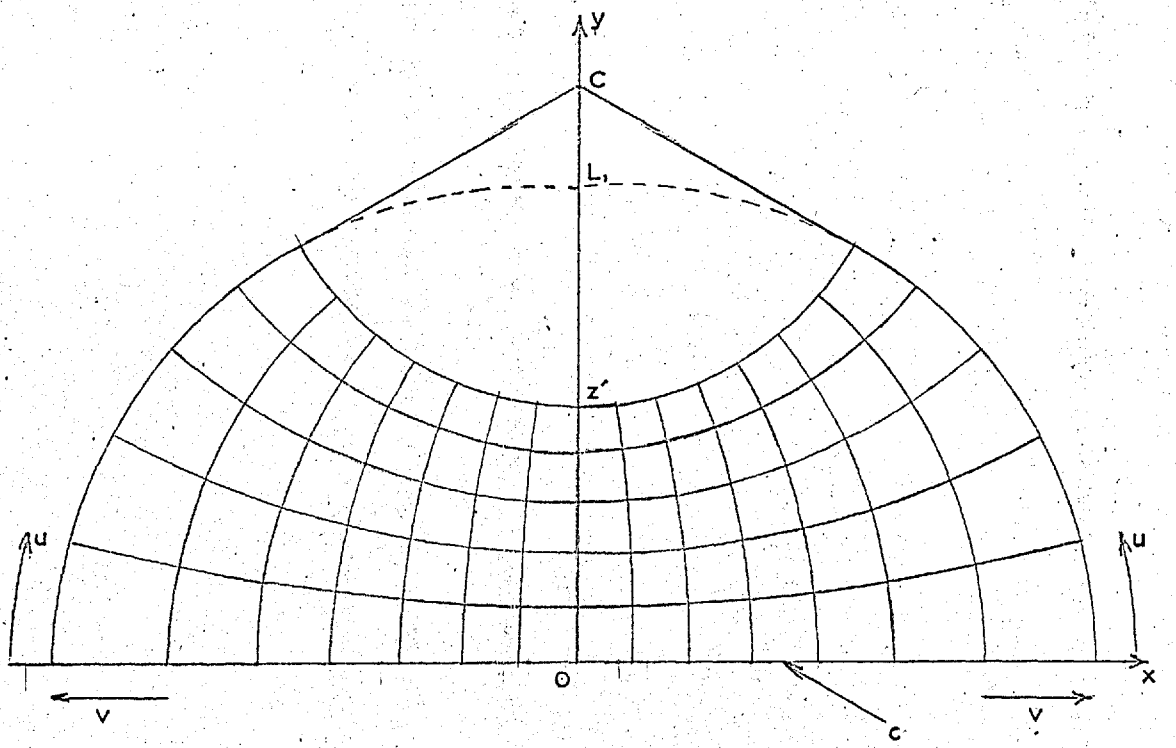


Fig. 4.1, First Coordinate System for Collimator.

Initially the transformation between the (u,v) plane and the (x,y) plane was assumed to be

$$u + jv = \log_e \frac{z - z'}{z - z''} \qquad (4.3)$$

where $z = x + jy$.

This is a system of coaxial circles with limiting points at z' and z''; a mesh of u and v lines was constructed for it, which covered the area of the collimator. In this particular system,

$$h_1 = h_2 = h \qquad (4.4)$$

and

$$\sqrt{h} = \frac{\frac{1}{2} z' - z''}{\cosh u + \cos v} \qquad (4.5)$$

so it was possible to calculate the potential at all the mesh points using (4.1) and assuming ϕ to be unity on the line $v = 0$. Unfortunately, the coordinate system assumed was not entirely suitable, because discontinuities in the radius of curvature of the principal rays occurred at both ends of the system, so it would have been physically impossible to produce the field. Therefore the mesh was modified, keeping the u = constant lines at the ends of the system the same. The new u = constant lines were made circles, and the v = constant lines were drawn orthogonal to them; in the new system h_1 was no longer equal to h_2. When the new mesh had been constructed and the potentials at the mesh points had been calculated, the trajectories of the electrons in the (w,u) plane, along the v = constant lines, were calculated using (4.2).

The accelerating lens was assumed to be a plane slot lens, with potential given by (3.9), where the principal rays travelled along the X-axis. The focal length of the lens was determined by integrating the paraxial ray equation (3.19) and obtaining the electron trajectories. The lens was then modified by adding an extra electrode at an intermediate potential which increased the focal length. When the results for the collimator and the accelerating lens were considered together, it became clear that the convergence of the collimator was too strong, so the u,v mesh was modified again. The potential distribution in this final system in the planes $w = 0$ and $w = 1.2$ are shown in Fig. 4.2 and Fig. 4.3.

4.3. Practical work on the collimator.

The theoretical design of the collimator was checked with a model which was tested in the electrolytic tank; the measurements indicated that there were no major errors in the electrode configuration, although the potential distribution in the plane $w = 0$ was not exactly that shown in Fig. 4.2. Some discrepancy had been expected, because the potential distribution in the plane $w = 1.2$ had been calculated assuming

$$\phi_w = \left(\phi\right)_{w=0} + \frac{1}{2} w^2 \left(\frac{\partial^2 \phi}{\partial w^2}\right)_{w=0}$$

which is hardly accurate when w is as large as 1.2. However, when the electron trajectories were plotted, it became apparent that the errors in the potential distribution were not very important.

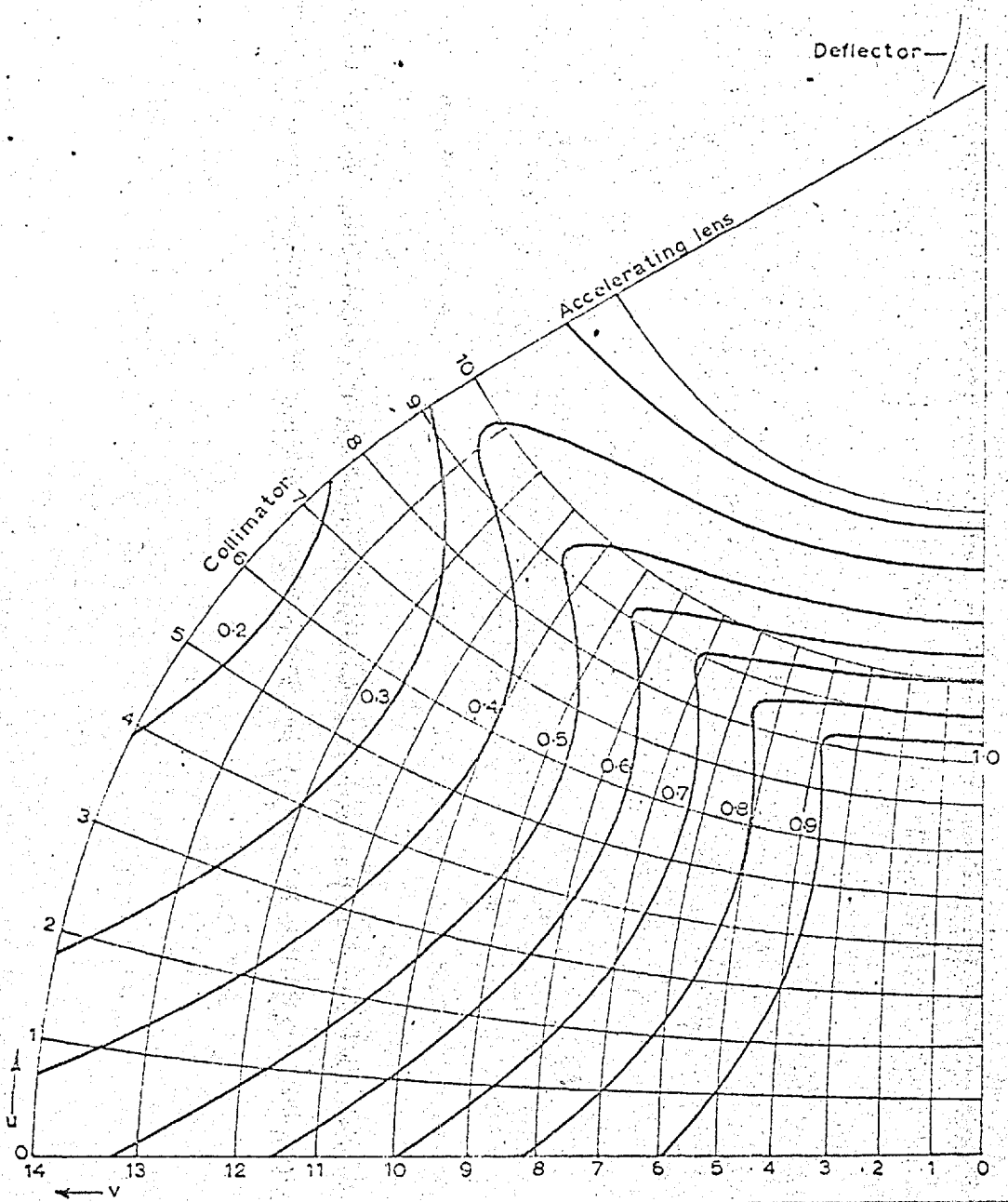


Fig. 4.2, Collimator Potentials in the Plane W – 0,
(by permission of Mrs. Wittington).

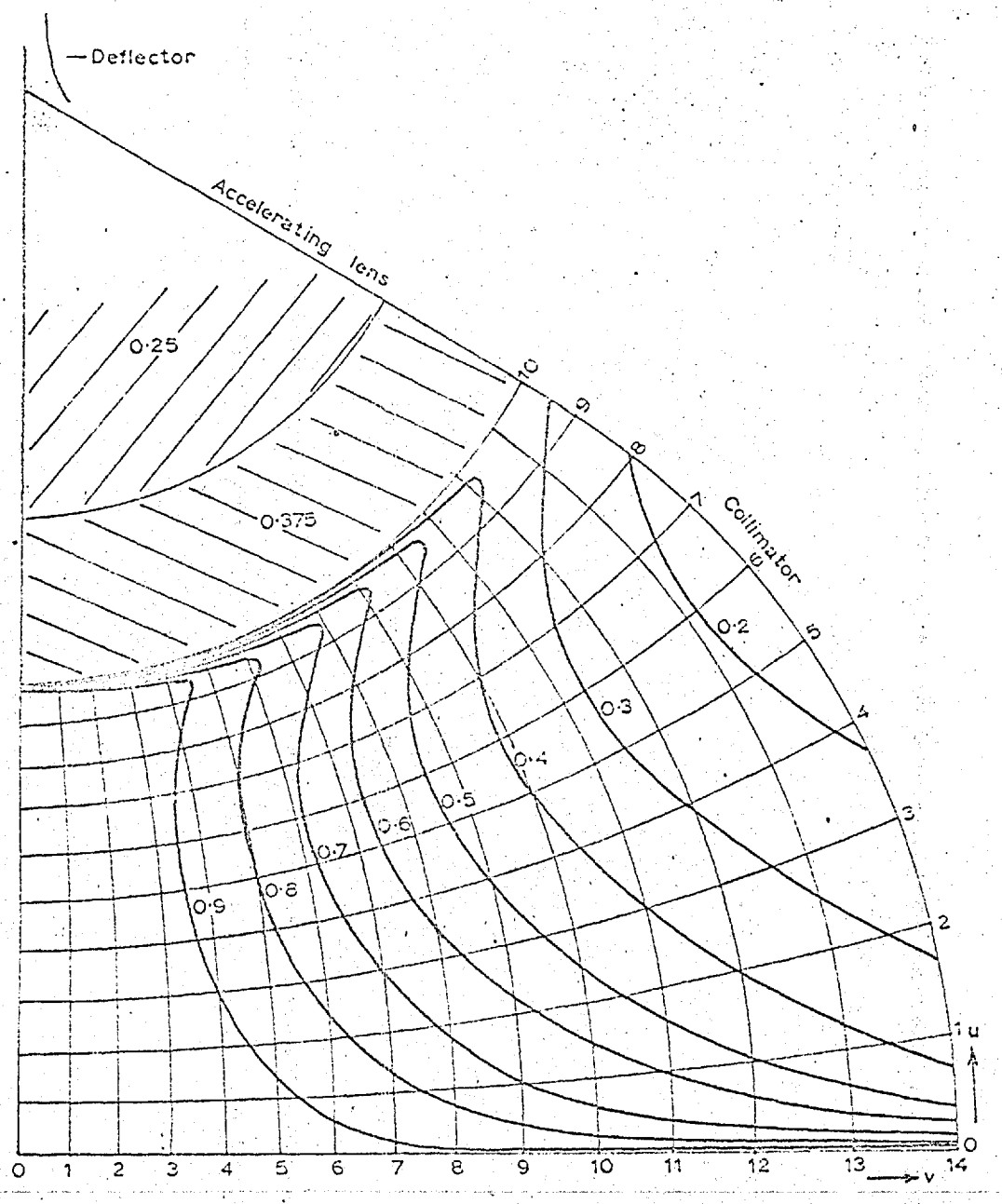


Fig. 4.3, Collimator Potentials in the Plane W= 1.2,
(by permission of Mrs. Wittington).

After some small corrections had been made to the electrode configuration as a result of the experiments in the electrolytic tank, the collimator was tested in the vacuum tank. At this time the primitive deflection system and poor alignment made measurements on the defocusing of the collimator almost worthless; however it was clear that the equipotentials were too close together in the v direction, as the beam tended to be bent through too large an angle. Soon afterwards, the general trend of the defocusing errors in the deflection system became apparent, so, in the next design, the area of minimum potential was moved towards the reversing lens, in order to compensate for these errors; in addition, the distance between the equipotentials in the v direction was increased. Later the collimator was modified again, in order to reduce irregularities in the potential distribution, which were apparent in a three-dimensional model of the electrode potentials plotted against the u and v coordinates.

It is only possible to assess the merit of a collimator when considering it in conjunction with a deflection system, because the best collimator is one for which the defocusing is exactly compensated by the deflection system. Thus measurements on either component alone are of limited value. Anyhow, it has not been possible to determine the defocusing properties of the collimator by itself, because these could only have been found by considering the difference between measurements on the deflection system alone and measurements on the deflection system and

collimator combined; the low accuracy of both sets of measurements made this method impossible. For these reasons, the development of the collimator was carried out at the same time as the development of the deflection system. The number of modifications, which have been made to the collimator in the course of its development, has been less than the number made to the deflection system, partly because a collimator took longer to build and partly because much less development was required, thanks to the theoretical design. Nevertheless, it is probable that the combination of deflection system No.11 and collimator No. 5 could still be improved upon.

A print from the master for the printed circuit boards of collimator No. 5 with deflection system No. 11 is given in Fig. 4.4; results of measurements on this combination, with the same initial beam conditions as before, have been plotted in Fig. 4.5 and Fig. 4.6. The deflection curve for the collimator and deflection system together, Fig. 4.5, has the same general shape as that of the deflection system alone, Fig. 3.18. Hence the distance of the beam from the centre line, where it left the collimator, was roughly proportional to the deflection angle where it entered it; the irregularities in the deflection curve appear to have come from the deflection system.

In the plots of divergence, Fig. 4.6, there seems to be a slight discontinuity at the centre line, particularly for measurements in the horizontal plane. There is no sign of this

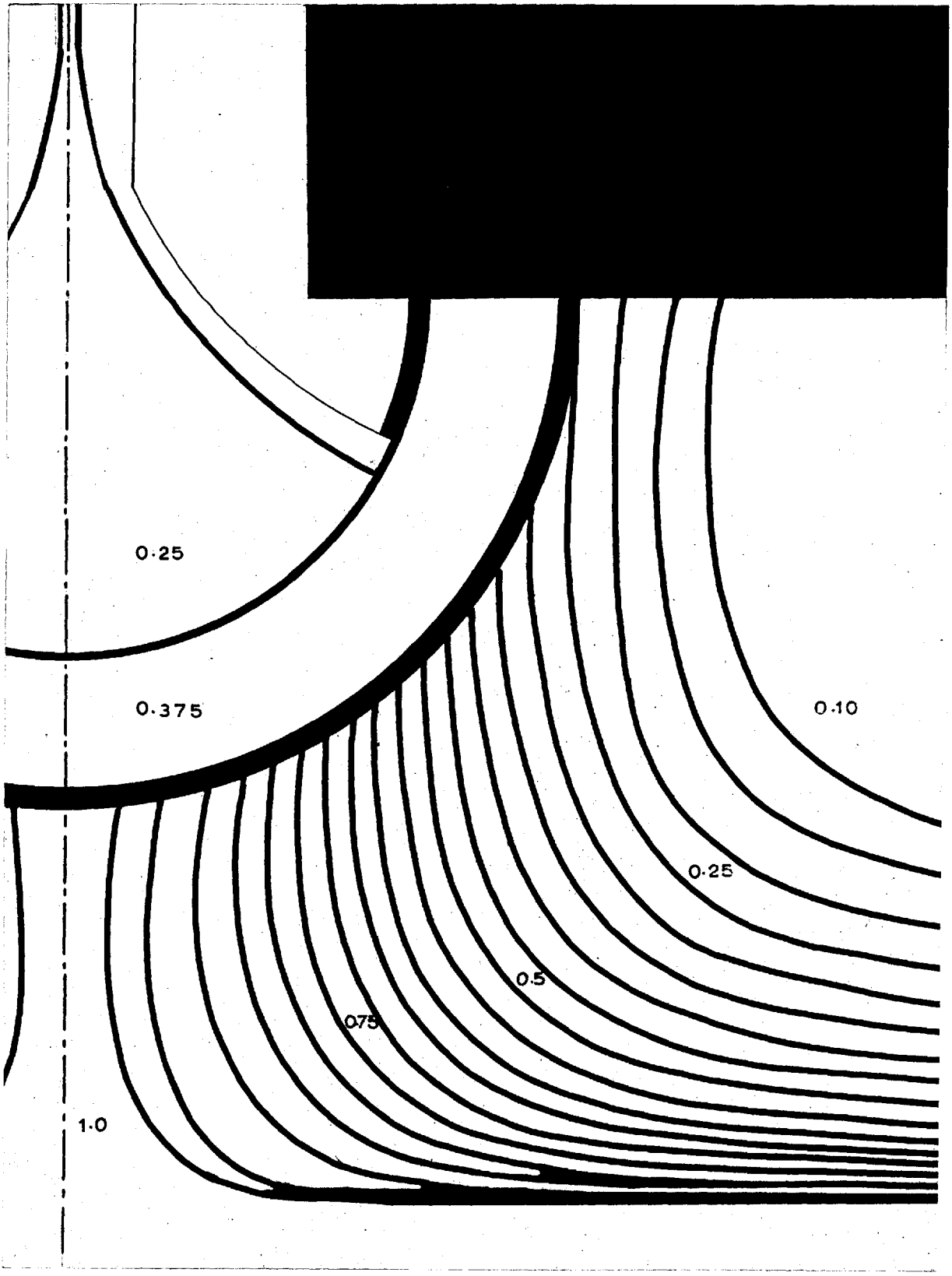


Fig. 4.4 : Part of print from Master for printed circuits forming latest collimator and deflection system.

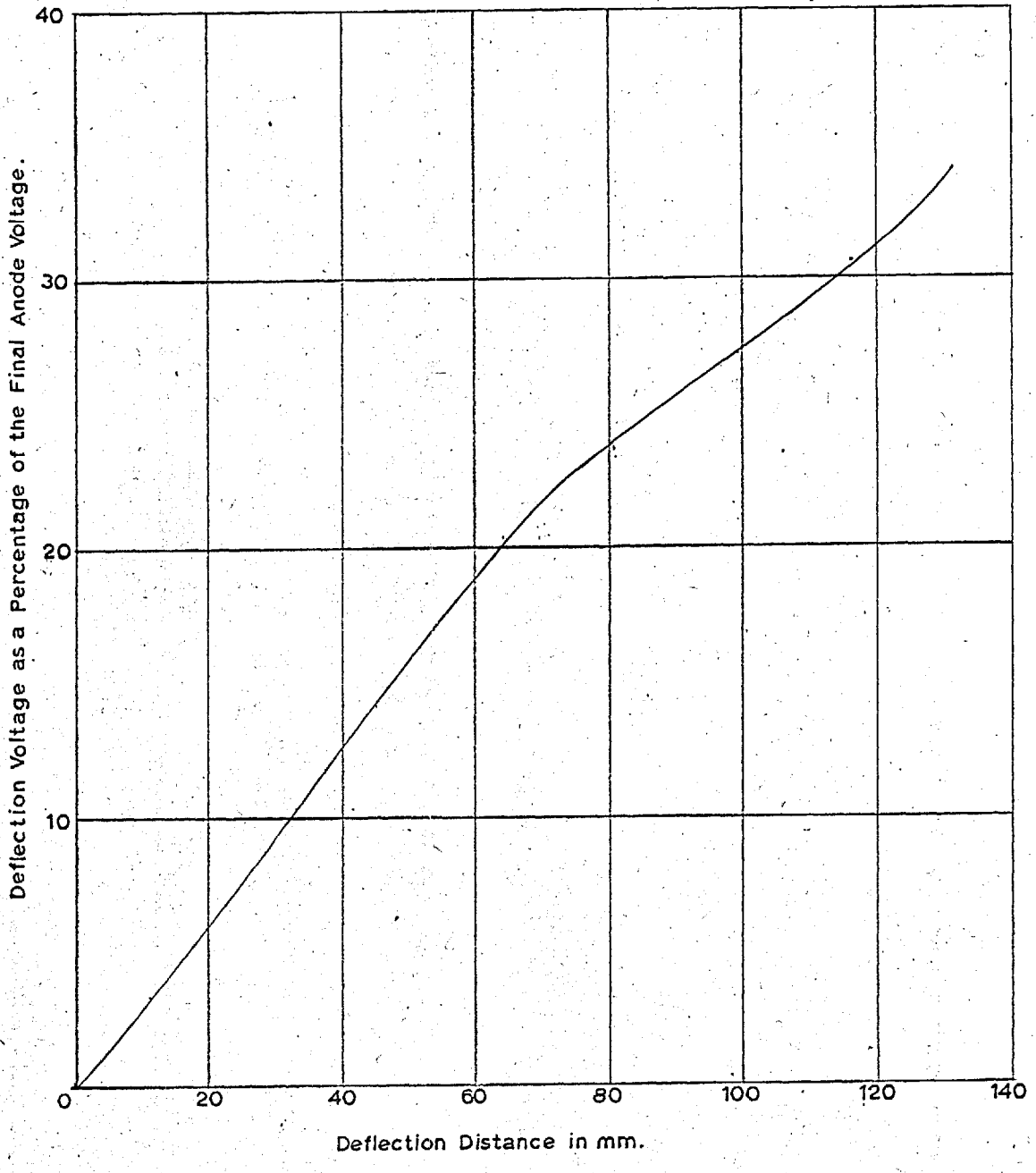
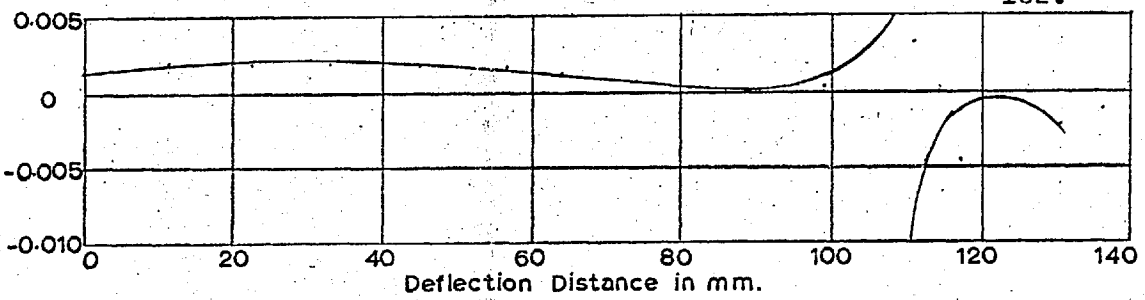
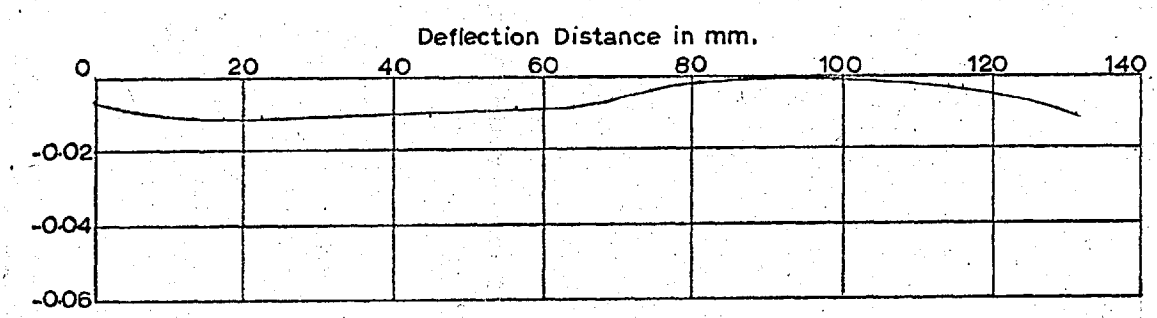


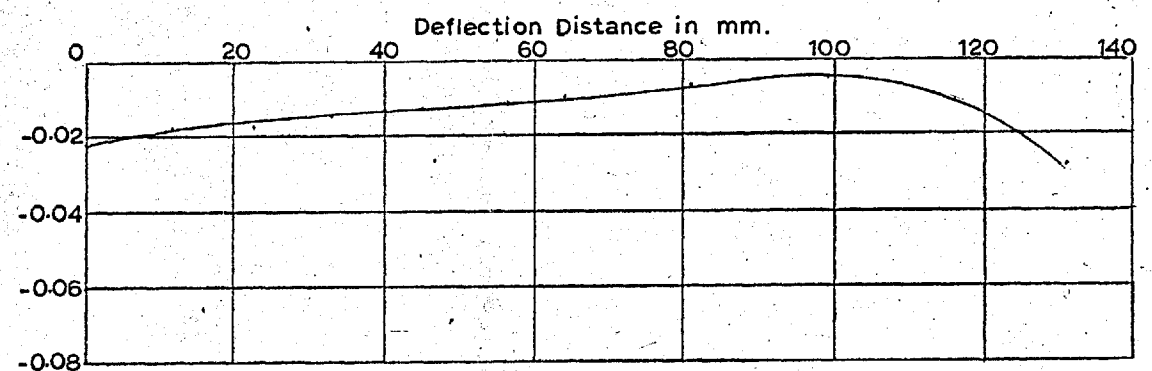
Fig. 4.5, Deflection Curve for Collimator No. 5 with Deflection System No. 11.



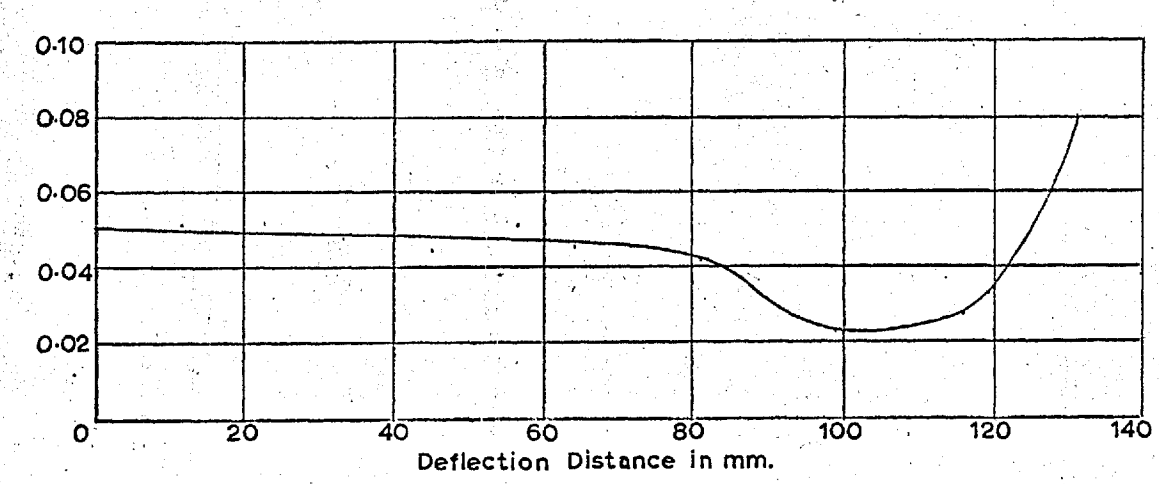
a). Reciprocal of Distance of Horizontal Crossover in Front of Collimator, $(mm.)^{-1}$



b). Horizontal Divergence Angle in Radians.



c). Reciprocal of Distance of Vertical Crossover in Front of Collimator, $(mm)^{-1}$



d). Vertical Divergence Angle in Radians.

Fig. 4.6, Divergence of Beam on Leaving Collimator No. 5.

effect in the results for the deflection system alone, so it must have come from the collimator. The most likely explanation is that the potential steps between the electrodes were too large near the centre line, so there were local irregularities in the potential distribution, although the two potential steps nearest the centre line were only 0.0125 and 0.0375 while all the others were 0.05. At the centre line $\frac{\partial \phi}{\partial w}$ was equal to 0 and $\frac{\partial^2 \phi}{\partial w^2}$ was almost certainly a maximum, so the divergence, which depended on $\frac{\partial^2 \phi}{\partial w^2}$, must have been critically dependent on the potentials of the surrounding electrodes.

For small deflection angles, the beam was convergent in the horizontal plane after it had left the collimator, although it was diverging when it left the deflection system. This is hardly surprising, because the principal rays entered the collimator radially from the deflection centre, but were parallel to each other when they left it, so, in the horizontal plane, the collimator was effectively a converging lens, with its focus at the deflection centre. Since the horizontal crossover of the beam, when it left the deflection system, was well behind the deflection centre, a real crossover could be expected to occur in front of the collimator, which would mean that the beam would be converging when it left the collimator. When this converging effect has been taken into account, the general shapes of the plots of the horizontal divergence appear to be similar to the corresponding curves for the deflection system alone, although the variations

in magnitude were much reduced by the presence of the collimator. The horizontal crossover shifted into the collimator from in front of it at large deflections, but this was to be expected, because this crossover occurred inside the deflection system at slightly larger deflections; the sign of the divergence angle was assumed to remain unchanged when this happened. In general, the collimator acted as a converging lens of almost constant focal length in the horizontal plane.

The collimator had a converging effect in the vertical plane, which occurred mainly in the second part of the accelerating lens, so there was always a vertical crossover inside the collimator. The general shapes of the vertical divergence plots are again similar to those for the deflection system by itself, although the variations in the vertical convergence angle, and hence in the position of the vertical crossover, were much reduced. As the deflection increased, the potential difference at the second part of the accelerating lens became less; although this introduced a potential increase inside the collimator proper, it was quite gradual, so the effective converging power of the collimator was reduced, thus compensating for the increasing convergence from the deflection system up to quite large deflections.

Although the variation in the defocusing of the beam when it left the collimator was considerably less than when it left the deflection system, it was still rather too large for a high definition television picture. It might be possible to improve

the collimator and deflection system sufficiently, but it would be easier to leave the deflection system and collimator as they are, and to use dynamic refocusing, by applying a voltage proportional to the square of the deflection voltage to the focus electrode of the writing gun. Full correction in both horizontal and vertical directions would require, of course, an astigmatic gun. As an alternative the vertical corrections could be applied in or near the reversing lens.

4.4. The Reversing Lens.

Previous workers on the flat tube have put a great deal of effort into the development of the reversing lens, so the writer was able to use their designs, suitably modified, spending little time on this component. In the earlier work, after careful investigations, Stuart[2] found a satisfactory cross section for the central plane; he then extended the design for beams at other angles of deflection. Upadhyay[5] found that the aberrations could be reduced, by replacing the rounded spine, by one which was shaped like an inverted T. In addition to designing a satisfactory reversing lens, these workers acquired a good insight into the working of the lens.

In the new version of the tube, the reversing lens has been made much less complicated than it was in the earlier version by the presence of the collimator between the lens and the deflection system, as this causes the beam to enter the reversing lens

travelling vertically downwards, for all angles of deflection. Previously the beam had entered the reversing lens at an angle to the vertical, which depended on the angle of deflection, and one of the functions of the lens had been to increase the angle of deflection, so the lens had been essentially three-dimensional. The central cross-section of the earlier lens has been taken as the cross-section of the new lens, which was symmetrical along its length, except at the extreme ends.

The other important difference between the two designs is due to the presence of a vertical crossover inside the electrostatic collimator, which has made the beam divergent in the y direction when it entered the reversing lens. In the earlier version, the beam had been almost parallel in this direction. In both versions of the tube, it has been essential that the beam should be parallel in the y direction when it left the reversing lens, so the new lens has been required to have a converging effect in this plane.

In the central plane of the earlier reversing lens, which was symmetrical about the vertical axis, the principal trajectories were identical in both the front and the back halves, because the beam was virtually parallel on entering, as well as on leaving, the lens. Hence, the optic axis could be defined as a trajectory, initially parallel to the axis of symmetry, which intersected the axis of symmetry nearer to the repeller than any neighbouring trajectory which was initially parallel to the axis. As this lens was symmetrical and telescopic, a narrow pencil of rays near

the optic axis was free from second order aberrations. However, the new lens is not telescopic, so these conditions no longer apply. Indeed as the divergence of the beam at entry differed from the divergence at the exit, the marginal trajectories were no longer symmetrical, so either the principal ray or the lens itself had to be asymmetrical. As the difference between the central cross section of the old lens and the cross section of the new lens was relatively small, it was decided to find the required modifications by making small changes to a few parameters on a model in the vacuum tank. The two most convenient parameters to vary were the horizontal and vertical position of the repeller; it no longer mattered if the lens was not symmetrical. Stuart's work indicated that the position of the spine was not critical, so changing these parameters effectively varied the distance of the principal trajectory from the central axis of the lens on entry, and the gap between the repeller and the positive side electrodes.

As a result of the experiments in the vacuum tank, it was found that shifting the repeller 1 millimetre towards the screen deflected the beam through 0.05 radians towards the screen, with very little effect on the divergence angle. Also, decreasing the gap between the repeller and the positive side electrodes by 1 millimetre increased the divergence angle by 0.005 radians and deflected the beam through 0.004 radians towards the screen. Second order errors were visisle when the measurements were being

made, but they were not unduly large. The reversing lens required readjustment when a mumetal magnetic screen was fitted, indicating that it had been affected by stray magnetic fields, but it was impossible to repeat the measurements with the magnetic screen in place. The cross-section of the lens is shown in Fig. 4.7. Trajectory plots for the earlier lens are shown in Fig. 4.8.

At the ends of the lens, some form of termination was required, in order to prevent the beam from being affected by the build up of electrostatic charge on the nearby insulating surfaces of the envelope. Instead of a large number of electrodes at different potentials, which would have eliminated distortion of the potential distribution, semi-circular electrodes were fitted to either end of the lens, as shown in Fig. 4.7. The optimum potential for these electrodes was found to be 0.75, so they were connected to the collimator resistor chain at the appropriate point. In addition, the ends of the repeller were filled in with a conducting surface, which was maintained at the potential of the repeller itself. Although the potential distribution at the termination was not exactly the same as in the central plane of the reversing lens, the difference was small. The effect of the error was to deflect the beam in the x direction towards the middle of the tube, but this was easily compensated by adjusting the potentials in the collimator, so that at extreme deflections, the beam had a small horizontal component of velocity away from the

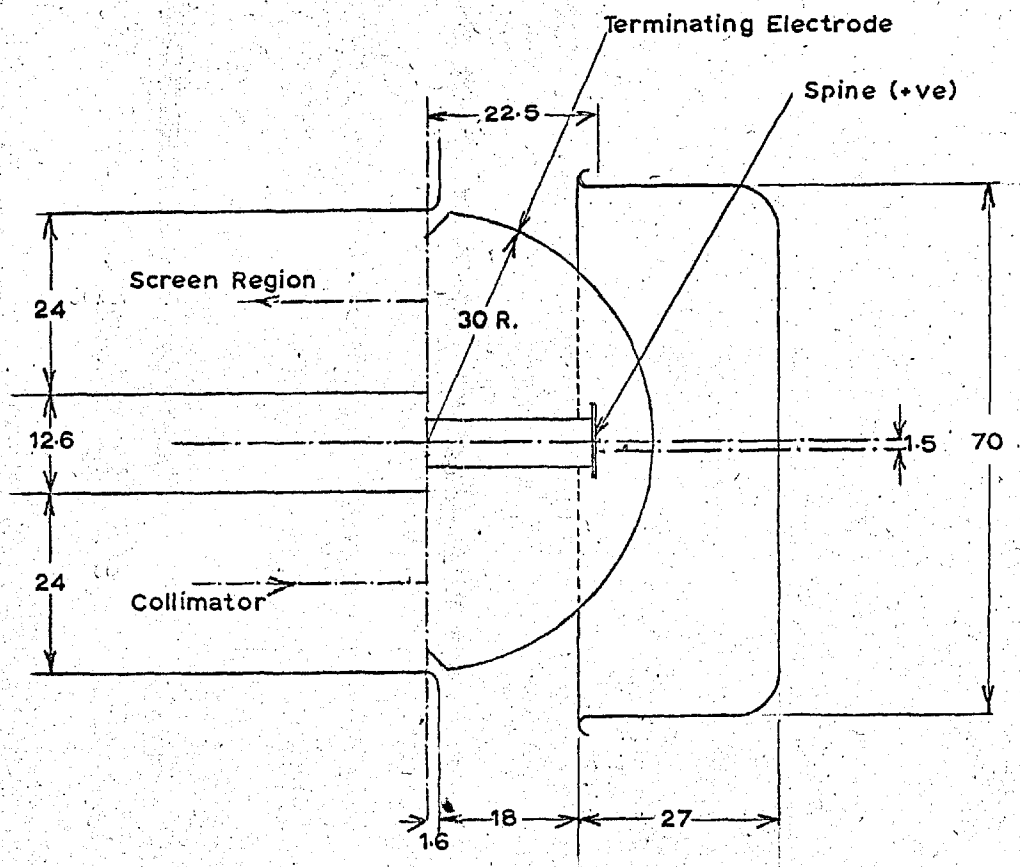


Fig. 4.7, Cross Section of the Reversing Lens.

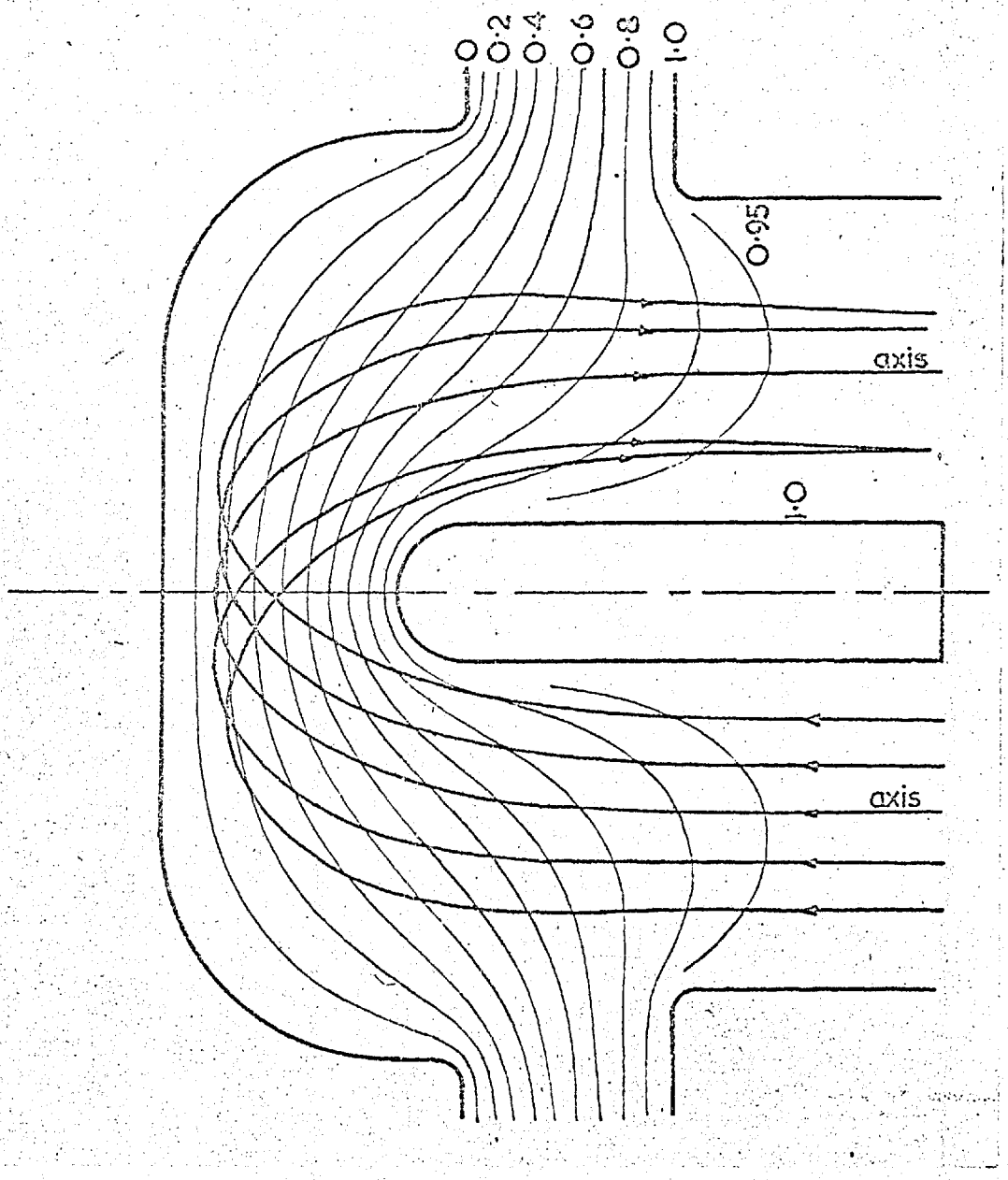


Fig. 4.8, Electron Trajectories in the Reversing Lens, (by permission of Dr. P. Stuart).

centre line when it left the collimator. Hence the errors in terminating the reversing lens gave a small but useful increase in deflection sensitivity at extreme deflections.

We have seen that it was necessary to modify the central cross-section of the earlier reversing lens in order to compensate for the divergence angle of the beam in the y direction as it left the collimator. However the results in section 4.3, in particular those in Fig. 4.5(d), indicate that the divergence angle of the beam was not the same for all angles of deflection; but this variation could be compensated by changing the correction for the divergence angle. This would involve varying the cross-section of the lens for different deflections.

Although the second order aberration was small, it might cause considerable difficulties in a colour version of the tube. However, it could easily be eliminated by fitting a converging lens between the collimator and the reversing lens, so that the beam would be parallel on entering the reversing lens. This extra component would increase the height of the tube slightly, but, if it were a linear version of an einzel or unipotential lens, it could be incorporated into the collimator in the same way as the accelerating lens. Compensation for variations of the divergence angle in the y direction could be carried out by changing the width of the central (negative) electrode; therefore the reversing lens would be symmetrical along its length and have the same cross-section as the earlier reversing lens. A further advantage of

fitting a converging lens would be that the effective principal plane, in the y direction, would be much closer to the crossover inside the collimator, so the diameter of the beam, in this direction, would be much less in the screen region, which would help to reduce the spot size.

CHAPTER 5. THE SCANNING ARRAY.

5.1. Introduction.

Undoubtedly the most unusual component in the flat tube is the scanning array, as it functions in a completely different manner to any other electronic device. Although the latest form of the scanning array is essentially similar to the earlier design, the writer has devoted a considerable amount of time to the development of this component. The earlier design had been shown to work in principle, but it was never entirely satisfactory. This was attributed to imperfections in the other components, so attention tended to be concentrated on improving the collimator and reversing lens, rather than the scanning array. It took some time to develop a satisfactory method of construction for the old array, because it had so many elements. When printed circuit techniques were used, flashover occurred across the surface of the substrate because the distance between adjacent strips was so small, but, when each strip was made separately, the whole array took a very long time to build. Thus it is not surprising that the scanning action had not been examined more closely, especially as it is difficult to take measurements on an array. Since the scanning process is essentially dynamic, static measurements are of little significance and a change in the capacitance of a strip, due to the presence of a normal measuring probe, would disturb the scan. Details of the methods which the writer has used for

measuring the performance and observing the operation of the scanning array have been described in section 2.5.

In the new design, the provision of separate rundown and flyback guns has eliminated the influence of the other components on the scanning action. A further advantage of this arrangement is that the rundown current can be supplied throughout the rundown period, instead of for a short fraction of each line time, immediately before the start of the line scan. By placing the flyback gun above the array, the upper strips can be charged positively, in preparation for the next frame scan, while the rundown is still in progress; thus the flyback potential transition follows the rundown potential transition. As the proportion of the frame time during which the scanning currents are supplied has been increased, the magnitudes of these currents have been reduced correspondingly. Hence the new design of scanning array overcomes one of the outstanding weaknesses of the earlier design, namely the exceedingly high scanning currents. The other change in the design of the scanning array has been a substantial reduction in the number of elements; the latest design has only 24 strips. As a result of this change, it was possible to build an experimental model using a printed circuit in which the gaps between the strips were sufficiently large to avoid flashover at 4 kilovolts.

After the success of the computer program for the deflection system, a program was written to calculate the electron trajectories

in the scanning array. This program has been most useful, both in the screen region, where it provided data for calculations on the alternative methods of colour selection, and in the scanning channels. One aspect of the scanning array which was not covered by the program, was the effect of secondary emission in the rundown channel.

5.2. A digital computer program for the scanning array.

In any study of the scanning array it is necessary to know the paths of the electrons, both in the scanning channels and in the screen region. It is particularly important to know where the electrons will land in the channels and on the screen, relative to the voltage wave. Obviously this depends on the design of the scanning array, the shape of the voltage wave and the trajectories of the electrons before they are influenced by it. During the earlier work on the scanning array, equipotential plots from the electrolytic tank were used for the calculation of the trajectories, but plotting a large number of trajectories was a slow process. More recently the screen region has been simulated experimentally with a stationary potential transition. As the measurements of the landing position were not very consistent, these results were only of use as a rough check. However, the computer program for the deflection system had been written when these difficulties became apparent, and it could obviously be adapted to solve the problem of the scanning array.

The function of the program for the scanning array is only to calculate the electron trajectories; the paraxial ray equations need not be solved in this case. The electron trajectories are calculated from the potential and field in the same way as in the program for the deflection system. In order to reduce the amount of output, only the initial and final positions of each trajectory are printed in this program, although, when the program was being checked, the positions of every point on the trajectories were printed.

If the potential transition is assumed to be abrupt, exact analytical expressions can be derived for the potential in the scanning array. This expression is, of course, two-dimensional and it is derived from the solution to Laplace's equation for the boundary conditions illustrated in Fig. 5.1, which is

$$V = \frac{2}{\pi} \tan^{-1} (\tan Y \tanh Z) \qquad (5.1)$$

If X and Y are rewritten as $\frac{\pi}{2}X$ and $\frac{\pi}{2}Y$, the system is scaled down so that the boundaries lie at $Y = \pm 1$ instead of $Y = \pm \frac{\pi}{2}$. Superimposing the potential given by $V = 2 - Y$ and dividing the resulting expression by 2 we get

$$V = 1 - \frac{Y}{2} - \frac{1}{\pi} \tan^{-1}(\tan \frac{\pi Y}{2} \tanh \frac{\pi Z}{2}) \qquad (5.2)$$

which satisfies the boundary conditions shown in Fig. 5.2. Since the second differential of $(2 - Y)$ is zero, this expression also satisfies Laplace's equation.

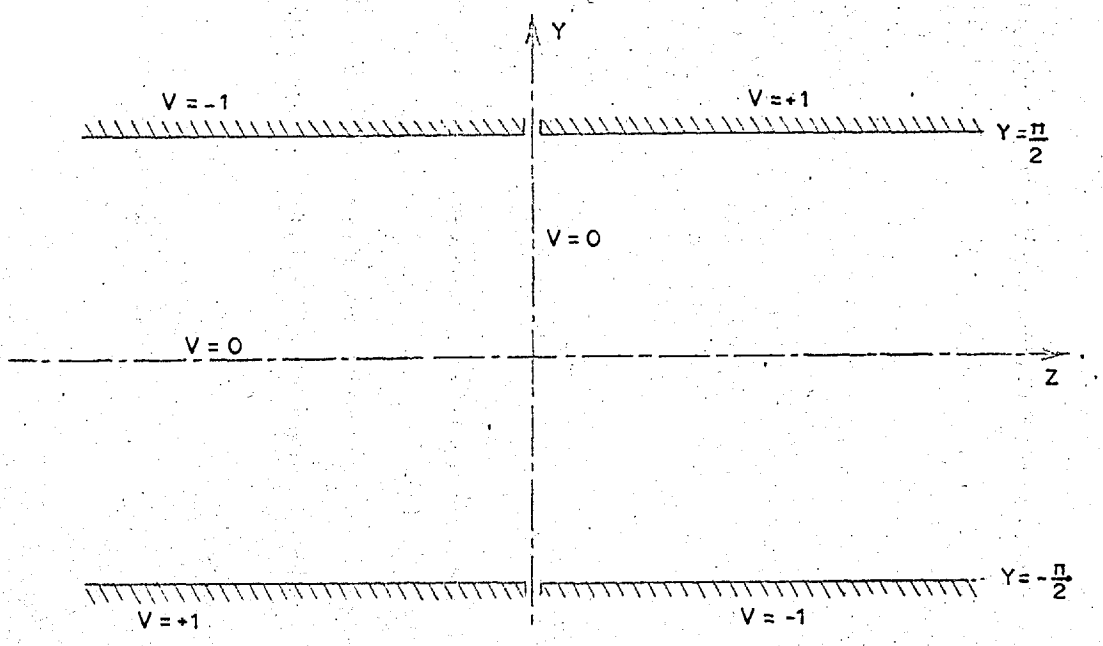


Fig. 5.1, Electrode Configuration of Basic Expression.

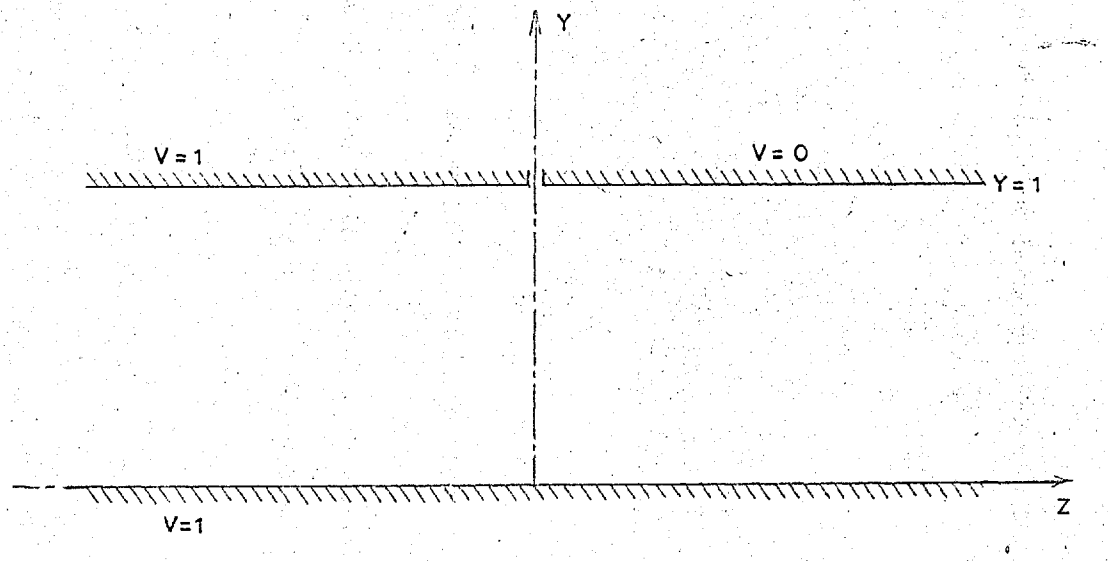


Fig. 5.2, Electrode Configuration of Simplified Expression.

Now the expression for the potential distribution in the screen region is the same as the corresponding expression for the scanning channels if the stagger angle is 90°, so both cases are covered by the electrode configuration of Fig. 5.3. In order to satisfy the boundary conditions of this figure, two solutions of the form of (5.2) must be superimposed and 1 must be subtracted from the resulting expression. In one of these solutions (Z-D) is written instead of Z, and in the other (1-Y) is written instead of Y. However, in general, the electrodes on the right hand side are not at zero potential, but at a finite fraction of the potential of the other electrodes. This can be taken into account by writing the expression for the potential in the scanning array as

$$V = 1 + (1-V') \left[\begin{array}{l} -\frac{(1-Y)}{2} - \frac{1}{\pi} \tan^{-1}\left\{ \tan \frac{\pi}{2}(1-Y) \tanh \frac{\pi Z}{2} \right\} \\ -\frac{Y}{2} - \frac{1}{\pi} \tan^{-1} \left\{ \tan \frac{\pi Y}{2} \tanh \frac{\pi}{2} (Z-D) \right\} \end{array} \right] \quad (5.3)$$

where $V' = \frac{V_{min}}{V_{max}}$ and V is the potential divided by V_{max}.

Not only are the potentials normalised in this expression, but the distances are, in effect, normalised with respect to the separation of the electrodes as well.

Due to the finite width of the strips, the potential transition can never be completely sharp. In practice the transition is fairly gradual and covers several strips; this is due to a number of effects such as secondary emission in the

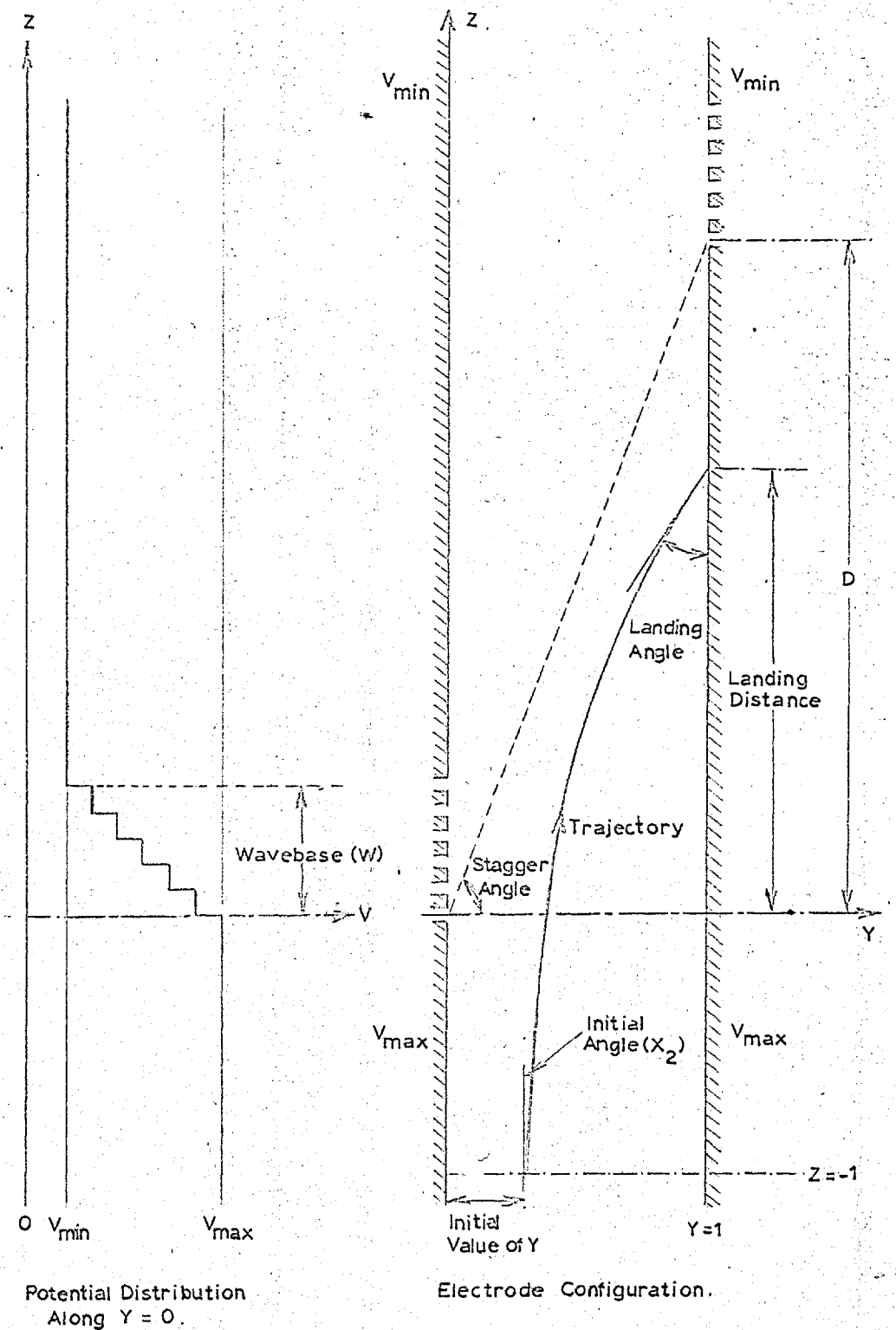


Fig. 5.3, Notation for Scanning Array.

rundown channel, mutual capacitance and leakage currents between adjacent strips and poor alignment or bad focusing of the scanning beams. The most convenient way of representing a gradual transition, for the purpose of the program, is to assume that the potential distribution is linear over the width of the transition, and then approximate to this by superimposing a number of expressions of the form of (5.3). Each has a slightly different value of X, and the difference between them depends on the width of the transition because, in the program, the number of expressions is always the same. If too many expressions had been used, the program would have been unduly long; in fact six were found to be sufficient.

The electron trajectories are calculated by a step by step method, but it is not easy to find the optimum size for a step because, if it is too short and potentials are calculated at an unnecessary large number of points, computing time will be wasted. On the other hand, excessive errors will arise where the potential or field change rapidly if the steps are too long. In the scanning array, the electrons are sharply deflected in a short distance, while close to the potential transition, so the step length must be short here. However, over most of the length of a trajectory the deflecting field is very weak and short steps are completely unnecessary. To overcome this problem, the program varied the length of the steps, depending on the radius of curvature of the trajectory. The ideal parameter to control the step length would

be the change in the radius of curvature with distance, because, if the potential or the field change abruptly, the radius of curvature will change abruptly too. However, in the scanning array, abrupt changes in the radius of curvature occur only where the radius of curvature itself is small; thus it is sufficient to use the magnitude of the radius of curvature, which is available in the program anyway, to control the step length.

A flow diagram for the whole program is given in Fig. 5.4, and an extract from the print out of the program covering the control of the step length is given in Fig. 5.5. The parameters are read in in three stages, first the initial step length C, then the stagger distance D and the wavebase W and finally V', which is $\frac{V_{min}}{V_{max}}$, and the initial angle X_2. When the computer has completed the calculations on these parameters, it reads in new values for V' and X_2, but, if it reads a value of V' greater than 1, it goes back and reads new values of D, W, V' and X_2.

After the parameters have been read in, the values of the working variables at the first point are set, for example Z = -1. The initial value of Y is varied successively from 0.1 to 0.5 in steps of 0.05. The values at the first points are stored and an integer S is set equal to 1; this is done at the beginning of the calculations for each point. The approximate coordinates of the next point are then calculated, by assuming that the radius of curvature remains unchanged. Next, the potential and field at

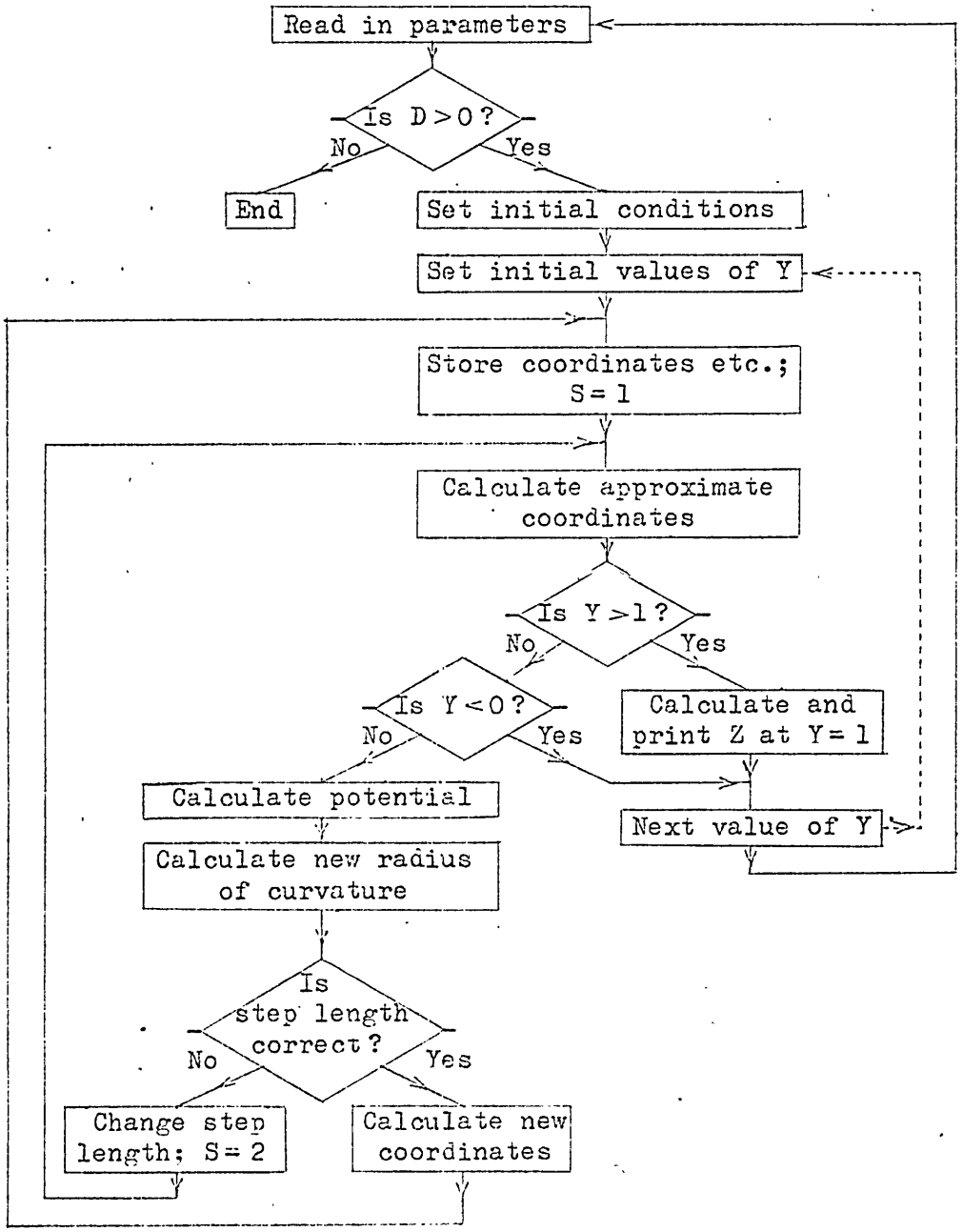
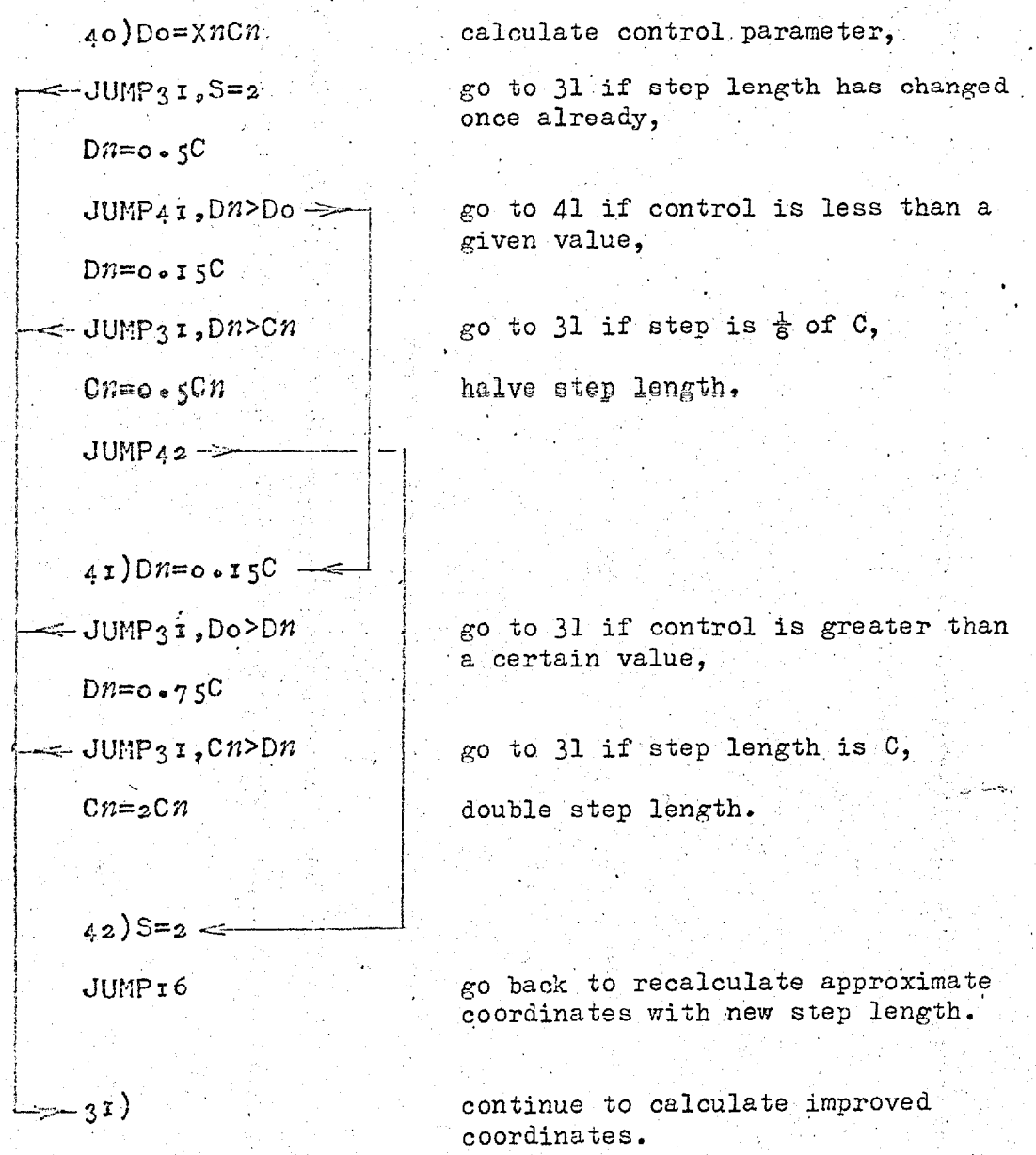


Fig. 5.4, Flow Diagram For Scanning Array Program.

Variables set previously in program:

C	Initial step length,
C*n*	Actual step length,
S	Integer, set at 1 before calculation for each point,
X*n*	Reciprocal of radius of curvature.



n represents a prime.

Fig. 5.5, Annotated Extract from Scanning Array Program (control of step length).

this point are computed, using equations of the form of (5.3) and their derivatives. The radius of curvature of the trajectory can now be calculated from the potential and the field, and so the step length is checkdat this stage.

At the beginning of a trajectory, the radius of curvature is almost infinite, so a standard step length which is relatively long is used in the program, but, near the potential transition, the radius of curvature decreases. When the product of the step length and the reciprocal of the radius of curvature exceeds a given value, the step length is halved and the coordinates of the point at which this occurs are recalculated using the new step length. If the product of the new step length and the reciprocal of the radius of curvature later exceeds the given value, the step length is halved again. Further on, the radius of curvature starts to increase, so, when the product of the step length and the reciprocal of the radius of curvature fall below a certain value, the step length is doubled. In order to avoid instability, the value which produces a reduction in step length is rather smaller than the value which produces an increase; as a further safeguard, once one change of step has occurred, a second change cannot occur until the computer has moved on at least one step along the trajectory. The step length can never exceed the initial value and cannot fall below one eighth of this value

If the step length is changed, the computer goes back to the beginning and recalculates the approximate coordinates using the

new step length; it follows on from there as before. If the step length is correct, the final coordinates of the point are calculated, using the radius of curvature at the previous point and the radius of curvature at the approximate point. These coordinates, the radius of curvature and the angle of the trajectory are stored as described above and S is set equal to 1 again; thus the process continues.

Results from the program have been compared with the trajectory plots, which had been derived with the aid of the electrolytic tank, and with the results of the experiments, which were carried out in the vacuum tank; they agree within reasonable limits.

5.3. Results of computations for the scanning array.

Results from the computer have been used for Fig. 5.6, in which the landing distance has been plotted against the initial value of Y; one curve is for $V' = 0$ and the other is for $V' = 0.25$. The wavebase W was assumed to be negligible, the stagger angle was taken to be 90° and the beam was assumed to have been parallel to the screen initially. Points based on experiments for these conditions with $V' = 0$ have also been plotted in this figure; in addition, the results which Stuart[2] obtained by ray tracing from electrolytic tank plots for $V' = 0.25$ are shown too. As the results from the computer agree fairly

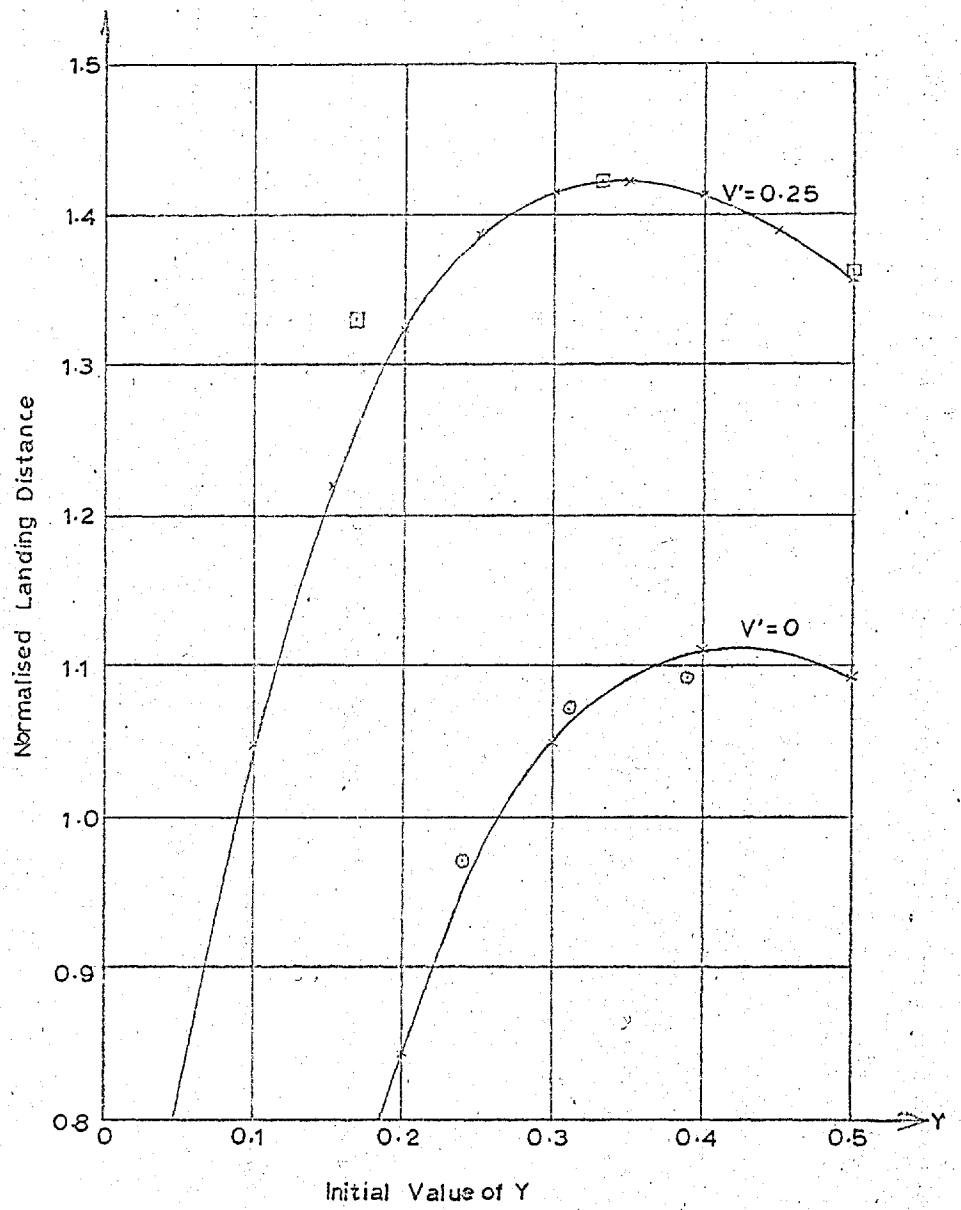


Fig. 5.6, Evaluation of Results from Computer Program.

well with the others, it is justifiable to assume that the computer program can be used to calculate the electron trajectories in the scanning array.

Using the computer program, electron trajectories for the above conditions with $V' = 0.25$ have been plotted in Fig. 5.7. The variation of the step length with curvature can clearly be seen. The initial step length was 0.2 units of length, and, although this might seem excessively large, there was little change in the computed landing distance when the step length was reduced by a factor of four. It is apparent that the electron trajectories come to a first order focus in the scanning array, but there is considerable second order aberration: it is a little misleading to describe this as a focus, because at a normal focus, in a system with rotational symmetry, no second order aberrations occur.

The effect of varying the value of V' is illustrated in Fig. 5.8, the other parameters remaining as in Fig. 5.6. When the value of V' is increased, the deflecting field becomes weaker so the landing distance increases; furthermore, the greatest landing distance for a particular value of V' occurs at a smaller initial value of Y. Fig. 5.9 shows the effect of varying V' on the angle of incidence of a trajectory at the screen; as might be expected, the angle increases as either V' or the initial value of Y increase. In fact the relationship is almost linear for both.

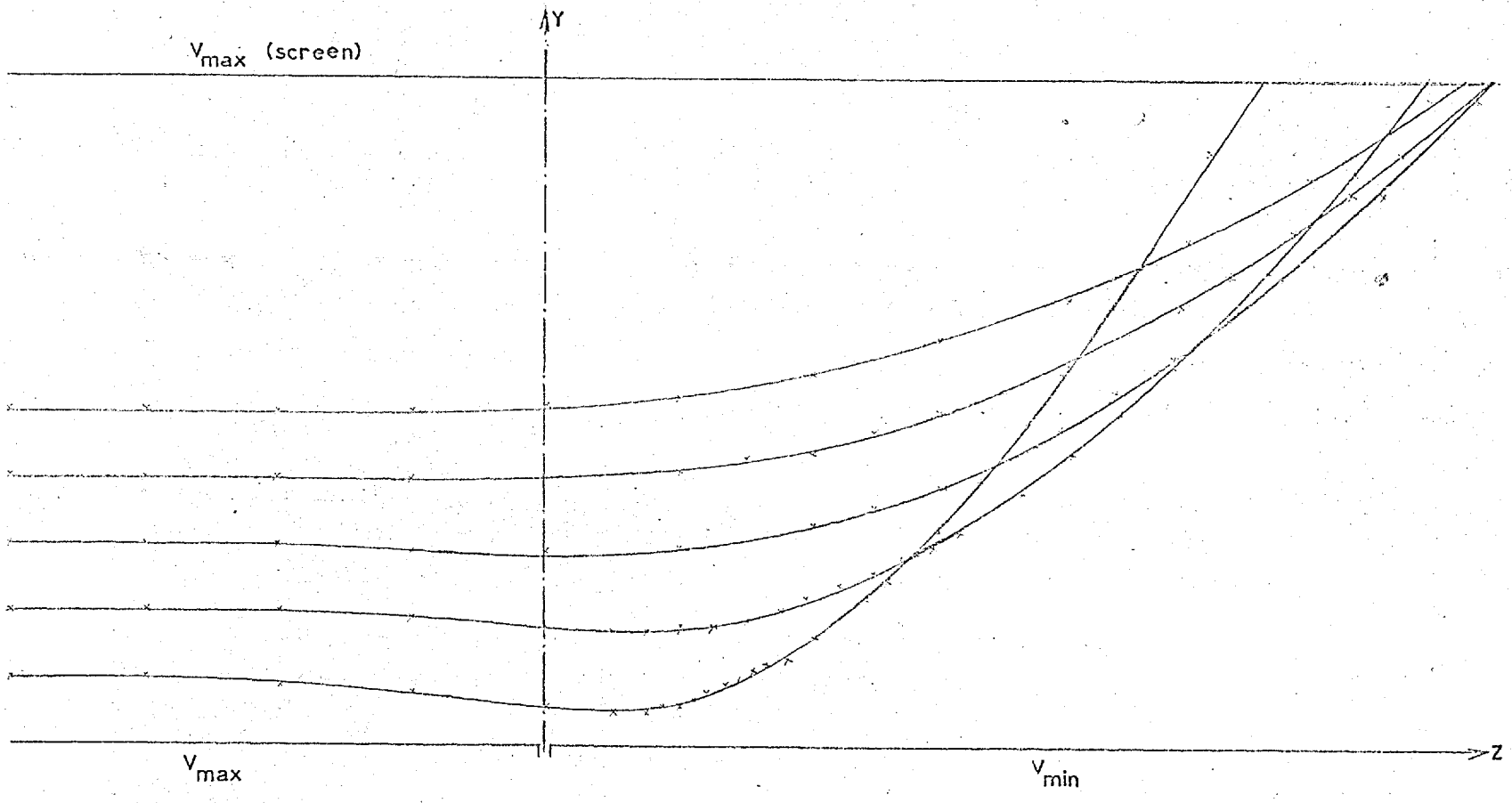


Fig. 5.7, Computed Electron Trajectories for V' = 0.25.

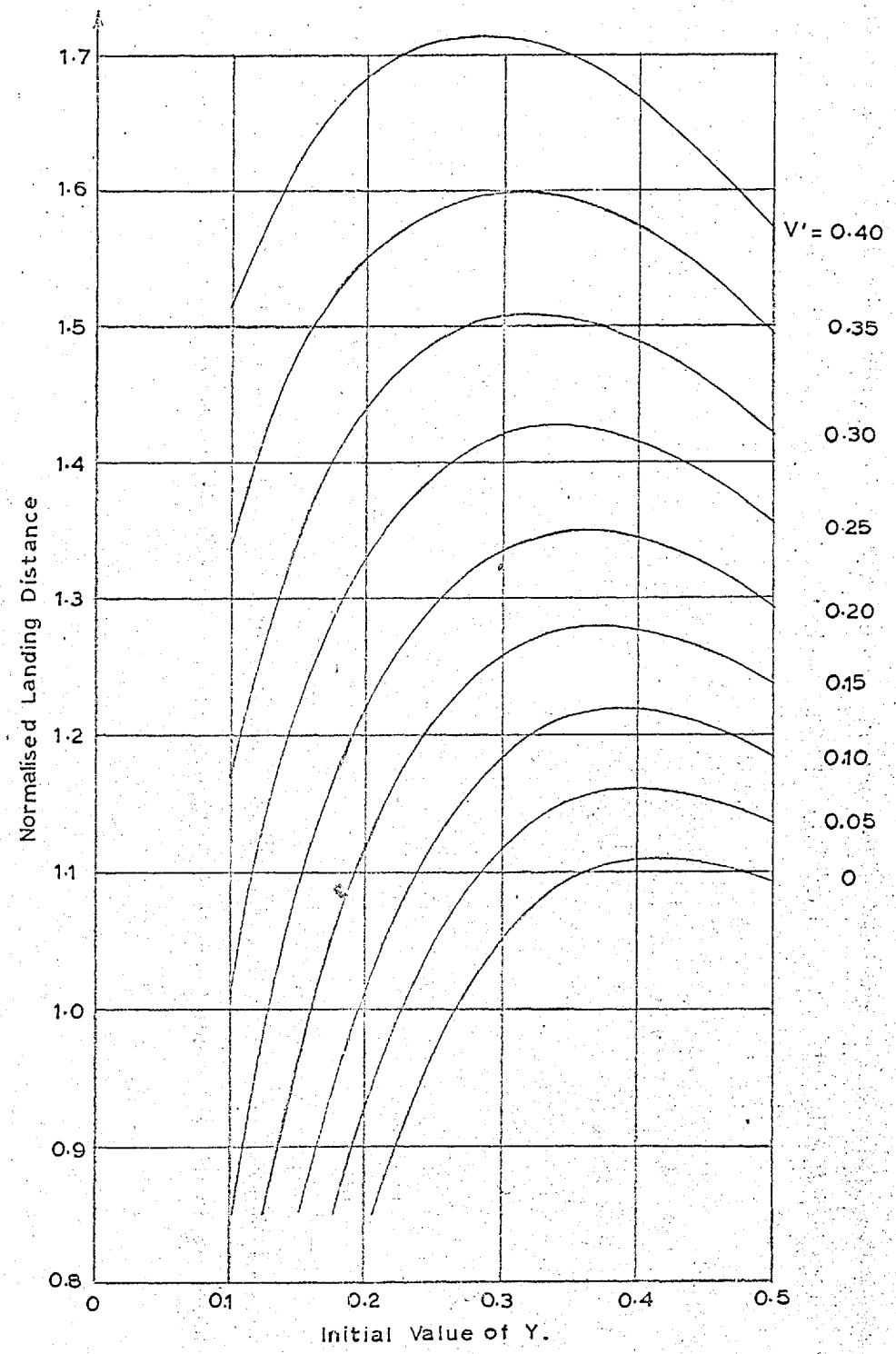


Fig. 5.8, Landing Distance for Different Values of V'.

The effect of changing the initial angle of the trajectory with the screen is shown in Fig. 5.10. The trajectories are assumed to radiate from a point on the line $z = 1$, and the image of this point lies on the screen when the initial value of Y is 0.23. For greater initial values of Y, the landing distance decreases with the initial angle, so that a trajectory which is initially inclined towards the screen will land closer to the starting point than one which was originally inclined away from it. For values of Y less than 0.23 the reverse is true. The dangers of considering the field in the scanning array to act as a simple lens have been pointed out; however, if this is done, the situation can be described by saying that the focal length of this lens increases with the initial value of Y. This could have been predicted because the lens effect, which is caused by the variation in potential, is strongest near the potential transition in the scanning array.

Any practical system has a finite potential transition width or wavebase, as will be shown later, and Fig. 5.11 illustrates the effect of varying this. In this figure the ordinate is the distance of the landing point from the centre of the potential transition. Although a small wavebase makes little difference, as the wavebase increases, the maximum value of the landing distance increases and, for a given wavebase, it occurs for smaller and smaller initial values of Y. Now a screen region with a long wavebase is roughly equivalent to a system with zero wavebase in

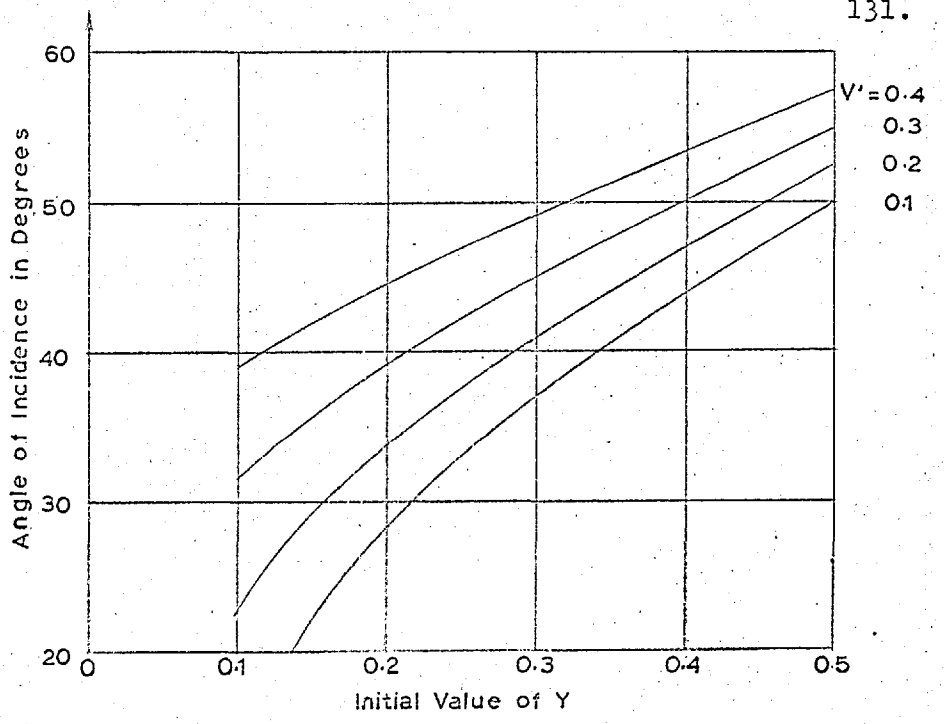


Fig. 5.9, Angle of Incidence for Different Values of V'.

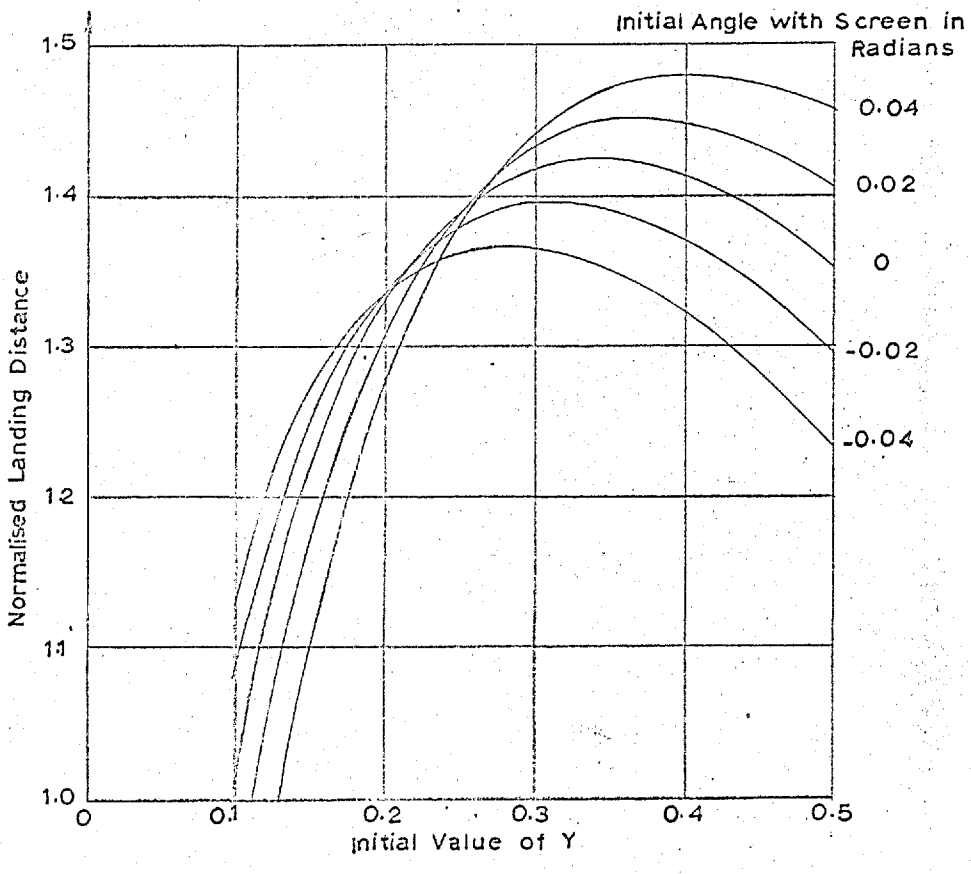


Fig. 5.10, Landing Distance for Different Initial Angles.

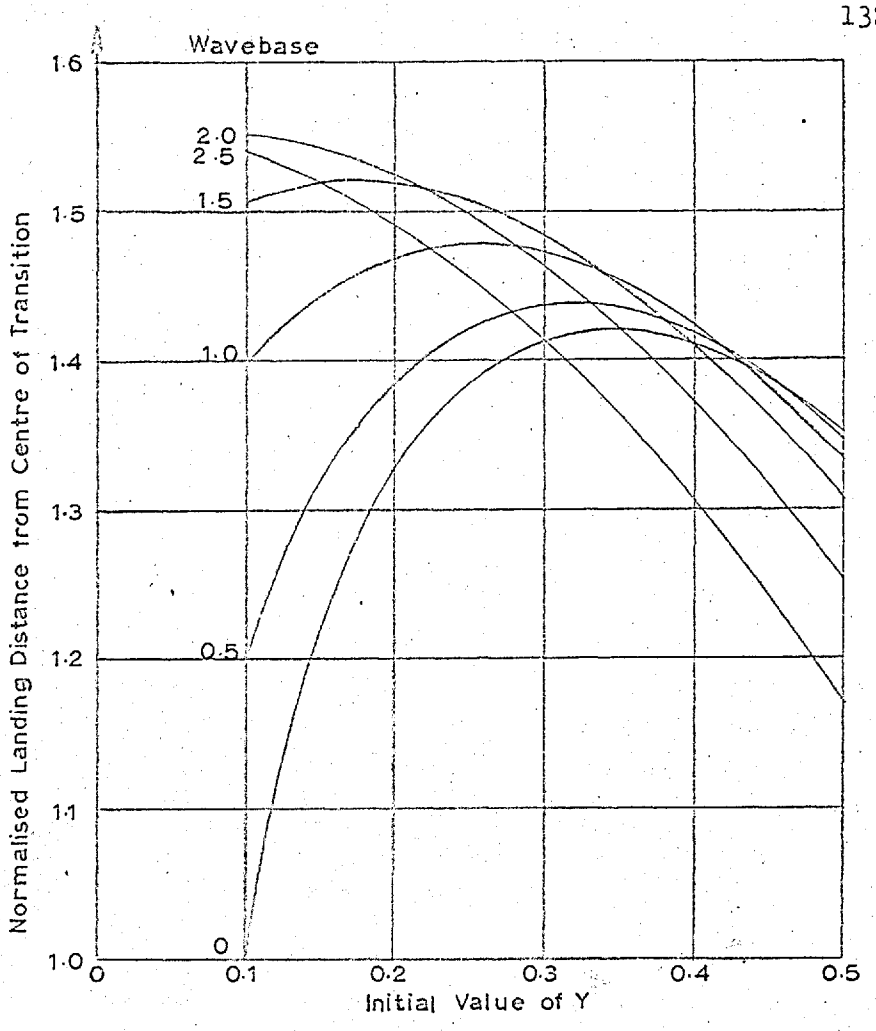


Fig. 5.11, Landing Distance for Different Wavebases.

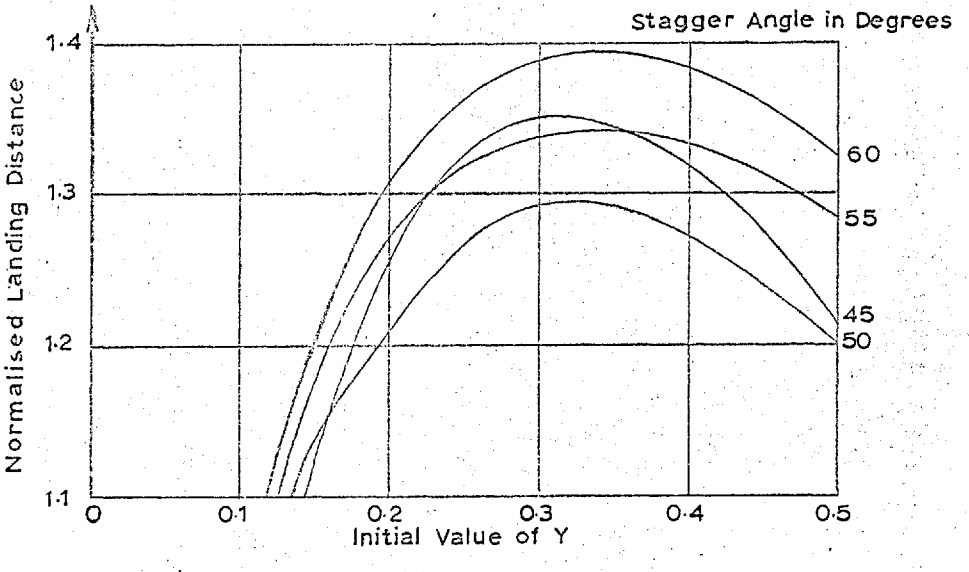


Fig. 5.12, Landing Distance for Different Stagger Angles.

which the strips of the array are further from the screen and the value of V' is lower. Although decreasing V' would have the effect of reducing the landing distance, this would be more than counteracted by the increase in dimensions of the equivalent system, which accounts for the increase in the maximum landing distance. Increasing the wavebase has the effect of increasing the equivalent initial value of Y rapidly, which explains why the maximum landing distances occur for smaller initial values of Y as the wavebase increases.

In Fig. 5.12 the landing distance is plotted against the initial value of Y for several stagger angles. As the stagger angle decreases from 90°, the second potential transition becomes increasingly important and deflects the beam so that the landing distance decreases. However, below a certain stagger angle, the landing distance starts to increase again because the beam is going past the second potential transition and into a region where the transverse field is small.

5.4. The scanning action.

As already described, the scanning action is the charging or discharging of the strips of the scanning array by bombarding them with electrons from the scanning guns. The scanning beams pass down channels which are, in the ideal case, designed so that the electrons strike the array only in the immediate vicinity of the potential transition. Assuming the potentials of the strips

of the array can only change when they are struck by one of the scanning beams, the width of the potential transition is equal to the width of the beam as it lands on the strips. Making this assumption, Gabor has proved for the rundown that such a wave will be stable, so it will travel with a constant speed and amplitude despite small disturbances.[7] However, this assumption is not necessarily valid in a practical system, because any physical array has a finite number of strips with an appreciable mutual capacitance between each strip: furthermore, in the rundown channel it is not easy to suppress secondary emission. Both these effects tend to increase the width of the transition.

The existence of mutual capacitance between the strips means that, when a certain voltage waveform is applied to one strip, the change in voltage of the adjacent strips has the same waveform, although it is attenuated. In order to investigate this effect in greater detail, we must consider the equivalent circuit illustrated in Fig. 5.13; the leakage resistances have been ignored here. This figure shows two adjacent strips, one of which receives a Dirac impulse of current. The mutual capacitance between the strips is C_m and the capacitance of each strip to earth is C_g. If the array is assumed to have an infinite number of strips, we can represent the effective capacitance at the (n+1)th strip of the (n+2)th strip and all the strips beyond by a simple capacitor C_c. Similarly we can represent the effect of all the strips on the other side of the n-th strip by another

capacitor C_c. However, as far as the n-th strip is concerned, we could also replace the (n+1)th strip in parallel with C_c simply by C_c.

Hence, $$C_c = \frac{C_m(C_g+C_c)}{C_m+C_g+C_c} \tag{5.4}$$

Now if a voltage step v_n is applied to the n-th strip, the capacitors C_m and C_g in parallel with C_c act as a voltage divider, so a voltage step

$$v_{n+1} = v_n \frac{C_m}{C_m+C_g+C_c} \tag{5.5}$$

will be induced on the (n+1)th strip. Similarly the voltage induced on the (n-1)th strip will be

$$v_{n-1} = v_n \frac{C_m}{C_m+C_g+C_c}$$

and the voltage induced on the (n+2)th strip will be

$$v_{n+2} = v_n \left(\frac{C_m}{C_m+C_g+C_c}\right)^2$$

Generalising these results we can write,

$$v_{n+k} = v_n \alpha^{|k|} \tag{5.6}$$

where k is an integer, and $\alpha = \frac{C_m}{C_m+C_g+C_c}$

Clearly $v(k)$ has a discontinuity at $k = 0$, so any expressions which are derived from this function will have discontinuities too. Thus it is essential to consider the physical

situation throughout this calculation. Actually the following expressions can be derived by means of differential equations, but then it is harder to relate them to the physical conditions.

If we now consider a potential transition in which a voltage step V_1 is applied to each strip in turn, to approach the n-th strip, when half the potential has been applied to the m-th strip away from the n-th strip, the potential of the n-th strip is

$$V_n = \sum_{k=\infty}^{m} V_1 \alpha^{|k|} - V_1 \frac{\alpha}{2}^{|m|}$$

Using the expression for the sum of a geometric progression, before the transition has reached the n-th strip,

$$V_n = V_1 \frac{\alpha^{|m|}}{1-\alpha} - \frac{V_1 \alpha^{|m|}}{2}$$

$$= V_1 \frac{(1+\alpha)}{(1-\alpha)} \frac{\alpha}{2}^{|m|} \qquad (5.7)$$

After the potential transition has passed the n-th strip,

$$V_n = V_1 \frac{(1+\alpha)}{(1-\alpha)} \left(1 - \frac{\alpha}{2}^{|m|}\right) \qquad (5.8)$$

By letting $m \to \infty$ in (5.8),

$$V_1 = V_o \left(\frac{1-\alpha}{1+\alpha}\right)$$

where V_o is the total voltage change across the transition.

Now $a^x = \exp(x \ln a)$

Hence, before the transition has reached the n-th strip,

$$V_n = \frac{V_o}{2} \exp(|m| \ln \alpha) \qquad (5.9)$$

and when the transition has passed the n-th strip

$$V_n = V_o - \frac{V_o}{2} \exp(|m| \ln \alpha) \qquad (5.10)$$

The above equations give the profile of the potential transition in terms of distance at any instant, but, by assuming that the velocity of the transition, u, is constant, we can transform these equations to give the variation of the potential of one strip with time. This variation can be measured with an oscilloscope, so it is possible to compare the actual profile with the theoretical predictions. The equations in terms of time are

$$V(t) = \frac{V_o}{2} \exp\left(\frac{t \ln \alpha}{u}\right) \qquad (5.11)$$

and

$$V(t) = V_o - \frac{V_o}{2} \exp\left(\frac{t \ln \alpha}{u}\right) \qquad (5.12)$$

From a simple consideration of the state of charge of the array,

$$u = \frac{I}{V_o C_g} \quad \text{strips per second,}$$

where I is the charging current im amps.

The effect of secondary emission in the rundown channel is much more difficult to deal with quantitatively. When the electrons of the rundown beam land on the strips of the channel, some secondary electrons are emitted. These are accelerated in the direction of the rundown gun by the electrostatic field which occurs at the potential transition. The shape of this field is such that the secondary electrons soon land on another strip, a little nearer the gun, where they may cause more secondaries to be emitted. However, the yield of secondaries for each primary is usually less than unity, so some negative charge is imparted to each strip which is struck by the electrons. Thus the secondary electrons increase the wavebase and, in extreme cases, will prevent the rundown from occurring at all.

In order to stop the secondary electrons from cascading down the rundown channel, the strips, where they are bombarded by the scanning beam, are fitted with small flaps on the edges nearest the rundown gun. These flaps act in two ways: firstly they reduce the field strength near the surface from which most of the secondary electrons are emitted and secondly they catch secondaries from the previous strip, preventing most of the secondaries from jumping more than one strip width. However the flaps are not entirely effective in eliminating the consequences of secondary electron emission, because some electrons land on the sides of the flaps facing the rundown gun, and secondaries from these go to the next strip down, (or even the one beyond). As the

yield of secondaries depends on the state of the emitting surface and the speed and angle of incidence of the primaries, it is clearly not feasible to calculate the increase in the wavebase, so the design of a rundown channel cannot be carried out from theory alone.

It is important to use a logical design procedure for a scanning array, and to begin with, the minimum voltage of the array must be decided. If the minimum voltage is too low, excessive scanning currents will be required, but, if it is too high, the angle of incidence of the writing beam on the screen will be unduly large and the spot size in the vertical direction may suffer. The required minimum voltage has been taken to be 0.25 because this is a reasonable compromise.

It is now possible to calculate the stagger angle of the rundown channel for zero wavebase. From Fig. 5.12, the landing distance can be plotted against the tangent of the stagger angle for a given initial value of Y and the required value of V' as in Fig. 5.14. Now for any given wavebase and initial value of Y, the value of V' is uniquely determined by the stagger angle. Hence, if a line is drawn through the origin with unit slope in Fig. 5.14, the tangent of the correct stagger angle will be given by the horizontal coordinate of the point where the line cuts the curve, because the beam will then land at the transition. Once the wavebase has been found for the first design, the procedure can be repeated to obtain an improved design, assuming the

wavebase to have that value instead of zero. A correction is required, however, because the rundown beam should land rather beyond the centre of the potential transition to compensate for the shift of charge towards the rundown gun by the secondary electrons.

Although, as was mentioned earlier, Gabor has proved that the rundown voltage wave is stable if secondary emission and mutual capacitance are neglected, the proof becomes invalid when these effects occur. The stability of the voltage wave can be treated qualitatively by considering the scanning action to be a closed loop control system. The forward path is the action of the scanning current in changing the voltage distribution on the array. The feedback path is the effect of the voltage distribution of the array on the landing point of the scanning beam, and hence where the scanning current is applied. Strictly, such a closed loop system exists for each strip with a feedback path dependent on the voltages of all the strips in the array; however it is more convenient to consider a single system, even if the transfer functions become more complicated. Fortunately the feedback path integrates the voltages on the array over a considerable distance, so the voltage wave will not be permanently affected by an irregularity in the voltage of one strip. Therefore the voltage wave is stable as far as high frequency oscillations are concerned, but we have still to consider the low frequency, or long term, stability.

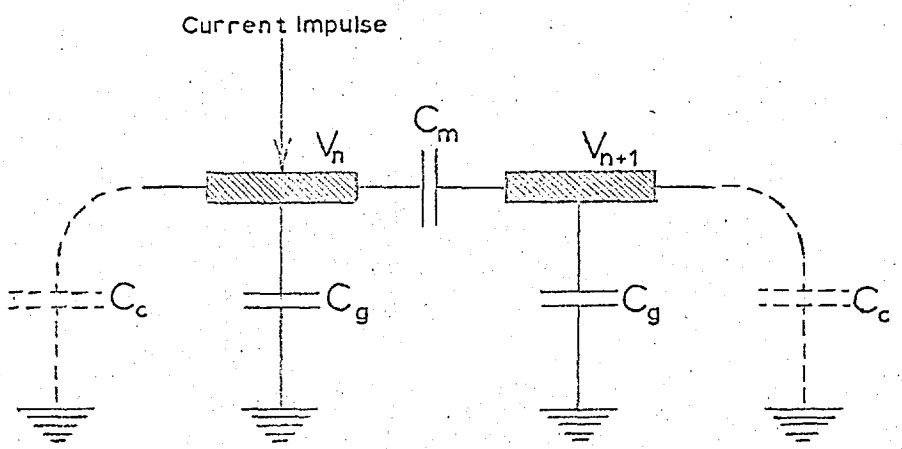


Fig. 5.13, Equivalent Circuit for Adjacent Strips.

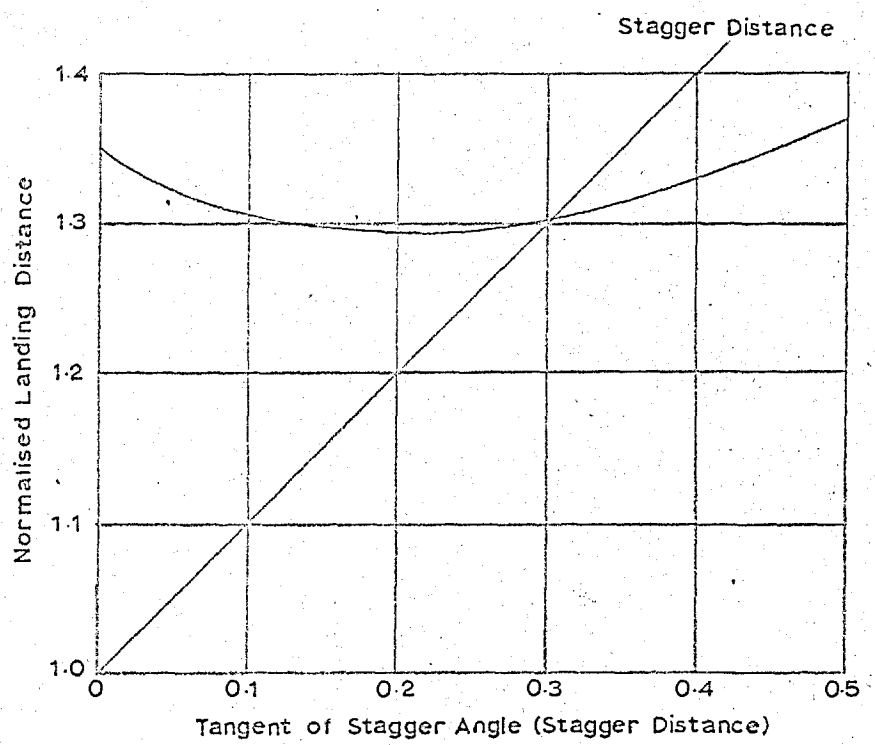


Fig. 5.14, Landing Distance Against Stagger Distance.
(initial value of Y = 0.33)

If for the moment we assume that the wavebase is small and we are only interested in long term stability, we can greatly simplify the transfer functions of our control system, by letting our frame of reference move down the array at a velocity equal to that of the voltage wave. The forward path is now the effect of the rundown current on the amplitude of the voltage wave, while the feedback path is the effect of the voltage wave on the landing point of the scanning beam. As we have assumed that the wavebase is small, for a given stagger angle and initial value of Y, the landing distance of the beam can only depend on the amplitude of the voltage wave, under steady state conditions. Fig. 5.8 shows that in general the landing distance increases as V' increases (or the height of the voltage wave decreases), so, if the amplitude of the voltage wave decreases, the tendency will be for the scanning beam to slow down which will increase the amplitude again. Thus under these conditions the wave is stable.

If we now consider the wavebase to have been increased, but assume that it is constant during the whole rundown, the same arguments apply as before and the voltage wave is still stable. If the beam had to land at the centre of the voltage wave, the amplitude of the wave would have increased slightly, but in practice the secondary electrons shift some of the charge from the landing point of the beam towards the region of high potential, so the landing distance must increase to compensate for this. As a result, the amplitude of the voltage actually decreases when the

wavebase is increased, if the stagger angle and initial value of Y remain unchanged. This can be represented in our simplified control system by applying the wavebase to the feedback transfer by an extra input.

We must now examine the wavebase in greater detail, because, if this remains unchanged, the voltage wave will be stable. Two effects which contribute to the wavebase have already been mentioned; one is due to the mutual capacitance between the strips of the array, which depends on the dimensions of the array and can be assumed to be constant. The other effect, which we have discussed already, is the emission of secondary electrons. The finite width of the beam as it lands on the array also contributes to the wavebase, but we can assume that this effect is constant. Unfortunately the effect of the secondary electrons cannot be taken to be constant, because the number of secondaries which cause an increase in the wavebase depends on the wavebase. We can consider this as another closed loop control system, in which the forward path is the effect of the secondary electrons on the wavebase and the feedback path is the effect of the wavebase on the number of secondaries which increase the wavebase. The forward transfer function is quite simple, because the secondaries which land on a strip charge it negatively. The feedback transfer function is too complicated to consider in detail, because there are quite a number of different effects working together; however it is worth discussing the action of the flaps in suppressing secondary emission. The flaps,

which have been described already, are intended to modify the field in the immediate vicinity of the landing point of the scanning beam, so that there is a potential barrier of sufficient height to contain the secondary electrons. Now the height of this barrier is proportional to the wavebase. Hence, if the wavebase becomes too long, a considerable number of secondary electrons can jump through the lowered potential barrier, which increases the wavebase and results in progressive deformation of the wave front. Fortunately some of the other effects tend to stabilise the wavebase, but even so there is the danger that, if the wavebase increases above a certain value, the effect which has just been described will cause the rundown to degenerate completely. In order to minimise the risk of this occurring, it is desirable to make the constant components of the wavebase as small as possible. Experiments have shown a tendency for the wavebase to increase during the course of a rundown, but with careful design this can be reduced to an acceptable level.

Fig. 5.15 is an oscillogram of the voltage on the fourth strip from the bottom of the scanning array during the course of a rundown. The sinusoidally varying trace, which is also in the photograph, is an indication of the rundown beam current which was $3\frac{1}{2}$ μA. Fig. 5.16 is derived from the oscillogram, after correction for the time constant of the coupling network. This figure is, in fact, the voltage profile of the rundown voltage wave at a given instant, because a transformation has been

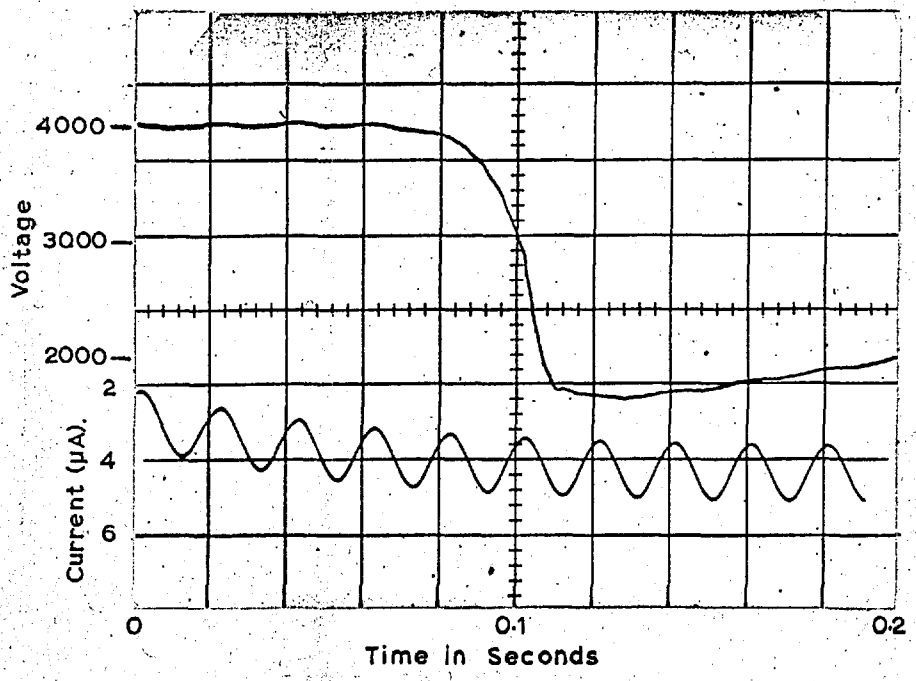


Fig. 5.15, Oscillogram of Rundown (Twentieth Strip from Top).

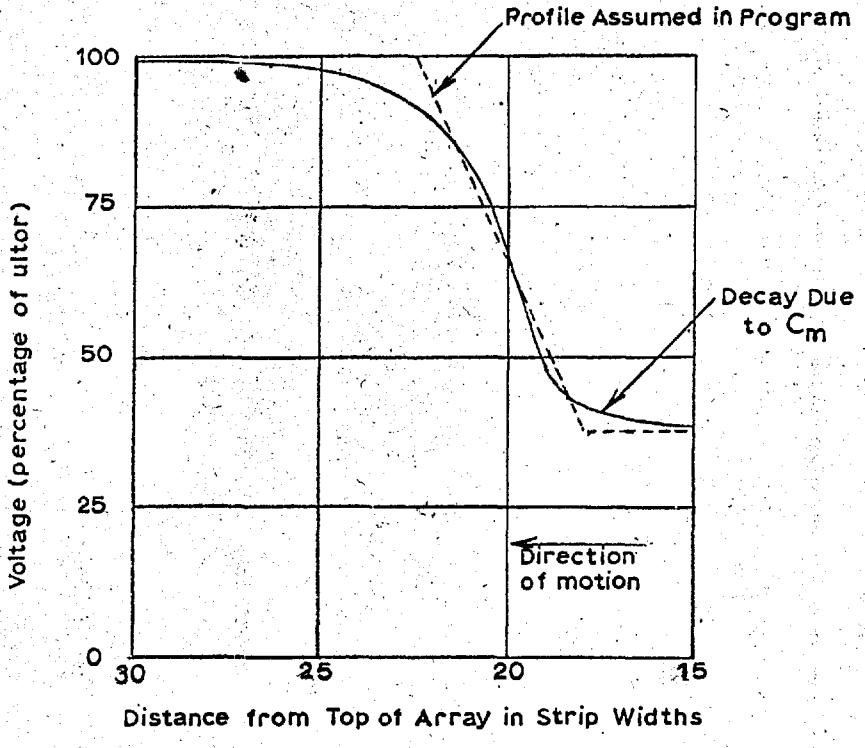


Fig. 5.16, Profile of Rundown.

carried out on the original oscillogram by multiplying the time axis by the speed of the voltage wave in strips per second; thus the units of the abscissa have been transformed into strip widths Unfortunately the speed of the voltage wave was not quite constant. in this case, so the transformation was not strictly valid; however the transformed result is much more useful than the oscillogram. The extra line which has been drawn on Fig. 5.16 represents the potential profile which has been assumed for the computer program. Fig. 5.16 shows that a number of effects which have already been predicted occur in practice. The first part of the voltage wave is much more rounded than the final portion because of the influence of secondary electrons; the primaries land behind the geometrical centre of the wave for the same reason. The effect of the mutual capacitance between the strips is clearly visible in the final portion of the wave; the decay constant agrees quite well with the value predicted from theoretical considerations.

So far we have been considering the scanning action in the rundown channel only, but we must now turn to study the flyback. The flyback is less critical than the rundown, because the profile of the voltage wave does not determine the focusing of the writing beam at the screen. Nevertheless it is desirable that the flyback should take the form of a well defined voltage wave which chases the rundown wave. We have seen that the rundown voltage wave is essentially stable; however, while the flyback wave is stable as far as high frequency oscillations are concerned because of the

integrating effect, it is not necessarily stable for low frequency oscillations. From Fig. 5.8, we have deduced that the landing distance of a scanning beam will increase as the height of the voltage wave decreases, so, as the amplitude of the voltage wave decreases, the scanning beam moves further ahead, thus producing a tendency to instability. Furthermore, if the flyback beam continues to land on a strip which has already reached the maximum potential, by the well known "anode potential stabilisation effect", the number of secondary electrons which go to the screen grid will exactly balance the number of primaries striking the strip, so it is possible for the flyback wave to stay completely stationary. This is never possible in the rundown channel because there are no electrodes for the secondaries to go to, apart from the other strips. These two effects, both of which tend to produce instability, are only the most obvious of a considerable number affecting the stability of the flyback; however, some of the other effects have a stabilising influence. These are too complicated to investigate theoretically, so the stability of the flyback can only be studied experimentally. In practice, it is possible to maintain the stability of the flyback wave profile for a considerable distance, but, so far, it has been impossible to do so for the full height of the array.

5.5. The screen region.

The results on the computer program permit detailed calculations of the focusing of the writing beam by the field in the neighbourhood of the potential transition. In this section, these calculations are given for both shadow mask and single gun colour displays, as well as black and white displays. Throughout the calculations we will consider a 625 line display 183 mm high; this corresponds to a tube with a 12 inch diagonal and a 4 : 3 aspect ratio. These dimensions have been chosen because all the experimental models of the flat tube have been based on a display with this diagonal measurement; however the calculations can easily be modified for tubes of different sizes, or for other line standards. For most of these calculations the wavebase has been assumed to be zero, but the effect of increasing it has been considered where this makes a significant difference. In these cases, the wavebase has been assumed to be 1.33, which corresponds to the wavebase of the rundown wave illustrated in Fig. 5.16, because the height of the scanning channels was 18 mm, and the distance between the screen and the scanning array was 27 mm. In these calculations, the distance between the screen and the scanning array has been assumed to be 30 mm. and V' has been taken as 0.25.

Ideal Black and White Display.

A 625 line display has 589 active lines, which corresponds to a line width of 0.31 mm. From Fig. 5.8 the maximum value of the landing distance is 1.422 for $V' = 0.25$ and this occurs for an initial value of Y of 0.355. Assuming that the beam is exactly parallel before reaching the potential transition, we also see from Fig. 5.8 that the spot will have the required vertical diameter if the beam initially lies between $Y = 0.294$ and $Y = 0.404$, which corresponds to an initial beam diameter of 3.3 mm. Thus, in the ideal case, there is a reduction in the beam diameter of more than 10 : 1 due to the focusing field of the potential transition.

Converging Beam.

In a practical system, it is impossible to ensure that the writing beam is exactly parallel before it reaches the potential transition, so we will now consider a beam which is converging to a point F mm. beyond the transition. We will assume that the axis of the beam is initially parallel to the screen and, coincides with the ray for which the landing distance is a maximum; we have already seen that the initial value of Y for this ray is 0.355. By elementary trigonometry, if the distance of a ray from the axial ray is r mm. at $Z = -1$, the angle of this ray with the screen is

$$\frac{r}{F + 30} \quad \text{radians.}$$

This angle can be plotted in Fig. 5.10 by interpolation between the curves for different initial angles, at the value of Y corresponding to r which is

$$-\frac{r}{30} + 0.355 \quad .$$

The landing distance of the ray is the ordinate of this point. Using this procedure for a number of different values of r, we can plot the landing distance against the value of Y at $Z = 1$; this may be used to find the vertical spot size on the screen for a given beam or the maximum initial beam diameter which will give the required spot size. Fig. 5.17 shows a curve of this type, calculated for $F = 300$ mm. This method can also be applied to the diverging beams by making F negative and Fig. 5.17 shows a curve for $F = -300$ mm. as well. From this figure, it can be shown that the vertical spot size will increase to 0.45 mm. if $F = +300$ mm. and 0.78 mm. if $F = -300$ mm., for the beam of the ideal display. If the spot size is to be satisfactory, although the focus of the undeflected beam approaches to within 300 mm. of the potential transition, the initial beam diameter must be reduced to 1.5 mm. This result assumes that the initial value of Y for the axial ray is still 0.355, but the initial beam diameter could be increased to 1.9 mm., if it was changed to 0.348.

The above method, although cumbersome, has been used in preference to considering simple equivalent lenses, so as to take second order aberrations into account.

Effect of Magnetic Fields.

Previously we have assumed that the axis of the writing beam was exactly parallel to the screen before it reached the potential transition, but it is unlikely that this will be so in a real tube. Fig. 5.10 indicates that the spot size will be critically dependent on the angle between the beam and the screen. One possible cause of misalignment of the beam is an imperfection in one or more components, but this can be corrected with the trimmer plates. However, if the tube is placed with its screen in the plane of the magnetic meridian, the horizontal component of the earth's magnetic field will deflect the beam either towards or away from the screen, producing a similar effect. This could be corrected to some extent with the trimmers, but it undesirable that the trimmers should require adjustment every time the television set is moved; so the design of the tube must be such that the spot size is not significantly changed by the earth's magnetic field.

The radius of curvature, r_e, of the path of an electron, of mass m and charge $-e$, which moves in a uniform magnetic field B_e with velocity v is given by

$$B_e r_e = \frac{m v}{e}$$

$$= \sqrt{\frac{2m}{e} V} \qquad \text{(where } V \text{ is the accelerating voltage)}$$

$$= 3.372 \times 10^{-6} \sqrt{V} \qquad \text{(using M.K.S. units).}$$

Now the maximum horizontal component of the earth's magnetic field is approximately 4×10^{-5} w/m^2, so

$$r_e = \frac{3.372 \times 10^{-6}\sqrt{V}}{4 \times 10^{-5}} \text{ meters.}$$

$$= 0.0842\sqrt{V} \text{ meters.}$$

The following calculation cannot be very accurate, so, for convenience, we will assume that the electrons always travel with a velocity equivalent to the ultor potential, but that the total distance which they travel is 0.5 meters, which is somewhat longer than the true distance. We will also assume that the ultor potential is 20 kV. Hence

$$r_e = 11.9 \text{ meters.}$$

The angle through which the beam is deflected by the magnetic field is

$$\frac{0.5}{11.9} = 0.042 \text{ radians}$$

and the displacement of the beam when it reaches the potential transition is

$$\frac{0.5}{2} \times 0.042 = 0.0105 \text{ meters.}$$

This corresponds to a change in the initial value of Y of

$$\frac{10.5}{30} = 0.35,$$

which is quite unacceptable, so magnetic screening will be essential.

If the residual horizontal component of the magnetic field after the screening has been fitted, is a fraction, B, of the horizontal component of the earth's magnetic field, the radius of curvature of the electron path becomes $\frac{11.9}{B}$ meters. Hence the angle through which the beam is deflected is now 0.042B radians, the displacement at the potential transition is 0.0105B meters and the corresponding change in the initial value of Y is 0.35B.

The method which was employed for converging beams can be used to calculate the landing distance of the axial ray for various values of B; it can also be adapted to give the landing distance of other rays for one value of B. In Fig. 5.18, the landing distance has been plotted against the initial value of Y, both for axial rays with a number of values of B and for other rays with B equal to 0.1. These curves indicate that the maximum initial diameter of the beam for which the spot size is satisfactory is 1.5 mm, if the beam is deflected away from the screen, and 1.05 mm, if it is deflected towards the screen, when B = 0.1. However the maximum initial diameters are increased to 2.4 mm. and 1.8 mm. if B = 0.05. If F varies between ∞ and 300 or $-\infty$ and -300, and B = 0.05, the initial diameter of the beam must be less than 1.1 mm. for the spot size to remain sufficiently small.

This calculation is not very accurate, because the horizontal component of the earth's magnetic field varies from country to country and the equivalent distance, at ultor potential,

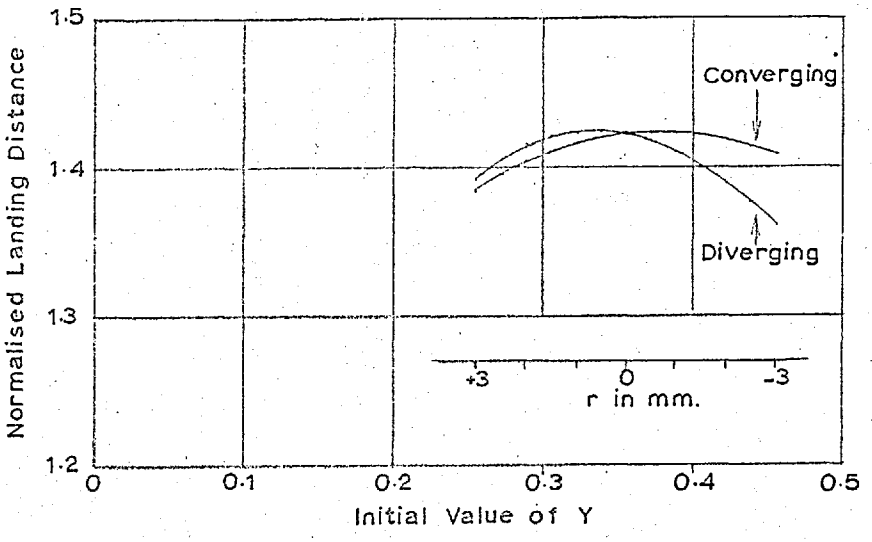


Fig. 5.17, Landing Distance for Converging Beam.

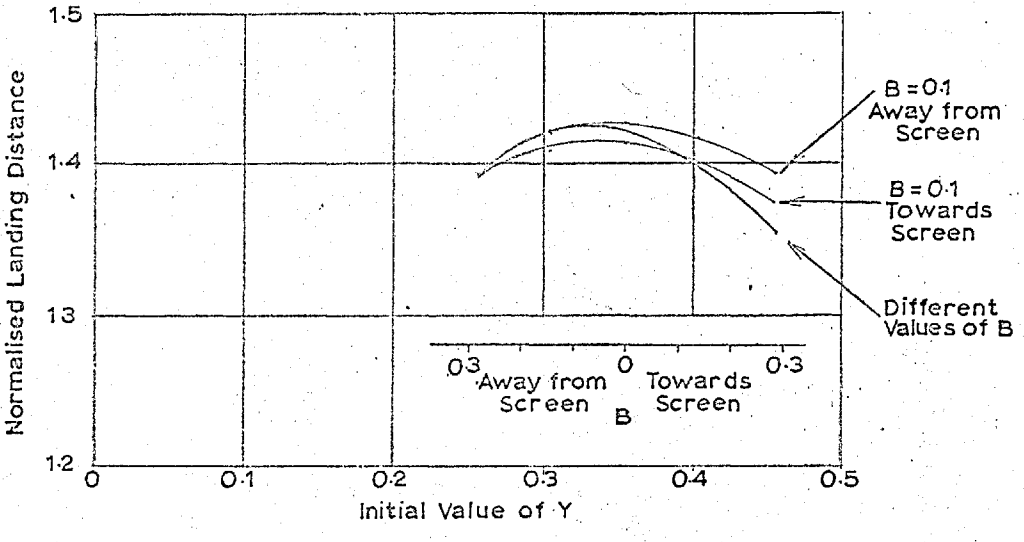


Fig. 5.18, Landing Distance with Magnetic Field.

travelled by the electrons varies between 0.52 meters and 0.76 meters, for a tube with a diagonal of 12 inches: Nevertheless, it demonstrates the need for effective magnetic screening, even for black and white displays.

Effect of the Wavebase.

If the wavebase is taken as 1.33 instead of zero, by using the methods which have been described and other results from the computer, it can be shown that the maximum diameter of the beam will be 3.8 mm. for an ideal black and white display, but it will have to be reduced to 1.2 mm. if F varies between ∞ and 300 or $-\infty$ and -300 while B = 0.05. In general the requirements for a spot of sufficiently small size are very slightly less stringent than would be the case for zero wavebase. The maximum landing distance is 1.508, if V' = 0.25, and it occurs when the initial value of Y is 0.200, which means that the width of the strips of the scanning array is more likely to cause periodic distortion of the rundown.

The Shadow Mask Colour Display.

The shadow mask method of colour selection requires the three primary colour beams to arrive at the shadow mask with different angles of incidence, but coincidently. In the flat tube, this would be achieved by locating the three beams in a line perpendicular to the screen, as was described in section 1.3. Fig. 5.9 indicates that, if the beams were parallel to each other initially, the angle of incidence of each would increase in

proportion to the initial value of Y, so each beam could only land on the appropriate phosphor, as shown in Fig. 1.4. However, it is clear from Fig. 5.8 that the central beam would land on the shadow mask beyond the other two, if all three beams were exactly parallel initially, and this would cause colour fringes. In order to correct this error, it would be necessary to ensure that the central beam was tilted slightly towards the screen.

As an example, we can consider the initial values of Y for the three beams to be 0.30, 0.35 and 0.40, which corresponds to a distance between adjacent beams of 1.5 mm. Fig. 5.10 indicates that the central beam would need to be tilted through 0.004 radians, or 0.23°, to coincide with the other beams at the shadow mask. From Fig. 5.8, the spot size of the outer beams would become excessive, if the initial diameters exceeded 0.9 mm., but some defocusing of the central beam would be required to ensure that all three beams covered the same area. From Fig. 5.9, the angles of incidence of the three beams would be 43.2°, 46.1° and 48.8°, if they were all parallel to the screen, but the angle of incidence of the central beam would actually be 45.9°, on account of its tilt.

We can now consider the action of the shadow mask itself in greater detail. Let s be the distance of the shadow mask from the screen, p be the distance between the slots in it and b be the width of these slots. We can see from Fig. 5.19(a) that, for full utilisation of the surface, in our example,

$$\frac{2}{3}p = s\,(\tan 48.8^\circ - \tan 43.2^\circ)$$

$$= 0.2032\,s.$$

Therefore $s = 3.28\,p$

$= 1$ mm. if p is assumed to be one line width.

Let the minimum angle for one beam be θ_1, the maximum angle for the adjacent one be θ_2 and the difference between them be $\Delta\theta$. From Fig. 5.19(b), if the beams just meet at the screen,

$$b = s(\tan\theta_1 - \tan\theta_2)$$

$$= \frac{s \sin\Delta\theta}{\cos\theta_1 \cos\theta_2}$$

$$\approx 2s\,\Delta\theta \qquad \text{(where } \Delta\theta \text{ is in radians)}$$

$$= 6.56\,p\Delta\theta\ .$$

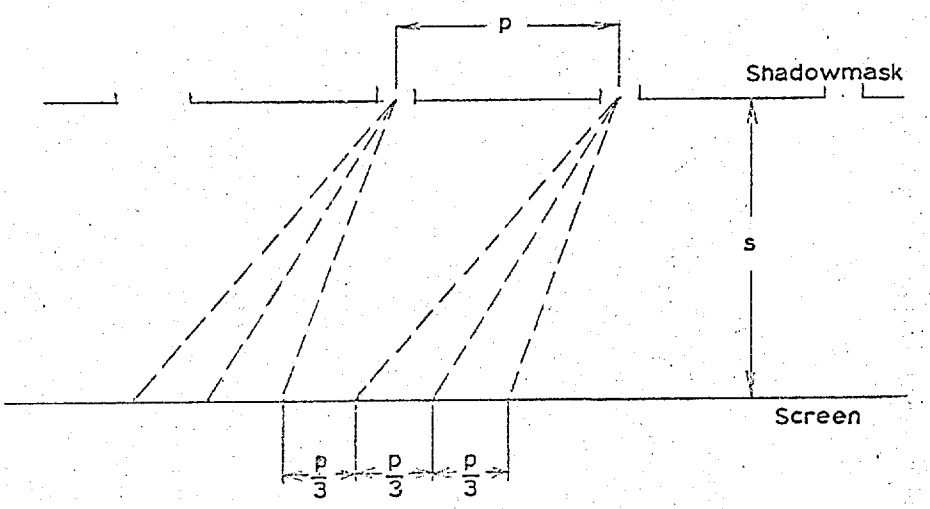
Therefore the mesh transparency, $\frac{b}{p}$, is $6.56\,\Delta\theta$.

In our example, if the diameters of all three beams are 0.9 mm.,

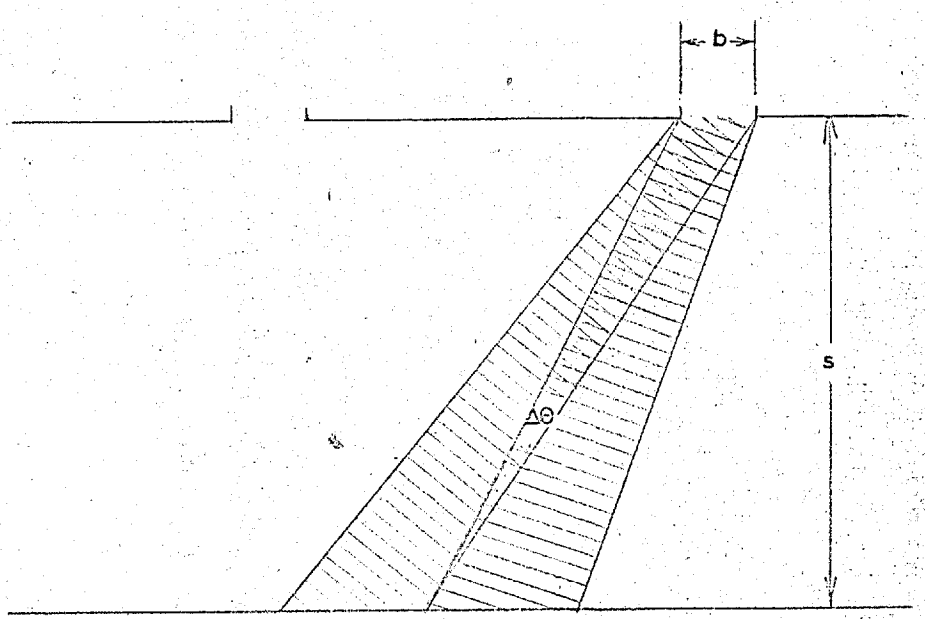
$$\Delta\theta = \frac{(1.5 - 0.9)}{1.5}\,\frac{(48.8 - 43.3)}{2} \text{ degrees,}$$

$= 1.12$ degrees or 0.02 radians.

Hence the mask transparency would be 13%. This could be increased by reducing the initial diameter of the beams; but, even so, this is an improvement on conventional shadow mask tubes.



(a) Shadowmask Distance.



(b) Mask Transparency.

Fig. 5.19, Action of the Shadowmask.

The Single Gun Colour Display.

The most important requirement for a single gun display is very small spot size. However, the calculations for spot size have already been carried out for black and white displays, so there is little point in repeating them; the only difference would be in the requirement for a much smaller spot. In order to obtain the very small spot, it would probably be necessary to use a converging beam at a smaller initial value of Y, although dynamic refocusing would then be needed.

One other electron optical requirement for a tube of this kind is vertical spot wobble, which could most easily be provided by changing the effective value of V'. Fig. 5.8 shows that the landing distance increases with the value of V'; in fact, changing V' by 0.1 would shift the landing point by 4.6 mm., if the distance between the screen and array were 30 mm. Hence V' should vary by 0.0067 for the spot to shift through one line width. The effective value of V' could easily be changed by applying a suitable voltage, ΔV, to the screen and a plate capacitively coupled to the strips of the array. The change in V', $\Delta V'$, would then be given by

$$V' + \Delta V' = \frac{V_{min} + \Delta V}{V_{max} + \Delta V}$$

Whence

$$\Delta V' \approx \frac{\Delta V}{V_{max}} (1-V') .$$

If V_{max} is 20 kilovolts, the change in V' would be 176 volts which is not excessive.

CHAPTER 6. CONCLUSIONS.

Before drawing detailed conclusions, the limitations of this investigation must be emphasised. All the vacuum experiments have been carried out in a mild steel demountable vacuum chamber; the voltages have never exceeded 5 kilovolts because corona on the resistor chains outside the vacuum tank and flashover on the vacuum models, made accurate measurements impossible whenever the voltage was greater than that. In view of the frequency with which the vacuum tank has been opened to permit adjustments and modifications, it was necessary to replace the oxide cathodes of the electron guns with tungsten hairpins. Hence it has never been possible to investigate the effects of space charge on the spot size with large beam currents. The mild steel walls of the vacuum tank produced an irregular magnetic field inside, which influenced the electron beam, even when magnetic screening was fitted; the effect of this field was accentuated by the low operating voltage. The magnetic field caused errors in the focusing measurements which were reduced, to some extent, by averaging, but even so they were considerable. In view of these limitations, it seems that further measurements with this apparatus would be of no great value; however, the resources required to build vacuum models and a vacuum system which would overcome them are rather beyond those available in a University.

The Deflection System.

It is clearly impossible to include every desirable property in a single deflection system, so some compromise has to be made. In the system which has finally been chosen, the worst feature is undoubtedly the deflection-defocusing, but the large maximum deflection angle, which is absolutely essential, could only be achieved at the cost of something else. However, the deflection-defocusing is compensated, to some extent, by the collimator. It is quite possible that a better design for a deflection system could be found, but none of the many designs which have been tested appeared to be much better, when considered in conjunction with the collimator.

The basic principle behind this form of deflection system, whereby it has been possible to improve the general performance because the beam always lies in the plane $Y = 0$, could probably be most useful in other applications.

The Collimator.

The theoretical design for the collimator was already in existence, so it was only necessary to show that it was satisfactory in practice and to modify the design slightly to help to compensate for the errors of the deflection system; this has been done. It has not, as yet, been possible to reduce the aberrations from the combination of the collimator and deflection system completely, so some further correction will probably be

required. This could be provided by a number of different methods such as dynamic refocusing, an astigmatic writing gun, shaping the electrodes of the reversing lens or fitting a correcting lens between the collimator and reversing lens. No detailed study of these methods of compensation has been made, however, because it would have been of little value, on account of the strong stray magnetic fields in the vacuum tank.

The Reversing Lens.

The modified form of the reversing lens has, in general, been successful, but second order aberrations occur if a beam, which is diverging when it enters the lens, is to be parallel when it leaves it. This could be avoided by fitting a converging lens between the collimator and the reversing lens.

The Scanning Array.

The scanning array had been shown to work, in principle, by Stuart, but some aspects required further work. The program, which was written to compute the electron trajectories, has been most useful, and has permitted fairly detailed theoretical studies both of the scanning action and of the focusing of the writing beam. These studies have confirmed that the rundown is fundamentally stable and indicated the effect of imperfections in the array on the profile and stability of the potential wave. It appears that the flyback is not entirely stable, but this does not affect the

size of the writing spot; fortunately, the instability only results in a decrease in the efficiency of the flyback, so it can be overcome by increasing the flyback beam current. Studies of the screen region show that the profile of the potential transition, in a practical system, can give a satisfactory writing spot; however, stray magnetic fields can be very troublesome and magnetic screening will be essential, even for a black and white display.

A method of measuring the variation of the potential on the strips of the scanning array has been devised which does not disturb the scanning action unduly. This has been used to check the theoretical predictions based on the computer program.

Future Work.

It has already been indicated that further experiments with the present vacuum system would be of little value. However, it would be desirable to study the scanning action, particularly the flyback in greater detail experimentally. This could be done in the present vacuum system, using the oscillographic technique which has recently been devised. A theoretical design for a correcting lens to be fitted between the collimator and the reversing lens could be prepared with the aid of a digital computer.

A system, electron optically identical to the one which has been developed and described in this Thesis, incorporating such a correcting lens, but with an ultor potential of 12 - 20 kilovolts and oxide cathodes in the electron guns, can be expected to give a satisfactory high-definition television display.

APPENDIX.

Paraxial ray and c-error equations.

This proof is essentially the same as that used by C.S. Upadhyay in a paper in which he considered the possibility of avoiding the third order errors in the reversing lens;[15] it has, however, been extended here to cover the c-error, although the third order terms in the paraxial ray equation have been omitted.

We start by defining a coordinate system, s,n,y, such that the s-axis lies along the central trajectory of an electron beam. We assume that the radius of curvature of this trajectory is R and the n-axis lies in the direction of increasing R; then the y-axis is orthogonal to the other two.

Consider now an electron at (s,n,y), the equation of motion is

$$\ddot{n} - \frac{\dot{s}^2}{n+R} = -\frac{e}{m}\frac{\partial \phi_n}{\partial n} \qquad (A.1),$$

where dots indicate differentiation with respect to time,

e and m are the charge and mass of the electron,

and ϕ_n is the potential at (s,n,y) relative to the cathode.

By the principle of conservation of energy,

$$\dot{s}^2 = -\frac{2\,e\,\phi_n}{m} \qquad (A.2)$$

Hence, eliminating $\frac{e}{m}$,

$$\ddot{n} - \frac{\dot{s}^2}{n+R} = \frac{\dot{s}^2}{2\phi_n}\frac{\partial \phi_n}{\partial n} \qquad (A.3).$$

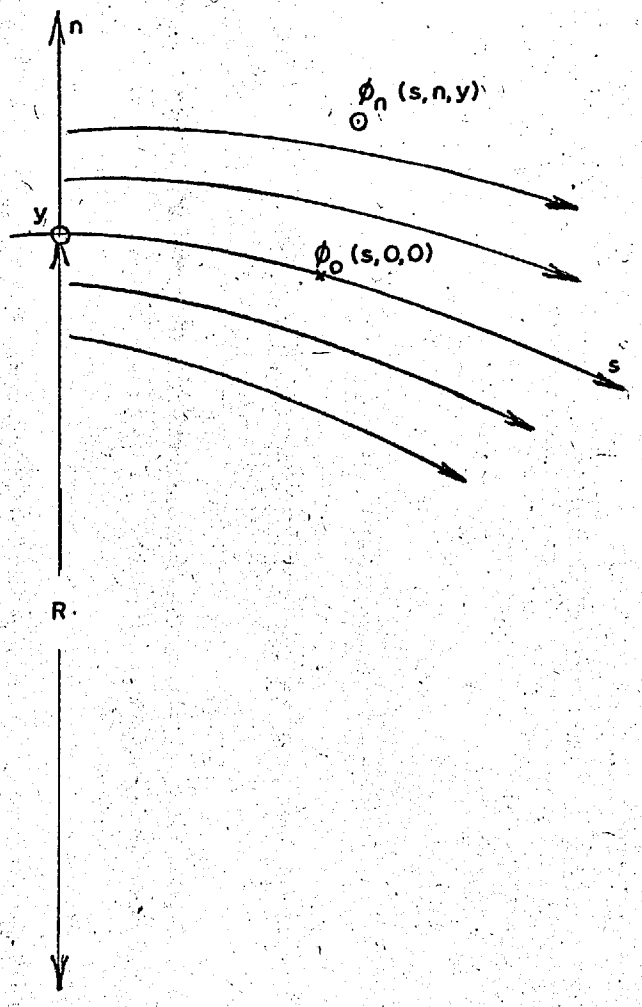


Fig. A.1, Curvilinear Coordinate System.

Differentiating (A.2) with respect to s,

$$\dot{s}\,\frac{d\dot{s}}{ds} = -\frac{e}{m}\left(\frac{\partial \phi_n}{\partial s} + \frac{dn}{ds}\,\frac{\partial \phi_n}{\partial n}\right) \qquad (A.4)$$

Now,

$$\ddot{n} = \dot{s}\,\frac{d}{ds}\left(\dot{s}\,\frac{dn}{ds}\right)$$

$$= \dot{s}^2\left(\frac{d^2n}{ds^2} + \frac{1}{\dot{s}}\,\frac{d\dot{s}}{ds}\,\frac{dn}{ds}\right)$$

Hence, using (A.4) divided by (A.2),

$$\ddot{n} = \dot{s}^2\left\{\frac{d^2n}{ds^2} + \frac{1}{2\phi_n}\left(\frac{\partial \phi_n}{\partial s} + \frac{dn}{ds}\,\frac{\partial \phi_n}{\partial n}\right)\,\frac{dn}{ds}\right\}$$

Substituting for $\ddot{n}$ in (A.3) and dividing by $\dot{s}^2$,

$$\frac{d^2n}{ds^2} + \frac{1}{2\phi_n}\,\frac{dn}{ds}\left(\frac{\partial \phi_n}{\partial s} + \frac{dn}{ds}\,\frac{\partial \phi_n}{\partial n}\right) = \frac{1}{n+R} + \frac{1}{2\phi_n}\,\frac{\partial \phi_n}{\partial n} \qquad (A.5)$$

We will first derive the paraxial ray equations and to do this we set $y = 0$. We can then write

$$\phi_n = \phi_o + n\,\frac{\partial \phi_o}{\partial n} + \frac{n^2}{2}\,\frac{\partial^2 \phi_o}{\partial n^2}$$

where ϕ_o is the potential at $(s,0,0)$, because n is small compared to s and the dimensions of the potential distribution.

Hence, $\quad \frac{1}{\phi_n}\,\frac{\partial \phi_n}{\partial s} \lesssim \frac{1}{\phi_o}\,\frac{\partial \phi_o}{\partial s}$

and

$$\frac{1}{\phi_n}\frac{\partial \phi_n}{\partial n} \approx \frac{1}{\phi_o}\frac{\partial \phi_o}{\partial n} + n\left\{\frac{1}{\phi_o}\frac{\partial^2 \phi_o}{\partial n^2} - \left(\frac{1}{\phi_o}\frac{\partial \phi_o}{\partial n}\right)^2\right\}$$

$$= -\frac{2}{R} - \frac{4n}{R^2} + n\frac{1}{\phi_o}\frac{\partial \phi_o}{\partial n}$$

since $\frac{1}{R} = -\frac{1}{2\phi_o}\frac{\partial \phi_o}{\partial n}$.

Substituting for $\frac{1}{\phi_n}\frac{\partial \phi_n}{\partial s}$ and $\frac{1}{\phi_n}\frac{\partial \phi_n}{\partial n}$ in (A.5),

$$\frac{d^2 n}{ds^2} + \frac{1}{2\phi_o}\frac{dn}{ds}\frac{\partial \phi_o}{\partial s} = \left(-\frac{3}{R^2} + \frac{1}{2\phi_o}\frac{\partial^2 \phi_o}{\partial n^2}\right) n \qquad (A.6)$$

which is equation (3.18).

By symmetry, if we had set $n = 0$, we would have obtained

$$\frac{d^2 y}{ds^2} + \frac{1}{2\phi_o}\frac{dy}{ds}\frac{\partial \phi_o}{\partial s} = \frac{1}{2\phi_o}\frac{\partial^2 \phi_o}{\partial y^2}\, y \qquad (A.7)$$

because the radius of curvature of the axis in the s,y plane is ∞ ; this is equation (3.19).

To derive the c-error equation, we must consider an electron at the point (s,c,y), so we write

$$\phi_n = \phi_o + c\frac{\partial \phi_o}{\partial n} + y\frac{\partial \phi_o}{\partial y} + \frac{c^2}{2}\frac{\partial^2 \phi_o}{\partial n^2} + cy\frac{\partial^2 \phi_o}{\partial n \partial y} + \frac{y^2}{2}\frac{\partial^2 \phi_o}{\partial y^2}$$

but $\frac{\partial \phi_o}{\partial y} = \frac{\partial^2 \phi_o}{\partial n \partial y} = 0$, because $y = 0$ is a plane of symmetry.

Hence it can be shown that

$$\frac{1}{\phi_n}\frac{\partial \phi_n}{\partial s} \backsimeq \frac{1}{\phi_o}\frac{\partial \phi_o}{\partial s}$$

and

$$\frac{1}{\phi_n}\frac{\partial \phi_n}{\partial n} \backsimeq -\frac{2}{R} - \frac{4c}{R^2} + \frac{c}{\phi_o}\frac{\partial \phi_o}{\partial n} + \frac{y^2}{2\phi_o}\left(\frac{1}{2}\frac{\partial^3 \phi_o}{\partial n \partial y^2} - \frac{1}{R}\frac{\partial^2 \phi_o}{\partial y^2}\right)$$

Substituting as before, we obtain

$$\frac{d^2c}{ds^2} + \frac{1}{2\phi}\frac{dc}{ds}\frac{\partial \phi}{\partial s} = \left(-\frac{3}{R^2} + \frac{1}{2\phi}\frac{\partial^2 \phi}{\partial n^2}\right)c + \frac{y^2}{2\phi}\left(\frac{1}{2}\frac{\partial^3 \phi}{\partial n \partial y^2} - \frac{1}{R}\frac{\partial^2 \phi}{\partial y^2}\right) \qquad (A.8)$$

which is equation (3.45).

REFERENCES.

1. D. Gabor, British Patent 739496; U.S. Patent 2,795,729.

2. P.R. Stuart. Ph.D. Thesis, University of London, 1957.

3. P.G. Kalman. Ph.D. Thesis, University of London, 1958.

4. P.M. Zollman. Ph.D. Thesis, University of London, 1962.

5. C.S. Upadhyay. M.Sc. Thesis, University of London, 1962.

6. J.E. Smith. Thesis for Diploma of Imperial College, 1962.

7. D. Gabor, P.R. Stuart, P.G. Kalman. Proc.I.E.E., 105, Part B, No.24, 1957, pp.581-606.

8. D. Gabor. British Patent 974093.

9. R. Graham, J.W.H. Justice, J.K. Oxenham. Proc.I.E.E. 108, Part B, No.41, 1961, pp.511-520.

10. W.R. Aiken. U.S. Patent 2,795,731.

11. W.R. Aiken. Proc.I.R.E., 45, No.12, 1957, pp.1599-1604.

12. H.B. Law, E.G. Ramberg, Proc.I.R.E., 48, No.8, 1960, pp.1409-1417.

13. J.J. Josephs. Proc.I.R.E., 48, No.8, 1960, pp.1380-1395.

14. J.R. Pierce. Theory and Design of Electron Beams, p.107, D. Van Nostrand & Co. Inc., New York, 1954.

15. C.S. Upadhyay. J. Inst. Telecom. Engrs., 9, No.4, 1963, pp.336-344.